Universidade de Aveiro
2020

Departamento de Geociências

Andrade António Francisco

Controlo de Qualidade dos Dados de Posicionamento em Reflexão Sísmica de Muito Alta Resolução

Quality Control of the Positioning Data in Ultra High Resolution Reflection Seismics

Universidade de Aveiro Departamento de Geociências
2020

Andrade António Francisco

Controlo de Qualidade dos Dados de Posicionamento em Reflexão Sísmica de Muito Alta Resolução

Quality Control of the Positioning Data in Ultra High Resolution Reflection Seismics

Dissertação apresentada à Universidade de Aveiro para cumprimento dos requisitos necessários à obtenção do grau de Mestre em Engenharia Geológica, realizada sob a orientação científica do Doutor Henrique Duarte, Diretor do Departamento de Geofísica Marinha da *Geosurveys* e do Professor Doutor Luís Menezes Pinheiro, Professor Associado do Departamento de Geociências da Universidade de Aveiro

Este fruto do meu crescimento académico, profissional e pessoal, dedico à Engrácia António e Rosénio António. Sei que não caminhei sozinho até ao fim desta jornada porque vocês continuam a olhar por mim de onde quer que estejam. Até breve...

o júri

Presidente	**Prof. Doutor Jorge Manuel Pessoa Girão Medina** Professor Auxiliar do Departamento de Geociências da Universidade de Aveiro
Arguente	**Doutor Omar Benazzouz** Consultor de Softwares de Geofísica da OB Tech
Orientador	**Doutor Henrique Canto e Castro Guerreiro Duarte** Diretor do Departamento de Geofísica Marinha Da Geosurveys
Co-Orientador	**Prof. Doutor Luís Fuentefria Menezes Pinheiro** Professor Associado do Departamento de Geociências da Universidade de Aveiro

agradecimentos

Primeiramente gostaria de agradecer aos meus orientadores Prof. Luís Menezes Pinheiro e ao Dr Henrique Duarte por todo tipo de apoio, ideias e sugestões que deram para a realização deste trabalho, e pela oportunidade que me deram de ver, enquanto estudante, como funciona na prática o mundo de indústria. Todas essas experiências contribuíram bastante para o meu crescimento a nível académico e profissional. Quero agradecer-lhes também que por mais atarefado que estivessem, não pouparam esforços para ajudar-me a superar as barreiras que surgiram durante este período.

Um obrigado muito especial à minha família, em especial à minha mãe, que apesar da distância mostrou-se sempre presente dando o apoio moral que precisava para concluir a formação. Ao meu Irmão Abecassis, obrigado pelos ensinamentos e pelo livro “Método Ser bom Aluno, bora lá?”, teve o efeito que se pretendia. À Academia da Sonangol EP e PUAÇA, por manterem o compromisso de custear todas as despesas inerentes a minha formação e estadia em Portugal durantes estes seis anos, mesmo numa época em que as condições financeiras e económicas do país eram menos boas.

Aos colegas da *Geosurveys*, pela ajuda e ensinamentos no uso das ferramentas e softwares utilizados neste trabalho. Ao meu colega de estágio, Eduardo Seabra, obrigado pela companhia durante estes meses e pelas boleias até a empresa. Um obrigado especial à Cíntia Pereira e Fábio Correia pela motivação e ajuda para fechar este trabalho numa altura em que o desleixo tomou conta de mim e a tendência era adiar cada vez mais.

Os meus agradecimentos são dirigidos também ao Analtino Martinho e Hermenegildo Tucale, pela amizade, cumplicidade, e disponibilidade que sempre demonstraram. Por fim, um agradecimento especial à Marta João, pela compreensão, companheirismo, pela incansável paciência comigo e por estar sempre presente.

palavras-chave

GeoSurveys, RadExPro, 3D UHRS, Controlo de Qualidade, Dados de Navegação, Erros de Posicionamento, DGPS, Offset, Ondas Diretas, Rejeição dos Dados de Navegação.

resumo

O controle de qualidade é uma operação muito importante durante as campanhas de aquisição de dados sísmicos. Tem como objetivo avaliar a qualidade dos dados adquiridos, detetar problemas ocorridos durante a aquisição, e finalmente assegurar que os dados têm a qualidade necessária para serem aceites ou se devem ser rejeitados. O tempo de operação tem consequências diretas sobre os custos e, por esta razão, esta é uma operação que deve ser feita rapidamente. Assim, devem ser avaliados os fatores mais relevantes que podem comprometer seriamente a qualidade dos dados.

O controle de qualidade da navegação é de extrema importância, visto que os erros de navegação contribuem para o *feathering*, que por sua vez constitui um dos principais critérios de rejeição. Por outro lado, a qualidade da navegação ou dos dados de posicionamento pode afetar fortemente a resolução sísmica pelo facto de serem usados para a determinação das posições das reflexões. Assim, dados de posicionamentos errados afetam os cálculos dos offsets e podem deslocar os pontos médios de reflexões para posições erradas, provocando uma discrepância entre a geologia real e a secção sísmica obtida. Deste modo, fica mais difícil a localização exata de blocos rochosos e a identificação de outros perigos em profundidade que colocam em risco a otimização das instalações das turbinas eólicas, trabalhos que a *Geosurveys* tem vindo a realizar.

As principais causas na origem destes problemas estão relacionadas com o mau funcionamento das antenas GPS usadas no sistema de aquisição, e outros problemas sistemáticos, como a atribuição de geometria. Existem erros típicos que afetam a geometria, tais como o erro na medição da distância entre o centro da antena da *lead buoy* e o primeiro canal, e erros na medição e atribuição das distâncias entre canais para as diferentes secções dos streamers. A solução proposta neste trabalho passou pelo desenvolvimento de métodos eficientes para diagnóstico destes tipos de problemas, onde através de padrões gráficos se torna possível detetar diferentes tipos de erros de posicionamentos e as respetivas causas.

O método desenvolvido baseou-se no controle de qualidade dos offsets calculados com os dados de posicionamento e no tempo de chegada das ondas diretas. Com essas duas informações foi possível estabelecer um critério de classificação dos dados de posicionamento quanto à sua qualidade, calcular os erros e obter indícios sobre a sua origem, levando sempre em consideração que os vários fatores têm diferentes influências sobre os erros e que alguns problemas são mais frequentes que outros. Com base neste procedimento, foram estabelecidos critérios de rejeição de dados com erros de posicionamento. As soluções obtidas foram testadas no software *RadExPro* e Kingdom Suite de modo a avaliar o efeito que esses erros têm sobre a sísmica.

acknowledgments

First of all, I would like to thank my advisors, Prof. Luís Menezes Pinheiro and Dr Henrique Duarte for all the support, ideas and suggestions given for the execution of this work, and for the opportunity they gave me, as a student, to see how the industry world works in practice. All these experiences contributed a lot to my academic and professional growth. I also thank them, because no matter how busy they were, they always found time to help me overcome the barriers that appeared in this period.

A very special thanks goes to my family, especially to my mother, who despite the distance was always present giving the moral support I needed to complete my academic education. To my brother “Abecassis”, I thank for all the life lessons he gave me and for the book “O método ser bom aluno, bora lá?”, it had the expected effect. To the Academy of Sonangol EP and PUAÇA, I thank for keeping the commitment of supporting all expenses related to my education and stay in Portugal during these six years, even at a time when the country's financial and economic conditions were less good.

To my colleagues at *Geosurveys*, for their help and lessons in using the tools and software used in this work. To my internship colleague, Eduardo Seabra, thanks for being my partner during these months and for the rides to the company. A special thanks to Cíntia Pereira and Fábio Correia for the motivation and support to finish this work at a time that I was sloppy and the tendency was to postpone again and again.

My thanks are also extended to Analtino Martinho and Hermenegildo Tucale, for the friendship, complicity, and availability they have always shown to me. Finally, a special thanks to Marta João, for understanding, companionship, endless patience with me and for always staying by my side.

keywords

GeoSurveys, RadExPro, 3D UHRS, Quality Control, Navigation Data, Positioning Errors, DGPS, Offset, Direct Arrivals, Rejection of the Navigation Data.

abstract

The quality control is a very important operation in the seismic data acquisition surveys and its main goals are to assess the quality of the acquired data, to detect problems during acquisition and finally to guarantee that the data has the required quality to be accepted for further processing, or if it must be rejected. The time spent in operations makes its cost to grow up and therefore the QC must be done efficiently and as early as possible., It is critical that the most relevant factors that can seriously compromise the data are evaluated onboard.

Navigation quality control is extremely important because the navigation errors can contribute to the feathering effect that by itself is one of the main rejections criteria. On the other hand, the quality of the positioning data can have strong influence on the seismic resolution, as it is used to calculate positioning for every reflection point. Thus, wrong positioning data affect offsets computing and can move the reflection midpoints to erroneous position causing a discrepancy between the actual geology and the seismic section obtained. This causes errors in the exact location of boulders and the identification of other in-depth hazards that threat the optimization of wind turbine installations, which is one of *Geosurveys* goals in this type of surveys.

The main sources of these problems are related to the bad functioning of GPS antennas used in the acquisition system and other systematic problems such as geometry assignment. There are typical errors which affect the geometry such as distance measurement between lead buoy center and first channel, distance measurements and assignment between channels in the different streamer sections. The solution proposed in this work consists on the development of effective methods to diagnose these types of problems, where through a graphical scheme it becomes possible to detect different types of positioning errors and their causes.

The method developed in the scope of this work was based on the quality control of the offsets calculated with the positioning data and the direct arrivals time. With this information it was possible to establish a classification criterion for the positioning data according to its quality, to calculate the errors and obtain indicators about its source of error, always considering that the various factors have different influences on the errors and some problems appear more frequently than others. Based on this, rejection criteria for data with positioning errors was established and solutions were tested in the software packages *RadExPro* and *Kingdom Suite*, in order to evaluate the effect of these errors on the seismic volumes.

Contents

List of Figures

List of Tables

List of Abbreviations

2D - Two Dimensions.

3D - Three Dimensions.

A - Amperes.

A.D - Anno Domini (epoch started from the birth of Jesus).

BP- Before Present.

CDP - Common Depth Point.

CHAN - Channel number.

CMP - Common Mid-Point.

DA - Direct Arrivals.

DGPS - Differential Global Positioning System.

FFID - Field File Identification Number.

FR - Fresnel Zone.

GMSS - Geomarine Survey System.

GPS - Global Positioning System.

GS - Geosurveys.

HZ - HERTZ.

ILine - Inline.

J - Joule.

Kyr - Thousand Years.

m - Meters.

Ma - Mega-annum, million years.

ms - Milliseconds.

NMEA - National Marine Electronics Association.

NMO - Normal Move Out.

QA - Quality Analysis.

QC - Quality Control.

RC - Reflection Coefficient.

SEG Y - Convention from the society of exploration geophysicist (SEG).

SVP - Sound Velocity Profile.

TWT - Two Way Time.

UHRS - Ultra High Resolution Seismic.

WAZ - Wide-Azimuth.

WTG - Wind Turbine Generators.

XLine - Crossline.

Z - Acoustic impedance.

Chapter 1

Introduction

1.1. Nature and Scope of the Thesis

This thesis is presented in fulfilment of the requirements for a master's degree in Geological Engineering, branch of Geological Resources, at the Geosciences Department of the University of Aveiro (UA), Portugal.

This is the result of the work developed during a 10 months' academic internship at *Geosurveys*, focused on navigation quality control, more specifically on offset and direct arrivals quality control and assessment, in order to detect problems in the positioning data provided by the acquisition system that can seriously compromise the quality of the data.

The internship consisted on a training with a set of software and methodologies used by the company. It started with a brief contact with NMEA files provided by the GPS antennas in order to understand the structure and meaning of the NMEA sentences. This was followed by the conversion of WGS84 NMEA data to projected coordinates using the *QGis* software. The projected coordinates were used to compute all node positions (positioning of the sources and receivers) and offsets with *GeoSuite Naviworks* software (from the Geomarine Survey System) for navigation processing purposes.

The computed offsets were loaded into the *RadExPro* Software (Deco Geophysical) and converted to time to compare with the direct arrivals time. When the differences between direct arrivals time and corresponding offsets were not expected, correction factors were calculated according to an analysis that was made of the positioning data to detect problems and their causes.

In summary, the training programme consisted on ultra high resolution seismic volume processing, and the development of a methodology to detect and diagnose bad positioning data, in order to improve the efficiency of navigation quality control, and the application of the appropriate rejection criteria to improve the quality of the data.

The present work was performed under the supervision of Dr Henrique Duarte, Director of the Marine Department of *GeoSurveys,* with co-supervision from Prof. Luís Menezes Pinheiro, from the Geosciences Department of the University of Aveiro.

1.2. Geosurveys – Geophysical Consultants, Lda

Based in Aveiro, *Geosurveys* was established in 1999 from an ambitious project designed for Geophysical Prospecting and Earth Sciences.

According to the market needs, *Geosurveys* specializes in Geophysical Prospecting and Geology (onshore and offshore) in several application domains, such as Groundwater Resources, Geophysics Planning and Project Managements, Environmental Impact, Archaeology and Patrimony, Geotechnical and Civil Engineering, Mining Exploration, estimates of Risks of Natural Disasters and Oil Exploration.

Thanks to continuous investments in hiring specialized human resources, as well as the purchase and development of latest generation technology in data acquisition and processing, *Geosurveys* has been consolidating in a sustained manner its position. Nowadays it is leader in the national market and has a prestigious position in the worldwide market.

In the latest years, the company´s strategy has been expanding and consolidating itself in international markets, with special attention to the so called “emerging economies”. With this bet *Geosurveys* has achieved and accomplished projects in a large number of countries, such as Qatar, Turkey, Ireland, Denmark, Iceland, the Netherlands, Angola, Mozambique, Cape Green Islands, Sao Tome and Principe, Guinea Bissau, Cameroon, Malawi, Ecuador, Peru, Brazil, USA, Venezuela, China, Vietnam, Singapore and India.

Geosurveys has available both technology for both offshore and onshore exploration. In onshore exploration it has available a full suite of geophysical methods, such as Georadar, Electrical Resistivity, Seismic, Electromagnetic Induction, Magnetometry, Gravity and Well Logging. For the offshore it presents a wide range of methods, such as Reflection Seismic, Refraction Seismic, Magnetometry, Side Scan Sonar, Echo-Sounder and Surface Sediment Sampling.

With special attention to the marine/blue economy, *Geosurveys* has available a set of geophysical solutions to exploration in nearshore, offshore, wind farm, port work and oceanographic studies. The company is highly experienced in the acquisition, processing, modelling and interpretation of single and multichannel reflection seismics (2D/3D), bathymetry with single beam and multibeam, side scan sonar, magnetometry, and sea bottom sampling with piston-corer, gravity-corer and vibro-corer.

Geosurveys provides high-resolution marine survey services for the implementation of wind farms and offers solutions such as ultra-high-resolution 3D reflection seismic with Geo-

Sparker and Geo-Boomer sources. The geophysical methods used have a major role to play in mapping stratigraphy, determining the thickness of superficial deposits and bedrock depth, the study of erosional and structural features and the detection of voids and buried objects and infrastructures. The port works include the acquisition of bathymetry, side scan sonar, magnetometry, seismics and drill execution. These techniques have an important role in determining the depth of bedrock for dredging and foundations. In the oceanographic studies, using gravity, magnetics, bathymetry and reflection seismics, *Geosurveys* provides its contribution to the knowledge of continental margins, determining the depositional areas, erosional surfaces and sediment transport pathways, mapping the thickness of sediments and mapping structural features of the bedrock, and through collaboration in scientific surveys.

The company is structured in a way that keeps its employees organized, attentive and ready to response to any request from potential clients, always providing an excellent service recognized by its clients and partners. This is evidenced by the increasing number of projects in recent years.

Considering the services provided and in order to effectively manage the resources and employees, *Geosurveys* is divided into three Departments: The Financial Department, led by the General Manager Francisco Sobral, the Department of Marine Geophysics, headed by Senior Geophysicist Henrique Duarte, and the Department of Geophysics on Earth, led by Senior Geophysicist Carlos Grangeia. The position of Executive Director is occupied by the Senior Geophysicist Hélder Hermosilha.

These departments consist on multidisciplinary teams of geophysicists, geologists and geological engineers, distributed between office and field, who work to give a good response to the various needs of the various clients.

1.3. Objectives

Marine seismic operations spend a lot of money on the operation team and vessel hire, and therefore the operations' cost can increase due to many factors such as the non-productive time, re-acquisition and infill lines. A good quality control is the base of effectiveness in this type of surveys because it allows the survey team to be able to detect problems during acquisition and act in a short interval of time to avoid re-acquisition and an increase of operations' cost.

One of the relevant steps in seismic data quality control is the navigation control. The quality of navigation has an important role in a marine seismic survey, and it is one of the most relevant criteria to accept or reject the acquired data. Bad positioning data affects offsets'

computing and can shift the reflection midpoints to erroneous positions causing a discrepancy between actual geology and the seismic section/volume obtained. This makes the exact location of boulders and the identification of other in-depth hazards that threaten the optimization of wind turbine installations, more difficult. Therefore, the main objectives of this thesis consist in detecting positioning problems, establishing criteria to classify and assess positioning data provided by GPS antennas from the acquisition system, and discuss the implementation of the best criterion to reject data affected by positioning errors according to its causes.

In order to achieve these goals some secondary objectives were established, such as developing an efficient way to detect errors, relating different types of errors to graphical patterns, and diagnosing and group the problems into different categories according to their causes.

An efficient way to detect erroneous offsets, which means errors in positioning data was developed, which consists of displays of iterative graphics (crossplots and histograms in *RadExPro*) with values of errors calculated by the difference between the offsets converted to time using sound velocity propagation in shallow water, and direct arrivals picks time. These iteratives graphics were analysed detect graphical patterns which give clues on the cause of the problem.

1.4. Dataset and Methodology

The dataset used for this work consisted of a 3D seismic volume with 600 Inlines (ILines) and 3800 Crosslines (XLines), with a CDP bin interval of 0.5 m, from a 3D UHRS data block named BLK2 that belongs to the NAPOLI 3D UHRS survey, carried out in the Tyrrhenian Sea (Bay of Naples). This dataset was acquired and quality controlled by *Geomarine* and *Geosurveys,* and partially re-processed in the scope of this work.

The methodology used in this work consisted on the implementation of methods for detecting positioning problems on the data provided by the GPS antennas used during the acquisition. A maximum acceptable positioning error value was defined to establish data rejection criteria and to evaluate the impact these errors have on the data after processing. *RadExPro* tests were performed, where through graphical patterns it was easier to detect the positioning errors and their causes, and then to reject the data affected by these problems in order to assess their impact on the data. Prior to applying the rejection criterion, the original volume was processed to obtain a standard stack to compare with the results obtained after applying the rejection methods. Since navigation data is being rejected, the impacts will be more noticeable on the time slices,

and therefore a final quality control was performed by comparing the horizontal sections of the Standard Stack and the post-rejection Stack.

1.5. Structure of this Thesis

This thesis is divided into six chapters. The first chapter gives a brief introduction about the scope of this work to get every reader more familiarized with the main objectives, dataset and methodology used in this work, and the structure of the company "*Geosurveys - Geophysical Consultants Ltd".*

Chapter two describes generically the geographical location and geological setting of the area where the survey was carried out. The third chapter introduces the marine seismic reflection method. It starts with the basic principles of reflection method, proceed with some important factors to consider in multichannel surveys (with special attention to 3D reflection seismic method) and this is followed by a basic seismic data processing flow to familiarize the reader with some important steps of seismic processing; this chapter finishes with an explanation about the 3D ultra-high-resolution system developed by *Geosurveys* and *Geomarine* and its processing sequence, and a brief highlight about the importance of the seismic data interpretation.

Chapter four, "Problem Setup, Data and Methodology", starts with the problem introduction, some information related to the acquisition parameters and proceeds with the processing of the seismic volume; after this, it is implemented the methodology developed in this work to assess the quality of the positioning data (Navigation Quality Control), to diagnose the problems and detect their causes.

Chapter five shows the results obtained from the developed method and the differences that different rejection criteria provide to the seismic data (mainly on time slices), ending with a short discussion around these results. Finally, chapter six presents a summary of the results achieved and the conclusions about the implementation of these methods.

Chapter 2:

Geological Setting of The Study Area

The area where the dataset used in this work was acquired is located in the Pozzuoli Bay of the Gulf of Naples in the Tyrrhenian Sea. This chapter starts with a general overview of the Tyrrhenian Sea, and then focuses on the area of the Gulf of Naples and the Bay of Pozzuoli where the survey area is located.

The Tyrrhenian Sea is part of the Mediterranean Sea, located off of the western coast of Italy (Figure 2.1). It is situated near where the African and Eurasian Plates meet. Therefore, mountain chains and active volcanoes such as Mount Marsili are found in its depths. This sea is bordered in the west by Corsica and Sardinia, in the north by the Isle of Elba, and in the south by Sicily.

Figure 2.1 - Tyrrhenian Sea. The study area, Pozzuoli Bay in Naples Bay is shown in the red box. (Source: https://www.worldatlas.com/aatlas/infopage/tyrrheniansea.html).

2.1. Geological Evolution of the Tyrrhenian Sea

The Tyrrhenian Sea is a young (<10 Ma) extensional basin that was formed within a complex convergent boundary between Africa and Europe (Figure 2.2a). It is surrounded by an arcuate orogenic belt consisting of the Apennines in the Italian peninsula, the Calabrian Arc in southern Italy and the Maghrebides in Sicily. This arcuate belt has been subjected to processes associated with subduction of a west dipping lithospheric slab, and simultaneously with back arc extension in the Tyrrhenian Sea (Malinverno & Ryan, 1986).

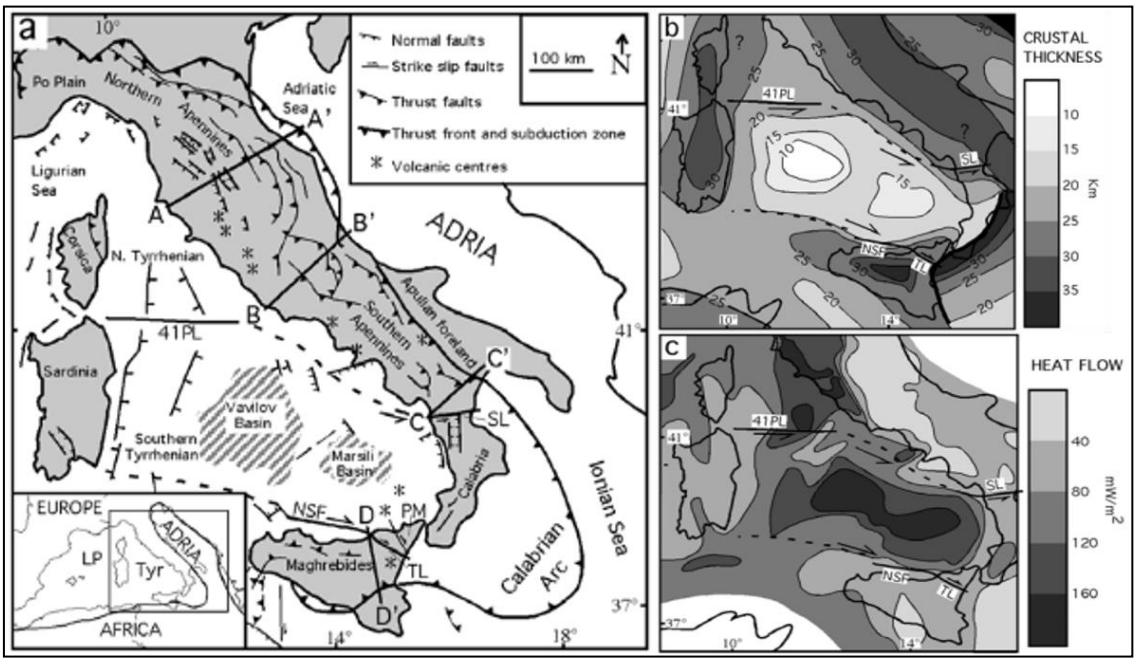

Figure 2.2 - Tectonic setting of the Tyrrhenian Sea. (a) Main structural features (modified from Patacca etal., 1993, in Rosembaum and Lister, 2004). (b) Crustal thickness (modified from Gvirtzman and Nur, 2001, in Rosembaum and Lister, 2004). (c) Heat flow (Della Vedova et al., 1991, in Rosembaum and Lister, 2004).

The Tyrrhenian Sea can be divided into a northern domain and a southern domain. The northern Tyrrhenian Sea is a wedge-shaped basin, bounded to the south by a major strike-slip fault zone, the *41 Parallel line* (41PL) (figure 2.2a), and floored by thin continental crust. Heat flow values and the spatial distribution of crustal thickness (Figures 2.2 b and c) indicate that the lithospheric discontinuity of the 41PL may continue farther southeast along the Tyrrhenian margin of Italy and into the sinistral strike-slip fault zone, the *Sangineto line* (SL) (see figure 2.2c), in northern Calabria (Rosenbaum & Lister, 2004). The Schematic cross sections AA', BB', CC' and DD' indicated in figure 2.2a, are presented in figure 2.3 for a better comprehension about the shortening and extensional systems associated with the formation of the Tyrrhenian Sea.

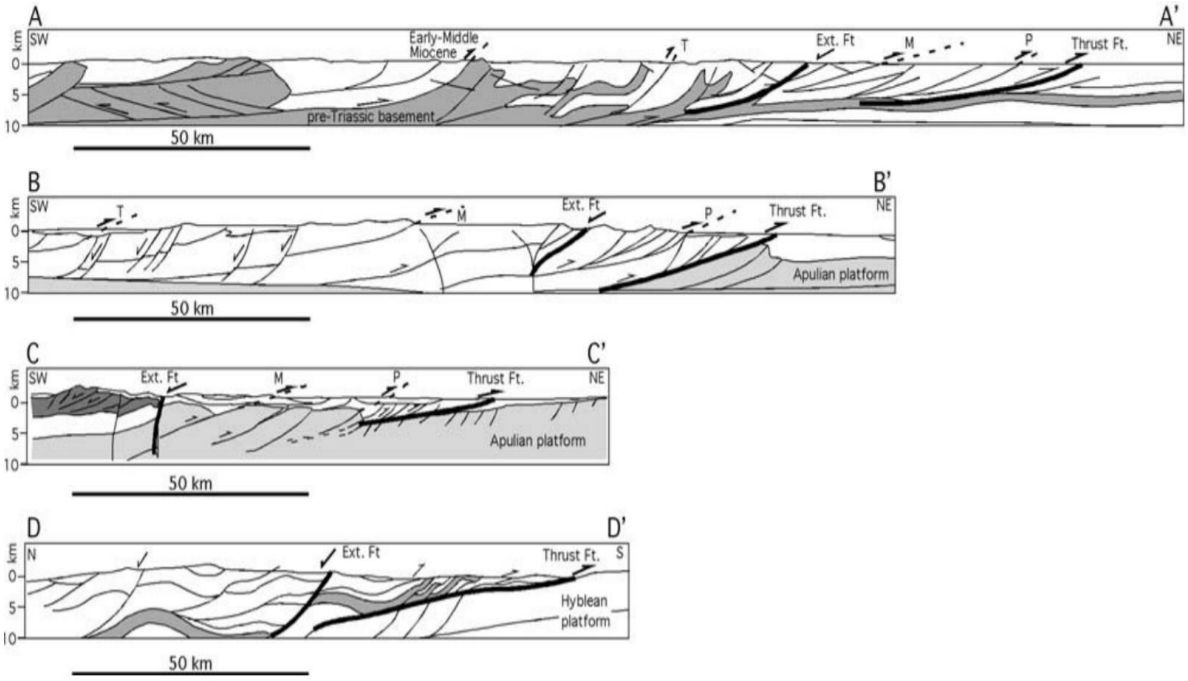

Figure 2.3 - Schematic cross sections AA', BB', CC' and DD' showing the approximate location of the thrust front and the extensional front. (from Finetti et al., 2001, in Rosenbaum & Lister, 2004, modified). Abbreviations are M, Messinian (7.5 –5.3 Ma); P, Pliocene-Pleistocene.

The southern Tyrrhenian Sea is separated from Sicily by another major strike-slip fault, the North Sicily Fault (NSF), which continues into northeast Sicily as the dextral strike-slip. In the southern Tyrrhenian Sea, there are stretched fragments of continental crust and deep basins (Vavilov and Marsili Basins) that contain Pliocene to Recent (<5 Ma) mid-ocean ridge basalt (MORB) (Kastens et al., 1988). These basins are considered to represent seafloor spreading in a back-arc position with respect to a northwest dipping subduction zone, presently located beneath Calabria. Further evidence of lithospheric stretching in a back-arc environment is based on high values of heat flow measured in the Tyrrhenian Sea (Della Vedova et al., 1984).

The Tyrrhenian-Apennine system has been subjected to simultaneous extension in the Tyrrhenian Sea and shortening in the Apennine-Maghrebide orogen since the late Miocene (10 Ma) (Malinverno and Ryan,1986; Lavecchia, 1988). Deformation in the Tyrrhenian-Apennine system followed an earlier deformational event during the late Oligocene-early Miocene that involved the opening of the Ligurian-Provençal Basin, as a result of the rollback of an older northwest dipping subduction zone (Faccenna et al., 1997; Rollet et al., 2002; Rosenbaum et al., 2002a). Rift basin sediments related to the earlier extensional event outcrop in eastern Corsica because they are located on the footwall of the younger fault. The opening of the Ligurian-Provençal Basin was accompanied by a counter-clockwise rotation (with respect to Europe) of the Corsica-Sardinia microplate, which led to progressive collision of Corsica-Sardinia with the

former western margin of Adria, and gave rise to the formation of the Apennines (Patacca et al., 1990). Paleomagnetic results indicate that Corsica and Sardinia stopped rotating at 16 Ma (Speranza et al., 2002, and references therein), while back-arc extension terminated in the Ligurian-Provençal Basin.

2.2. Geological Context of the Gulf of Naples

The Gulf of Naples also called the Bay of Naples (Figure 2.4), is a gulf located along the south-western coast of Italy (province of Naples, Campania region). It opens to the west into the Mediterranean Sea. It is bordered on the north by the cities of Naples and Pozzuoli, on the east by Mount Vesuvius, and on the south by the Sorrento Peninsula and the main town of the peninsula, Sorrento.

The Gulf of Naples is a NE-trending set of faults globally shaping a half graben characterized by thick volcanic units erupted from the Campi Flegrei and Vesuvius volcanoes (Milia, Torrente, Russo, & Zuppetta, 2003). The structure of the Gulf of Naples is controlled by numerous Quaternary fault systems, NE–SW trending SE-dipping and NW– SE trending SW dipping, linked to the last stages of the opening of the Tyrrhenian Sea (Fedele et al., 2015; Milia, 2010). Between the Middle and Upper Pleistocene, the fault systems were responsible for the development of the half-graben of the Gulf of Naples and Sorrento Peninsula fault block ridge (Milia & Torrente, 2003). This extensional basin covers about 1000 km^2 and has the typical physiographic features of a passive continental margin, with its continental shelf slope (between −140 and −180 m of depth) and basin (Aiello et al., 2001; Milia & Torrente, 1999).

Figure 2.4 - Gulf of Naples area (Source: https://www.wordatlas.com/gulfnaples.html). Study area in the red box.

The Gulf of Naples, characterized by both monogenic volcanoes and other volcanic and pyroclastic rocks, is bordered to the south by the carbonate succession of the Sorrento Peninsula, to the north by the Campi Flegrei volcanic area and to the east by the Vesuvian coast (Bonardi, d'Argenio, & Perrone, 1988; Fedele et al., 2015; Iannace et al., 2015; Santacroce & Sbrana, 2003) (Figure 2.5). The Campi Flegrei volcanic district includes Procida island and several submarine events and monogenic volcanos (Passaro et al., 2016) mostly made of pyroclastic rocks, such as Nisida island in the western part of the city of Naples (Fedele et al., 2015). The Campanian Ignimbrite (39.28 ky BP) and the Neapolitan Yellow tuff (15.3 ky BP) eruptions were the two largest caldera-collapse events of Campi Flegrei volcano (De Vivo et al., 2001; Deino, Orsi, de Vita, & Piochi, 2004). The Somma – Vesuvius is a 1281 m-high stratovolcano, composed of the older volcano Mount Somma and the younger cone Mount Vesuvius, formed from the caldera collapses produced by the three main Plinian eruptions (Santacroce et al., 2008). These two large volcanic complexes are separated by two alluvial plains: the Sebeto and Sarno plains, mainly formed of pyroclastic fall deposits related to upper Pleistocene to Holocene volcanic activity, and alluvial deposits. The present morphology of the gulf basin and its coasts has been influenced by the interaction between tectonics, volcanism and sea-level fluctuations that have greatly contributed to its evolution during the Quaternary cycle (Bruno et al., 2003; Cinque et al., 1997; Milia & Torrente, 1999, 2003, 2007).

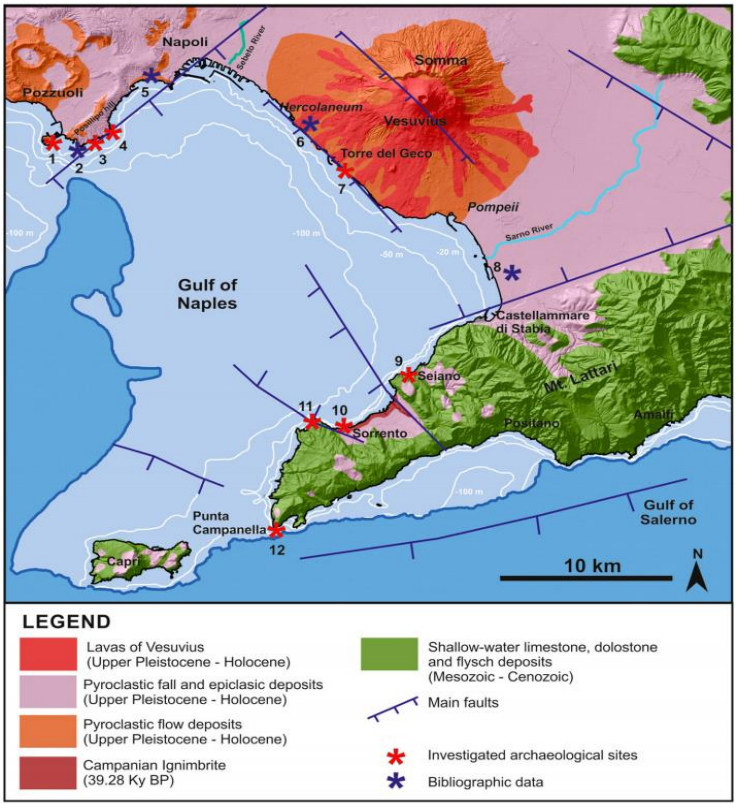

Figure 2.5 - Geological sketchmap of Gulf of Naples. (from Pietro P.C. Aucelli, 2017).

The Gulf of Naples represents an excellent natural laboratory, in which basin filling recorded the interplay of tectonic, volcanic and depositional/erosional processes, together with the tectonic uplift and deformation of adjacent onshore areas during the Pleistocene. The stratigraphic architecture of continental shelf and upper slope settings appears strongly influenced by the volcanoclastic input of centers of the Phlegraean Fields, Somma-Vesuvius and Ischia and Procida islands (Rosi and Sbrana, 1987; Santacroce, 1987; Vezzoli, 1988). Rapid lateral variations between acoustically transparent seismic units, interpreted as volcanic deposits, which erupted during multiphase volcanic activity of the Phlegraean Fields, Ischia and Procida islands complexes, and regularly stratified sedimentary units supplied by the Paleo-Sarno River mouth and by the Sorrento Peninsula tectonic uplift occurred (Aiello et al., 2005).

The Phlegraean Fields volcanic district surround the western part of the Gulf of Naples has been active since at least 50 kyr (Rosi and Sbrana, 1987). They correspond to a resurgent caldera (Rosi and Sbrana, 1987; Orsi *et al.*, 2002) with a diameter of 12 km and resulting from the volcano-tectonic collapse induced from the eruption of the pyroclastic flow deposits of the Campanian Ignimbrite (35 kyr BP). Coastal sediments ranging in age from 10000 and 5300 years crop out at 50 m altitude on the sea level in the marine terrace of *La Starza* (Gulf of Pozzuoli), indicating a volcano-tectonic uplift of the calderic center (Rosi and Sbrana, 1987; Dvorak and Mastrolorenzo, 1991).

The continental shelf of the Gulf of Naples has a variable width, ranging between 2.5 km (offshore the western sector of the Capri Island) and 10-15 km (offshore the Sorrento coast). Such a submarine topography is controlled by the interactions between subaerial and submarine volcanism, strongly involving the gulf during the Late Pleistocene and the linear erosion and sediment drainage along main axis of the Dohrn and Magnaghi canyons. The eruption centres occurring on the islands of Procida, Vivara and Ischia have an age ranging between 150 kyr and historical times (Rosi and Sbrana, 1987; Vezzoli, 1988). The volcanic activity in these islands played a major role in the formation and the activity of the Dohrn canyon western branch and of the Magnaghi canyon, since they drained a great volcanoclastic input on the slope during major eruptive phases. Polyphasic submerged volcanic edifices around Ischia Island (*i.e.* Banco di Ischia) and monogenic edifices in the Phlegraean Fields offshore - Banco di Pentapalummo, Banco di Nisida, Banco di Miseno - are also known (Latmiral *et al.*, 1971; Pescatore *et al.*, 1984; Fusi *et al*., 1991; Milia, 1996). These banks represent volcanic relic morphologies characterized by polycyclic erosional surfaces cropping out at the sea bottom, eroding volcanic deposits and covered by Holocene sediments (Banco di Pentapalummo, Banco di Ischia) or by a thick Holocene sedimentation. In the center of the Gulf of Naples, between Capri and Ischia islands a NE-SW trending morpho-structural high, the *Banco di Fuori* or *Banco di Bocca Grande*, occurs.

This bank looks like an asymmetrical ridge with the southeastern flank steeper than the north-western one (Aiello et al., 2005). (Figure 2.6).

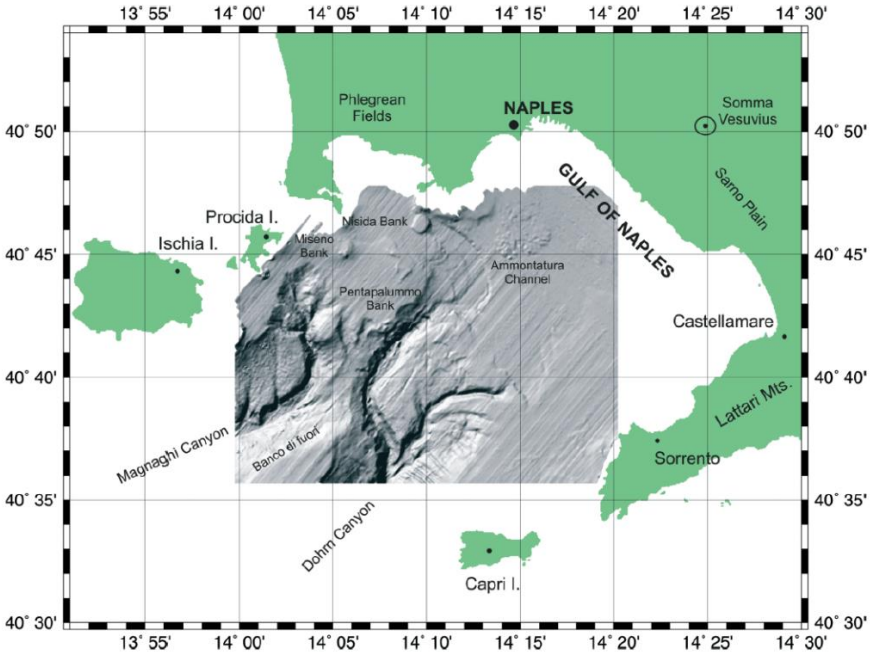

Figure 2.6 - Sketch map showing the main morphological lineaments in the Gulf of Naples reported from Multibeam bathymetry recorded by CNR-IAMC Geomare Institute (Aiello et al., 2001a).

2.2.1. Marine Sediments of the Late Quaternary Depositional Sequence

According to Aiello *et al.* (2011), the geological maps in this area show that the physiographic domains, mostly developed during the last Highstand Systems Tract, are characterized by specific sedimentary processes and volcanic events. They include the littoral zone, the continental shelf (marine platform, erosional or depositional, often at the base of coastal cliffs, relic or preserved morphologies of monogenic volcanic edifices, hummocky chaotic morphologies due to gravitational instability) and the continental slope (the latter deeply incised by canyons, evolving downslope in tributary channels).

The littoral zone is composed of the base of cliff deposits, submerged beach deposits, relic deposits, submarine slide deposits and beach rocks. The base of the cliff deposits is represented by heterometric blocks, often volcanic, with dimensions from metric to decametric, alternating with poorly sorted heterometric gravels, with heterogeneous texture. The submerged beach deposits are composed of gravels, gravelly sands and coarse-grained sands with pebbles (tuffs and lavas), as well as by coarse to medium grained sands, often with gravels and, subordinately, pebbles and isolated blocks. The relic beach deposits are composed of well-rounded heterometric volcanic pebbles, immersed in a sandy silty matrix. There are also

sandstones and conglomerates. The inner shelf zone includes inner shelf deposits and bioclastic deposits. The inner shelf deposits are composed of gravels, sandy gravels and coarse grained lithobioclastic sands. The lithic component is made up of volcanic elements (tuff and other pyroclastic particles). The bioclastic component is formed by fragments of Molluscs and Echinoderms. The sandy fraction is represented by heterometric gravels, gravelly sands and bioclastic sands in a scarce pelitic matrix. The outer shelf environment includes clastic deposits and bioclastic deposits. The bioclastic deposits are composed of organogenic sands and gravels with scarce pelitic matrix, bio-detritic coarse-grained sands with scarce pelitic matrix ("coastal detritic"), draping on pelitic and sandy pelitic sea bottoms. The muddy coastal detrital assemblage is formed by pelites with bioclastic gravels and sands (Aiello *et al.*, 2011).

The slope zone includes the deposits of the Transgressive Systems Tract of the Lowstand Systems Tract and Pleistocene relic marine deposits of the Falling Stage Systems Tract. Pelites with a remaining sand fraction are diffused in correspondence of the canyon´s heads. The Transgressive Systems Tract is composed of volcanoclastic pebbles, alternating with thick pumice levels, often in a pelitic matrix. These deposits have a mounded external morphology, exhibit acoustically-transparent seismic facies and crop out on the outer shelf, offshore the Naples town, in a bathymetric interval ranging between – 140 m and – 180 m. The Lowstand Systems Tract includes relic littoral deposits, composed of well sorted sands and gravels with bioclastic, as well as middle to fine sands, organized as coastal prisms overlying the shelf break. The Pleistocene marine units are represented by coarse to fine grained marine deposits, forming relic morphologies of beach and continental shelf environments (Aiello *et al.*, 2011).

2.2.2. Volcanological Background – Products of Vesuvius flowed into Naples Bay

Vesuvius, in southern Italy, has been one of the most active volcanoes in the world. More than 80 eruptions of Vesuvius are listed in a recent worldwide directory of volcanic activity (Simkin and Siebert, 1994). Most geologic studies of Vesuvius have concentrated on subaerial exposures, even though a significant amount of the material erupted in 79 and 1631 flowed into Naples Bay.

Vesuvius produced at least four major Plinian eruptions before A.D. 79 (Arnò et al., 1987). Because the breached crater of Monte Somma opens southward toward Naples Bay, these earlier eruptions certainly sent surge and pyroclastic flows toward the sea. The extent and thickness of these earlier flows are unknown, because they are covered by the extensive deposits erupted in A.D. 79.

Besides the A.D. 79 eruption, the only other historic eruption of Vesuvius that sent voluminous flows into the sea occurred in 1631 (Rosi et al. 1993). A contemporary engraving of the 1631 eruption shows distinct flows entering the sea at a half dozen sites. A map of these

flows, compiled from recorded eyewitness accounts and field work, confirms that deposits of that eruption are found along half of the coastline of Vesuvius (Rosi et al. 1993). Those flows formed deltas that extended into Naples Bay at Granatello, Torre del Greco, and Torre Annunziata (Milia et al., 1998).

2.3. Structure and Evolution of the Bay of Pozzuoli

The Campi Flegrei is an active volcanic area located on the coastal zone of the Campania region of SW Italy, a large part of which develops off the Naples (Pozzuoli) Bay. In the Pozzuoli Bay, the structural elements of this caldera collapse have been largely inferred, on the basis of seafloor morphology and associated deposits (Pescatore et al., 1984; Fusi et al., 1991; Fevola et al., 1993; Orsi et al., 1996; Di Vito et al., 1999).

The volcanic activity of the Campi Flegrei spans throughout the latest Quaternary (Di Girolamo et al., 1984; Lirer et al., 1987; Rosi and Sbrana, 1987; Di Vito et al., 1999; Pappalardo et al., 1999; Rolandi et al., 2003; Scarpati et al., 2013) and is characterized by at least one large caldera collapse structure produced during the eruption of the Neapolitan Yellow Tuff (NYT). The caldera is represented by a quasi-circular area of approximately 8 km in diameter, that developed in the central sector of the Campi Flegrei, including the inland area and part the Pozzuoli Bay (Lirer et al., 1987; Rosi and Sbrana, 1987; Barberi et al., 1991; Scandone et al., 1991; Scarpati et al., 1993; Wohletz et al., 1995; Orsi et al., 1996; Florio et al., 1999; Judenherc and Zollo, 2004; De Natale et al., 2006; Dello Iacono et al., 2009; Sacchi et al., 2009).

2.3.1. Ground Deformation in the Pozzuoli Area

An uplifted coastal sector of the Pozzuoli Bay is exposed on-land at the marine terrace called "*La Starza"*, at 30 to 55 m above sea level. The youngest marine deposits nowadays exposed at *La Starza* display a maximum elevation of approximately 30 m above sea level and were originally deposited in water depth of 30 to 50 m below sea level (Amore et al., 1988). The total uplift at *La Starza*, on-land, can be estimated in the order of 60–80 m. Archaeological remains of Roman age, nowadays found at a water depth of approximately 10 m along the western coast of the Pozzuoli Bay (Dvorak and Mastrolorenzo, 1991; Orsi et al., 1996; Passaro et al., 2012) indicate that the entire area underwent subsidence since Roman time.

2.3.2. The Pozzuoli Bay

The Pozzuoli Bay shown in Figure 2.7 is a minor inlet of the Gulf of Naples characterized by a central depression with maximum water depth reaching approximately 110 m below sea

level, bounded seaward by submerged volcanic banks (De Pippo et al., 1984; Pescatore et al., 1984). The oldest stratigraphic units are relics of volcanic edifices associated with explosive activity older than 40 kyr, overlain by products of the Campania Ignimbrite (De Vivo et al., 2001; Rolandi et al., 2003; Deino et al., 2004) and NYT eruptions (Neapolitan Yellow Tuff, caldera offshore the Campi Flegrei). The sedimentary succession of the last 15 ky is represented by marine epiclastic deposits interbedded with volcaniclastic layers (Milia, 1998, 1999, 2010; Milia and Torrente, 2000; Insinga et al., 2002; Milia and Giordano, 2002; Sacchi et al., 2009; Budillon et al., 2011), mostly deposited inside the NYT caldera collapse.

There is a general consensus regarding the location of major morpho-structural lineaments, mostly described in terms of NE–SW, EW and NW–SE trends (Pescatore et al., 1984; Di Vito et al., 1999; Milia and Torrente, 2000; Milia and Giordano, 2002; Milia et al., 2003; Bruno, 2004). Acocella et al. (2004) and Acocella (2010) have suggested that NE–SW transfer faults likely played an important role in controlling the evolution of volcanic activity at Campi Flegrei.

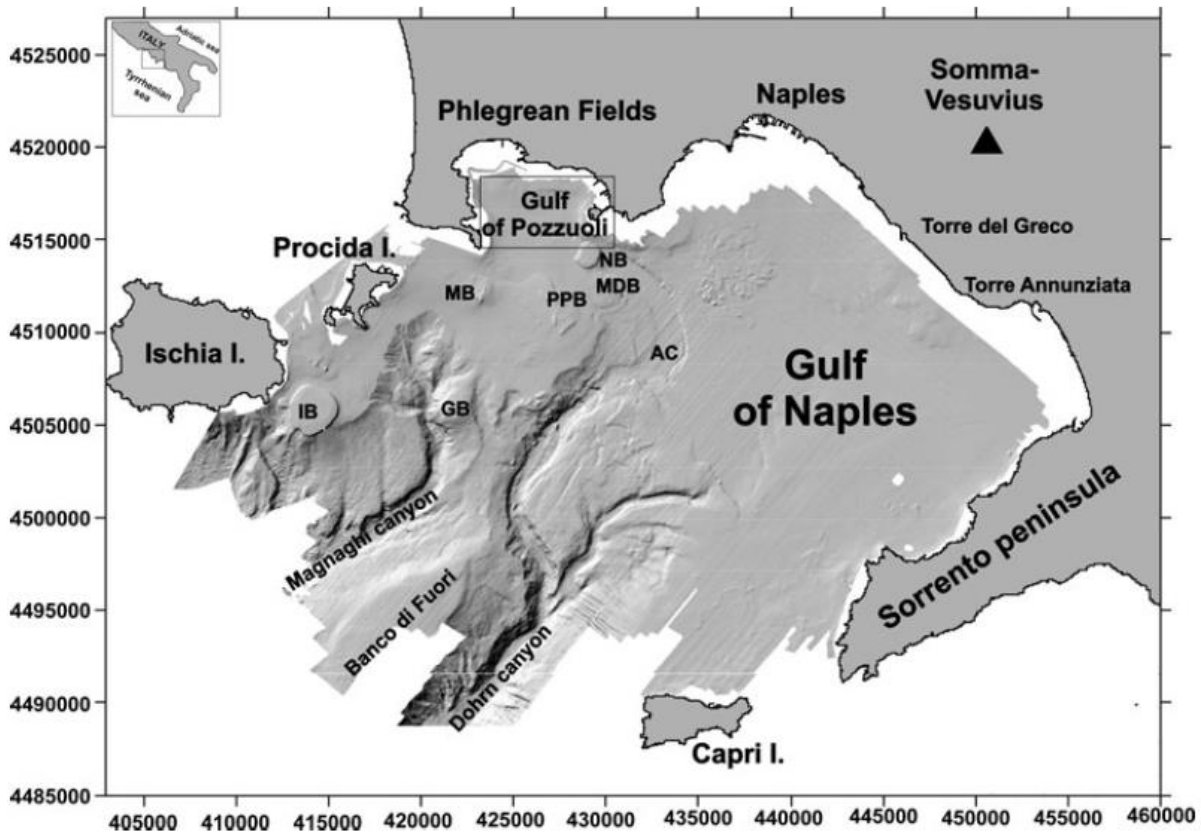

Figure 2.7 - Shaded relief map of the Multibeam bathymetry (ELAC, BottomChart MK2) recorded in the Bay of Naples. AC Ammontatura Channel, MDB Monte Dolce Bank, NB Nisida Bank, PPB Pentapalummo Bank, MB Miseno Bank, GB Gaia Bank, IB Ischia Bank (source: Aiello et al 2012).

The morphological sketch map of the Pozzuoli Bay (Figure 2.8) shows several offshore morphological units, including the inner continental shelf, the central basin, the submerged

volcanic banks and the outer continental shelf. The inner shelf is positioned in the northern sector of the gulf, whose shelf break occurs at about 50 m water depth. It grades through a weakly inclined slope to a central basin, developed at about 100 m water depth. The basin is bounded seawards by a belt of submarine volcanic highs (Aiello *et al.,* 2012).

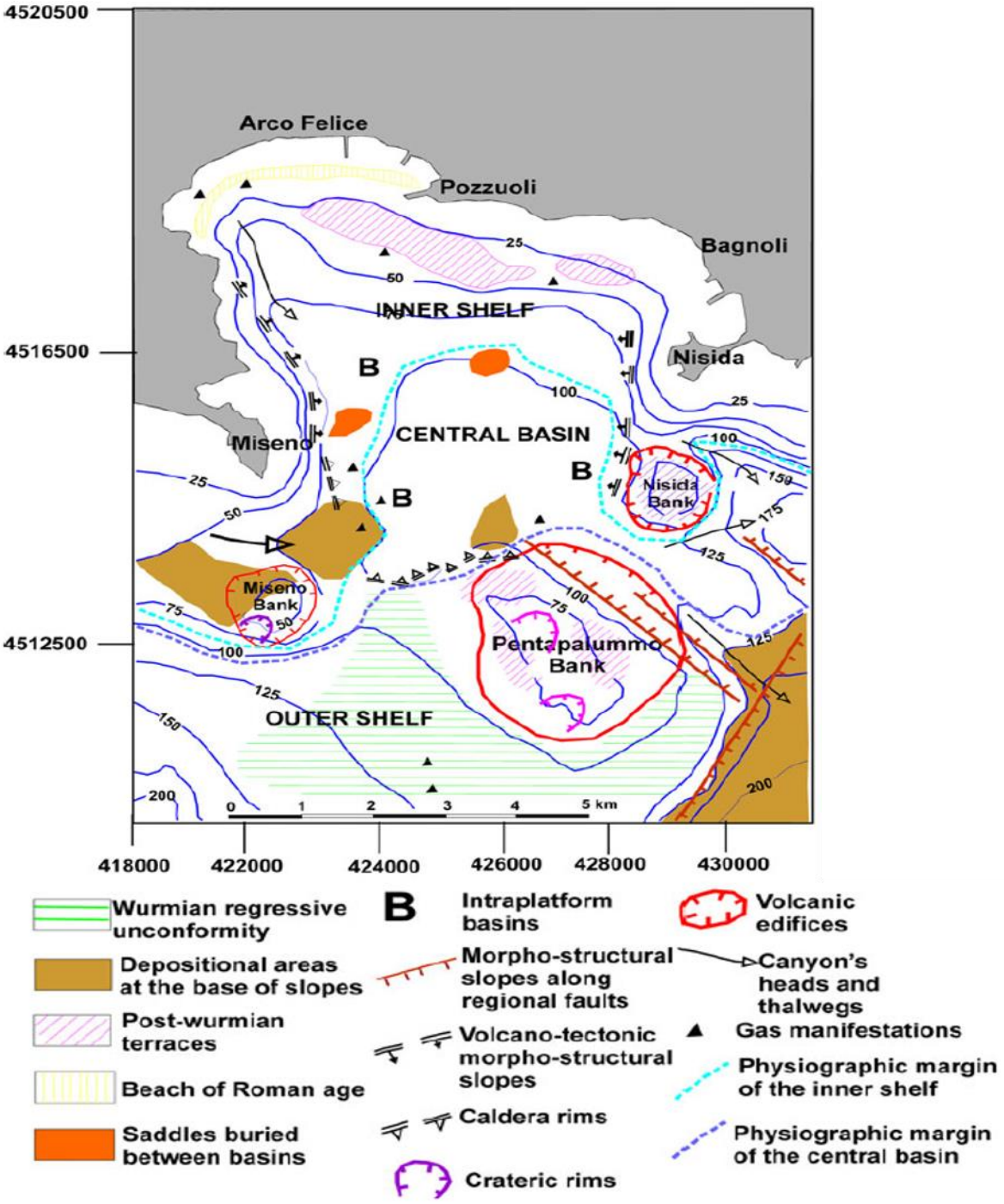

Figure 2.8 - Morphological map of the Pozzuoli Bay (modified after De Pippo et al. 1984, in Aielo et al 2012).

Chapter 3:

The 3d Marine Seismic Reflection Method

According to Yilmaz (2001a) the seismic method has three principal applications which are delineation of near-surface geology for engineering studies, coal and mineral exploration within a depth of up to 1km, hydrocarbon exploration and development within a depth of up to 10 km, and the investigation of the earth's crustal structure within a depth of up to 100 km.

The seismic reflection industry can be divided into three main sections: data acquisition, data processing and data interpretation. The data acquisition is a difficult operation that requires a lot of skill and experience from the operating personnel. Data processing is normally handled by the same contractors who carry out the acquisition, with the addition of some smaller firms who may focus on particular advanced techniques. The last section, data interpretation, is mostly handled by the client companies, who employ both geophysicists and geologists as seismic interpreters (Ashcroft, 2011)

The conventional seismic methods are widely applied to map the subsurface regional geology, the geometry of layered sedimentary sequences and in the search of oil and gas. Ultra-High Resolution Seismics (UHRS), which usually consists on denser data acquired with wider frequency bands above 500Hz up to 5kHz, can be used to study the near-surface geology for the geotechnical investigation of foundation conditions, essential, for example, for the construction of an offshore windfarm (Correia, 2017).

3.1. Basic Principles and Fundamentals of the Reflection Method

The seismic reflection method is based on the propagation of compression waves in the interior of the earth that are reflected in the interfaces between layers with different properties, then return to the surface. The structure of the subsurface geological formations is mapped by measuring the time required for a seismic wave emitted at or near surface to return to the surface after reflection on the interfaces between formations, which have different physical and acoustically properties. The incident wave is split into a reflected part that travels upward and a refracted part that continues to propagate downward in a slightly different direction, according to the Snell's Law (Equation 3.1).

$$\frac{\sin(\theta_i)}{\sin(\theta_r)} = \frac{V_1}{V_2} \tag{3.1}$$

where θi is the incident angle, θr is the refracted angle and V_1 and V_2 are the velocities of the seismic waves in the two different media (Figure 3.1)

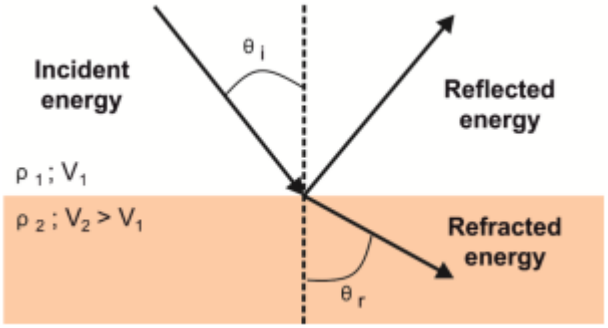

Figure 3.1 - Schematic image of the seismic wave between two media with different physical properties. The non-normal incidence, the density values for the two different layers and the velocity values of the seismic waves (adapted from Ribeiro, 2011).

Both equation 3.1 and figure 3.1 are simplified case in which there is no wave mode conversion. In the wave general case, for non-normal incidence, there will be wave mode conversion at the interface and longitudinal waves (P-waves) are converted to shear waves (S-waves) and vice versa.

In reflection seismics, the travel time also known as TWT (two-way-time) is the time taken for the seismic waves to travel from the source, to an interface between two layers with different physical properties (specifically the density (ρ) and the seismic wave velocity(v)), and then the time the waves take to reach the receivers. The acoustic impedance (Z), that characterizes the partition of the sound propagation from a media or formation to another with different properties, is the product of the density the formation by the velocity of propagation of the waves in that formation.

For the simplified case of the normal incidence and no wave mode conversion, the Reflection Coefficient (RC) is proportional to contrast between acoustic impedance of the formations with different physical properties and can be calculated by Equation 3.2.

$$RC = \frac{\rho_2 V_2 - \rho_1 V_1}{\rho_2 V_2 + \rho_1 V_1} = \frac{Z_2 - Z_1}{Z_2 + Z_1} \tag{3.2}$$

Seismic resolution is an essential parameter for a good quality seismic data. It is defined as a measure of how large an individual object needs to be to make itself detectable with seismic data, or the ability to recognize two different objects very close in seismic data.

The frequency of waves transmitted by the source depends on the type of seismic source, leading to different frequency bands used in the survey. Depending on the purpose of the survey different frequency bands can be used to acquire seismic reflection data, and this happens because higher frequencies are more rapidly absorbed with depth, while lower frequencies propagate deeper. Therefore, higher frequencies have higher resolution but a low penetration, making these higher frequency bands to be more used for near-surface studies; lower frequencies have lower resolution. These concepts are important for the choice of the acquisition equipment.

Vertical resolution

The vertical resolution of a seismic wave (Figure 3.2) is a measure of its ability to recognize individual, closely spaced reflectors and is determined by the pulse length of the record seismic section. For a reflected pulse represented by a simple wavelet, the maximum resolution possible is between one-quarter and one-eighth of the dominant wavelength of the pulse. The vertical resolution increases with increasing wave frequency. Frequency is expressed as the number of cycles per second (1cycle per second = 1Hertz) and higher frequencies mean sharper pulses and therefore better resolution. Two reflectors, such as the top and the base of a stratigraphic unit, can be recognized as separated seismic events only if the distance between them is at least $\frac{1}{4}$ of wavelength (λ) of the seismic wavelet, defined by Equation 3.3, where *V* is the seismic wave velocity in the layer and *f* frequency, that depends on the type and characteristics of the seismic source.

$$\lambda = \frac{V}{f} \tag{3.3}$$

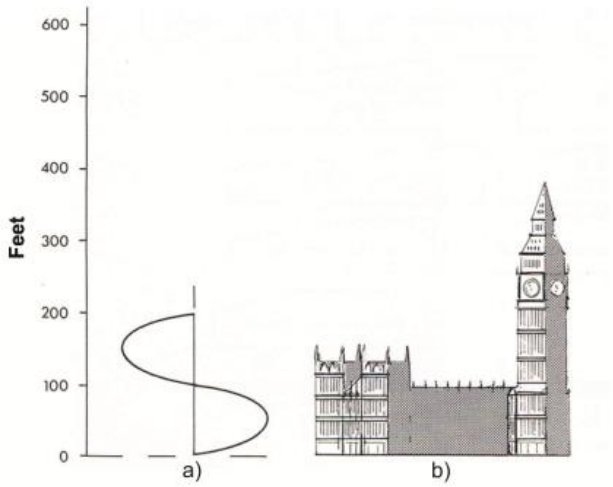

Figure 3.2 - Vertical scale of a seismic wavelet: a) A single cycle wave of 30 Hz in medium velocity of 1830m/s; b) The Big Ben, London, 115 meters (modified from McQuillin et al., 1984, in Ribeiro, 2011).

The frequency changes as the waves travel in the subsurface and the seismic wave will lose higher frequencies in depth since they are more rapidly absorbed. Therefore, high-frequencies waves are attenuated much faster than low-frequencies. The higher the frequency the lower will be the penetration, but the higher will be the vertical resolution.

Horizontal resolution

The horizontal resolution of a seismic wave is mainly controlled by the so-called "First Fresnel Zone" (Figure 3.3), the part of reflector illuminated by the seismic wavefront at a certain depth. The Huygen's principle states that each part of a wavefront acts as a source of a new wave and the area where the waves interfere with each other constructively is the area of interest called the "First Fresnel Zone" (Sheriff, 1991,1996).

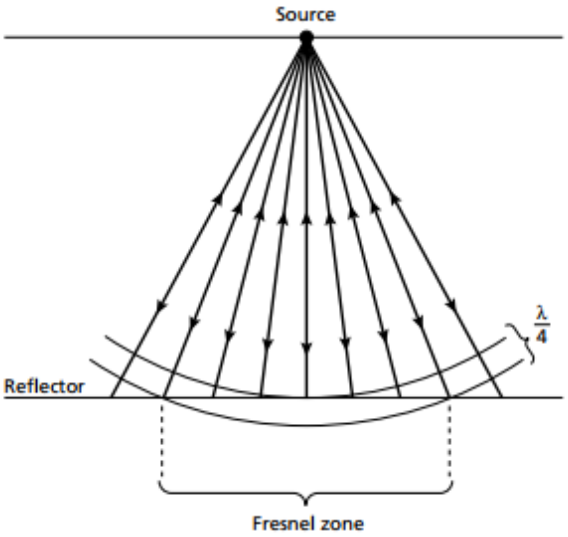

Figure 3.3 - Schematic representation of the Fresnel Zone (Kearey et al., 1991).

The reflected waves will interfere constructively where their travel paths differ by less than a half wavelength. A reflection that is coming back to the surface is being reflected not from a reflector point, but from an area with the dimension of the First Fresnel Zone. The radius of the First Fresnel Zone (FR) depends on the seismic velocity (V), the depth of the target (*t*, in two-way-time) and the frequency of the seismic source (f) (Equation 3.4; Sheriff and Geldart, 1995; Sheriff, 1996). With increasing velocities, increasing travel-time and decreasing signal frequency, the Fresnel Zone increases and consequently the horizontal resolution decreases. Therefore, both vertical and horizontal resolution decrease in depth.

$$\boldsymbol{FR} = \frac{\boldsymbol{V}}{\boldsymbol{2}}\sqrt{\frac{\boldsymbol{t}}{\boldsymbol{f}}} \qquad (3.4)$$

3.2. Multichannel Seismic Reflection Data

A multichannel seismic survey aims to get a multi-fold coverage, where with correct geometry the reflections from each point along the reflector are recorded in more than one seismic trace, for different shots (Figure 3.4). By using multiple sources and receivers per reflection point and summing the common reflection point traces, a significant improvement of the signal to noise ratio can be achieved (McQuillin et al., 1984).

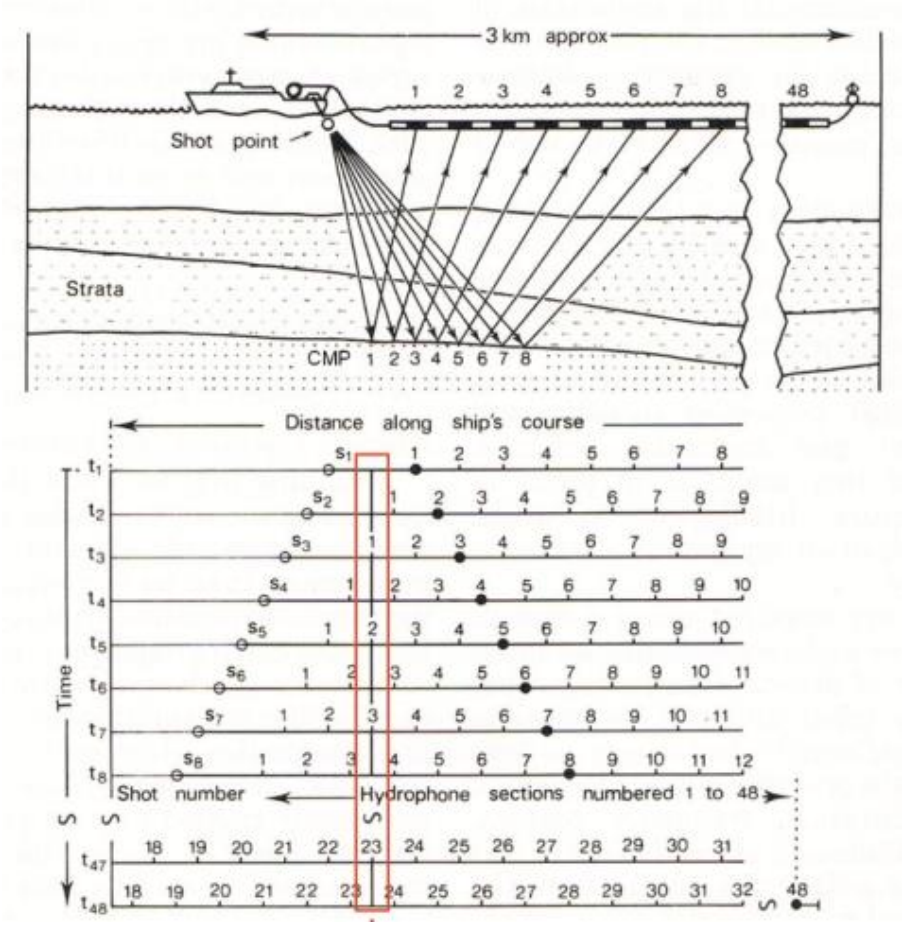

Figure 3.4 - Diagram of a multichannel marine acquisition geometry, with multi-fold coverage (In Ribeiro, 2011, modified from McQuillin et al., 1984). The red rectangle represents the common midpoint location.

3.2.1. Marine Seismic Sources and Receivers

The choice of marine source to be used in a survey depends on its objectives, such as the seismic resolution and depth penetration. Both depth and seismic resolution are depending on frequencies range of the seismic sources. Acoustic sources should aim to produce a signal as close as possible to a spike. There are many marine seismic sources (Figure 3.5), such as Airguns, Pinger, Boomers, and Sparkers.

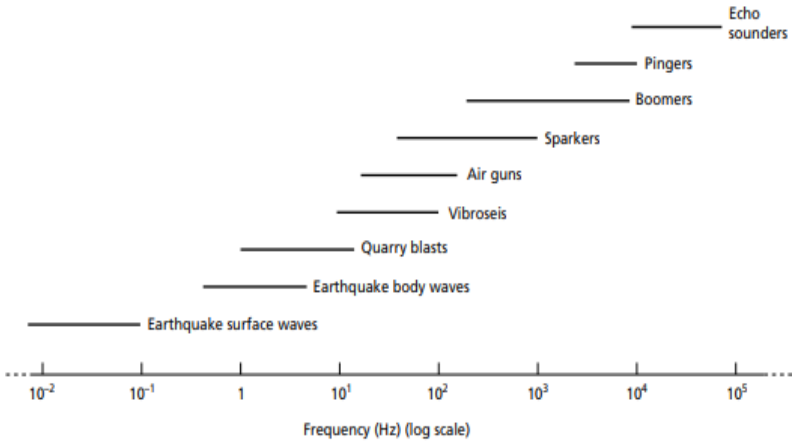

Figure 3.5 - Acoustic spectrum of different seismic sources (Kearey et al., 2002).

The Sparkers, the seismic source used in this survey, convert electrical energy into acoustic energy (Figure 3.6). It is a relatively high-powered acoustic source, that consists of two closely spaced electrodes arrays immersed on a conducting fluid (seawater) that are connected to a capacitor bank (power supply) and a switch, to open and close the power supply to the capacitor. Discharging the capacitor creates a voltage between the electrodes high enough to cause dielectric breakdown (an abrupt increase in the electric current) of the fluid in between. During this breakdown, the fluid becomes first ionized and a current start to flow between the electrodes causing a short spark that produces heat which vaporizes the surrounding water, then a vapor bubble of high pressure and temperature is formed (Heigl et al., 2013). This vapor bubble begins to force outwards the fluid around and generates a pressure shock wave. The collapsing bubbles produce a high frequency signal (up to 5 kHz). As sparkers generate broad-band acoustic pulses and can be operated over a wide range of energy levels, this type of source can be tailored to the needs of a particular survey.

Figure 3.6 – High frequency marine source, Sparker. (from https://www.geomarinesurveysystems.com).

When the survey is carried out at sea, the receivers used are hydrophones. In a multichannel survey the hydrophones are placed inside the streamer which is a neoprene tube filled with a liquid lighter than water (e.g. kerosene) to turn it neutrally buoyant (Figure 3.7). Connection wires in between hydrophones and from the receiver to the recording system are also included inside the streamer (Sheriff and Geldart, 1995). Standard hydrophones are piezoelectric sensors which transform the compressional p-waves into an electrical signal. Within the hydrophone a piezoelectric transducer produces an electrical signal in response to the pressure changes caused by the passage through the surrounding water of the seismic pressure waves. Each crystal element consists of an annular piezoelectric ring, covered by metal on both surfaces, bonded at the open ends by thin convex metallic diaphragms (Dobrin and Savit, 1988).

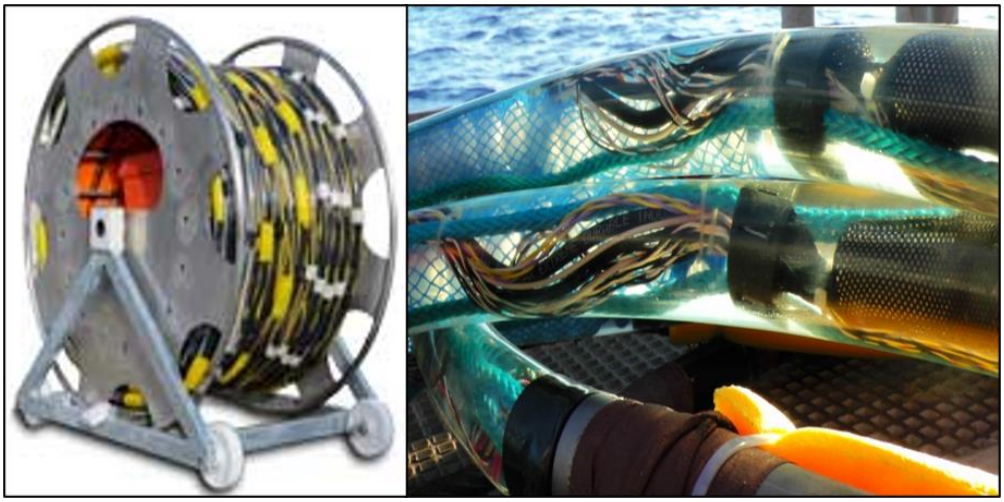

Figure 3.7 - Left: When the vessel is not acquiring seismic data, the streamer is kept onboard coiled on a reel. (from https://www.geomarinesurveysystems.com/products). Right: detailed seismic streamer array with hydrophones (https://www.oceanblogs.org/mappingtheoceanfloor/2016/06/28/radio-rock-research/).

A streamer is divided in several functional parts as it is shown in Figure 3.8. The first component connects the vessel and the first group of hydrophones. This ensures the minimum interference from the vessel's movement in the streamer (Pereira, 2009). Hydrophones are arranged in sections called "live sections" and in each section, can be implemented with twenty or more hydrophones spaced approximately 1m. The signals received at each hydrophone inside the same section are summed up and this is considered as a single receiver group (or channel). This technique improves the signal-to-noise ratio but when there is a great component of noise acquired with the signal, it can damage the quality of the data (Alfaro et al., 2007).

The "dead sections", or sections without hydrophones, are placed between live sections to give the desired length and configuration to the streamer. In the tail of streamer there is a buoy

equipped with positioning system tools that can communicate with the vessel (Figure 3.8). The buoy is used both to calculate the positioning of the streamer and to reduce the drift of the streamer due to water currents (Alfaro et al., 2007; Pereira, 2009). As it will be discussed further in the next chapter, the acquisition system used in this survey has a specific and efficient method to compute the positioning of every receivers and sources, to keep the desired geometry.

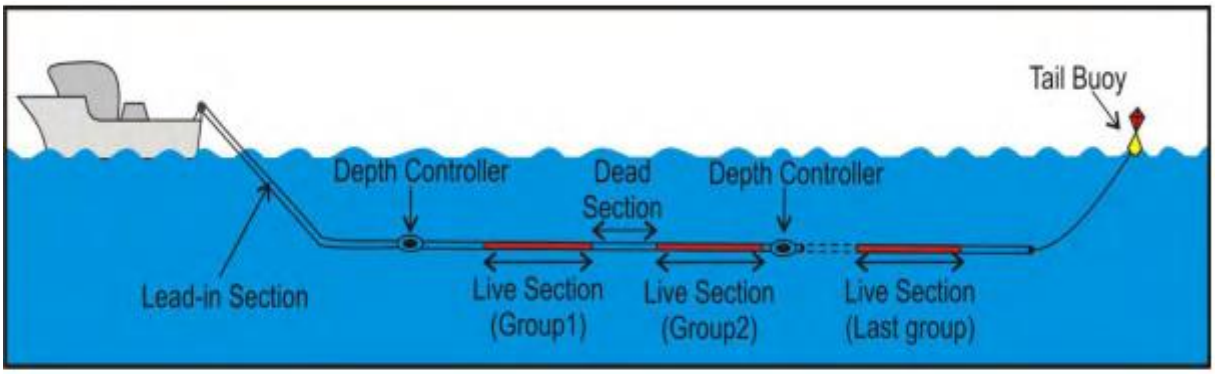

Figure 3.8 - Schematic representation of a streamer configuration (Modified from Sheriff and Geldart, 1995).

In seismic surveys, to minimize the noise generated due to the vibration of the cable and the vessel's movement, McQuillin et al. (1984) suggests several methods to reduce these effects:

- Ship motion is decoupled from the streamer by using an elastic non-active lead-in section; this absorbs the ship's heave motion allowing the cable to be towed at a constant speed through the water;
- Streamer depths controller "birds" - are used to maintain a constant depth along the length of the streamer;
- Lead-in sections to the cable can be "smoothed" (rubber or tissue strips can be attached to it) to reduce noise induced by tugging;
- Instead of single crystal element hydrophones, dual crystal element hydrophones are used which have very low sensitivity to horizontal accelerations, one of the main sources of noise problems.

3.2.2. The 3D Marine Seismic Surveys

According to Brown (2011), three-dimensional surveys were first performed on a contractual basis in 1975, and the following year Bone, Giles, and Tegland (1976) presented the technology to the world. 3D marine survey aims to record reflections that come from out of the

plane of seismic line, so sources and streamers are not confined to working along a line but cover a swath of the surface. The normal procedure is to tow several streamers behind the ship, with sources firing alternately (Ashcroft, 2011) (Figure 3.9).

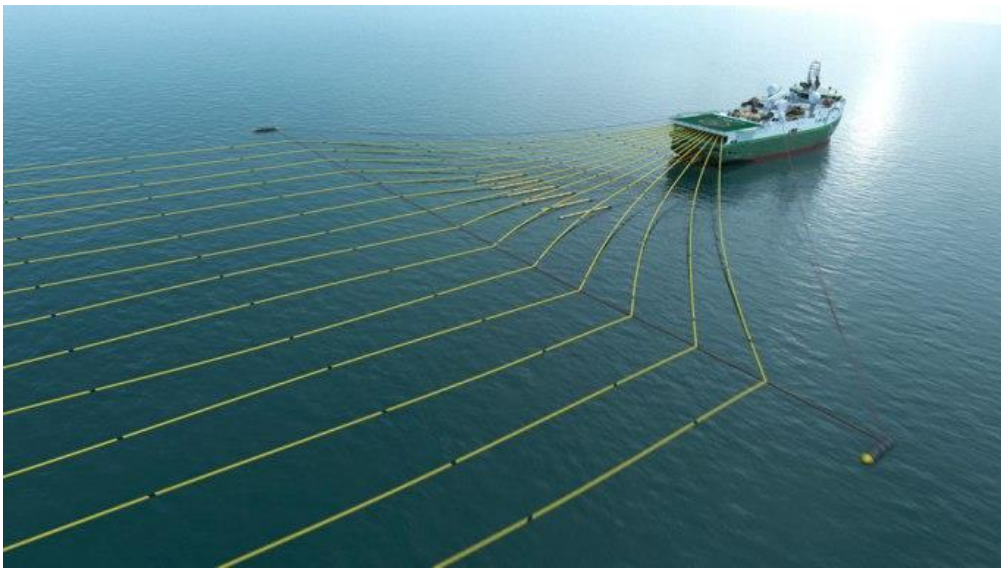

Figure 3.9 - Representation of the traditional 3D seismic surveys (from http://www.shippingherald.com).

3D seismic is distinguished from 2D seismic by the acquisition of multiple closely spaced lines that provides regular data that allows 3D data migration during processing. Three-dimensional surveys provide seismic data volumes making possible the interpretation of seismic events in 3D along the survey. Besides this, while in 2D the seismic data is sorted into common-midpoint gathers, in 3D seismic data requires binning the record data into common-cell gathers (Yilmaz, 2001a).

The geometry can be tailored to the survey goals. According to Volkhard and Florian (2017), in an offshore windfarm survey, a 3D model can provide a comprehensive overview of the study area, focused planning of sites, optimized planning of expensive coring/cone penetration tests, high flexibility throughout the entire planning phase (e.g., when offshore wind turbine locations are changed at a later stage).

Between the end of a swath and the beginning of another, there is non-productive time, there are also some imaging limitations depending on the geological context and the objective of the survey, in order to solve these problems different geometries can be used, such as wide azimuth and Coil Shooting (Buia et al., 2008) (Figure 3.10). Wide azimuth method is quite identical to the traditional method, but with at least two seismic sources. The Wide azimuth acquisition technique provides a general increase in coverage for all azimuth-offsets.

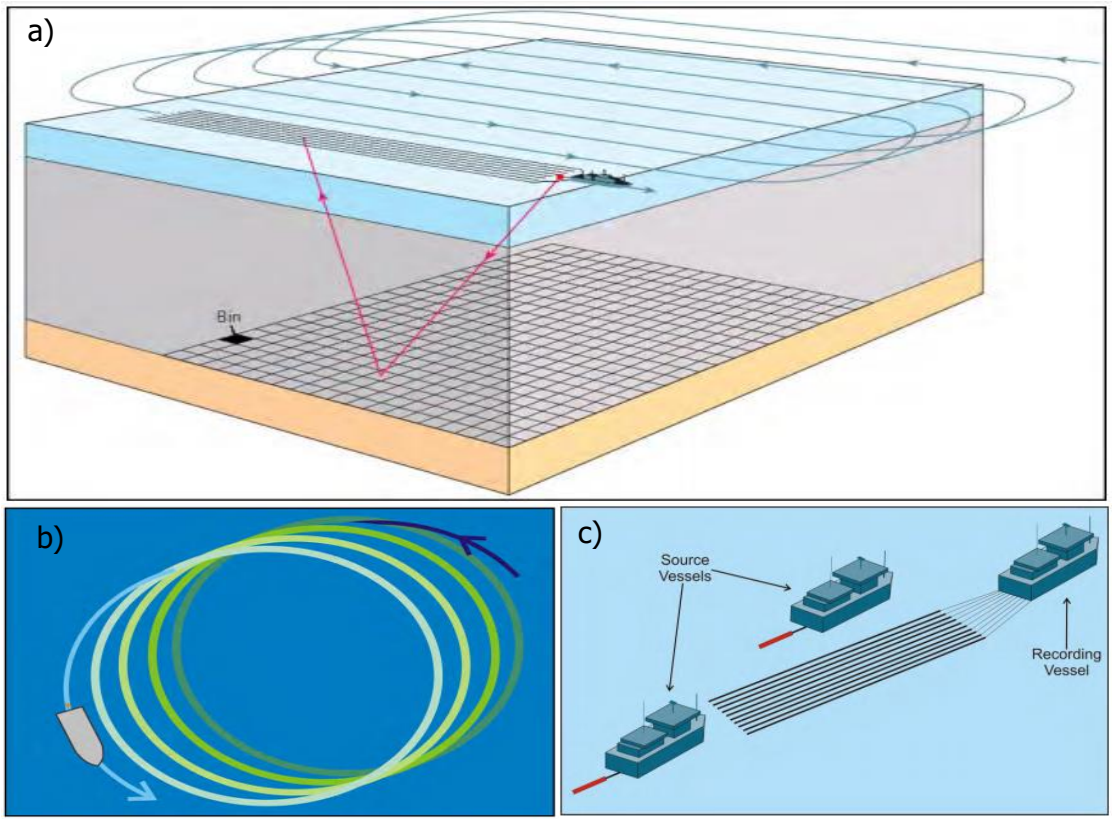

Figure 3.10 - Schematic images of different geometries to 3D seismic acquisition on sea. A) The basic 3D Acquisition, this is the most traditional way (Buia et al., 2008). B) The Coil shooting acquisition technique (Buia et al., 2008). C) The Wide-azimuth survey (Buia et al. 2008).

3.3. Basic Seismic Data Processing Flow

The typical seismic processing flows are implemented to increase the seismic vertical resolution, improve the signal-to-noise ratio of the data and to display the seismic events in their correct spatial position (Yilmaz, 2001a; McQuillin et al., 1984; Kearey et al., 1991). According to Yilmaz (2001a), there are three primary steps in multichannel processing seismic data:

Deconvolution: acts along the time axis to improve the vertical seismic resolution by compressing the wavelet. This step can be applied before and after stacking. Besides improving vertical resolution, it can also attenuate the receiver ghosts and seabed multiple reflections.

Stacking**:** it is also a process of compression. The seismic traces from each CMP gather are reduced to an only one trace at zero offset, first by applying normal moveout correction to traces from each CMP gather, then by summing them along the offset axis. The result is a stacked section. This step improves also the signal/noise ratio, as noise is random and signal is coherent, when traces are summed the signal usually get stronger and noises are annulled.

Migration: migration commonly is applied to stacked data in conventional processing. It is a process that collapses diffractions and maps dipping events on a stacked section to their supposedly true subsurface locations. In this respect, migration is a spatial deconvolution process that improves spatial resolution.

Besides those primary processes, there are other processing techniques that can be considered secondary, they help improve the effectiveness of the primary processes. For example, dip filtering may need to be applied before deconvolution to remove coherent noise. Wide band-pass filtering also may be needed to remove very low and high-frequency noise, correction for geometric spreading before deconvolution to compensate for the loss of amplitude caused by wave front divergence. Velocity analysis, which is an essential step for stacking, is improved by multiple attenuation and residual statics corrections.

A common simple processing flow for multichannel seismic data is composed of a pre-processing stage with demultiplexing, trace editing, amplitude and geometry corrections, and it is followed by a processing sequence which normally includes: deconvolution, CMP sorting, velocity analysis, normal moveout correction, CMP stack and migration (Yilmaz, 2001a).

In demultiplexing step the data are converted to a convenient format that is used throughout processing. This format is determined by the type of processing system and the individual company. A common format used in the seismic industry for data exchange is SEG-Y, established by the Society of Exploration Geophysicists.

Trace editing consists on the correction or removing of noise or polarity reversed traces. The marine data are most of the times contaminated with very low frequency noise due to swell and movements of the streamers. This noise can be easily removed with the application of lowcut filters. However, if these effects are still observed in some traces, even after applying the filter, the common practice is to delete them, as otherwise they will decrease the signal-to-noise ratio of the seismic data (Yilmaz, 2001a).

Following the demultiplexing and trace edit steps, amplitude adjustments are performed in order to correct the amplitude decay with time due to spherical divergence and energy dissipation in the Earth. The spherical divergence correction is a spatially averaged velocity function which is applied to compensate the effects of spherical wave front divergence. Additionally, a gain function is sometimes used to compensate for attenuation losses. In the end of the pre-processing stage it is done the geometry assignment, where the seismic data is adjusted with the acquisition geometry used in the field, the data is corrected for the position of shots and receivers and the true position are stored on trace headers. Many types of processing

problems arise at later stages due to the wrong setting up of the field geometry, and as a result the stacked profiles can be severely degraded (Yilmaz, 2001a).

Once pre-processing stage is finished, the main processing steps start with deconvolution that aims to improve the vertical resolution by compressing the source wavelet. Deconvolution is the inverse filtering technique used to compress source waveform, often seen on marine data, into a spike (unit-impulse function), as closest as possible. Ghosts, seabed multiples, and near surface reverberations can often be attenuated through deconvolution approaches. Many deconvolution techniques use the autocorrelation of the trace to design an inverse operator that removes undesirable and predictable energy (Dobrin and Savit, 1988). As can be seen in Figure 3.11, there are two main classes of multiples: long-path and short-path multiples (Sheriff and Geldart, 1995). A long-path multiple is one whose travel path is long compared with primary reflections (e.g. seabed multiples). A short-path multiple arrives soon after the associated primary reflection and can interfere with the original event, these are also known as ghosts. Near-surface multiples and ghosts are short-path multiples, originated by the deep tow of the seismic source/receivers producing a high amplitude pulse of negative polarity.

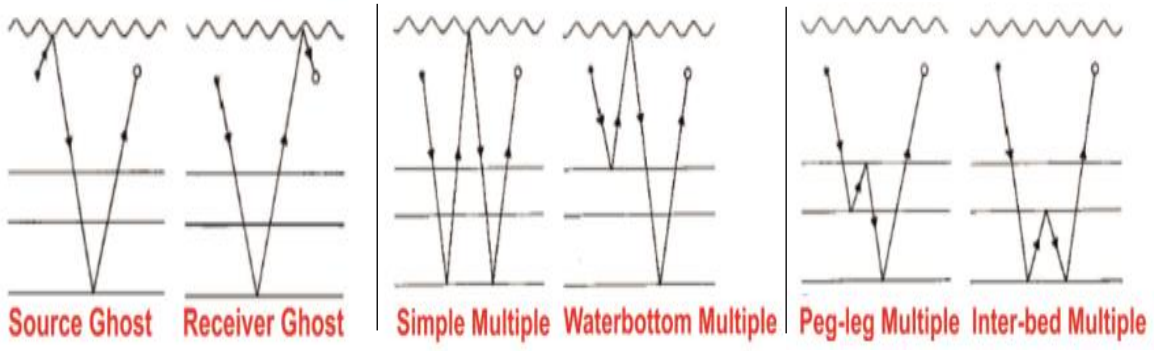

Figure 3.11 - Ray paths of some common multiple families (modified from Hatton et al., 1986, in Ribeiro, 2011).

The geometry of acquisition is set in a way that a group of traces recorded at different offsets for different shots contains reflections from a common midpoint (CMP) on the same reflector (Figure 3.12). A CMP is a point at the surface located at half-offset between the source and the receiver that is common to several source-receiver pairs. CMP gather is formed by all the traces from the source-receiver pairs that correspond to the same common reflection points. The fold refers to the number of traces in the CMP gather that can be summed.

Velocity analysis is performed on selected CMP gathers or group of gathers also known as Super Gathers. The output from the velocity analysis is a table of numbers as a function of velocity versus two-way zero-offset time. At this step, for each reflection hyperbolae in the CMP Gathers, velocity that best fits are determined. This velocity is known as root mean square velocity

(RMS velocity) and it is the velocity that provide a good stack when applied in the normal moveout correction (Stacking Velocity).

The velocity model is then used to correct the normal moveout (NMO) of the CMP gathers. The NMO is a correction of time delay due to offset, assuming horizontal interfaces. This correction removes the source-receiver offset effect in a non-dipping seismic reflector, considering that the reflection travel-time follows a hyperbolic trajectory. After this, most hyperbolic event will be horizontal allowing a good stack (Figure 3.12).

The common midpoint stack is the data-compression technique generally used. After a detailed velocity analysis and after the NMO corrections, the seismic traces in each CMP gather are summed to form a stacked trace at each midpoint location – CMP stacking (Figure 3.12). This process will increase the signal-to-noise ratio, will also attenuates noise such as multiples, because reflected signal and coherent noise usually have different stacking velocities (Yilmaz, 2001a).

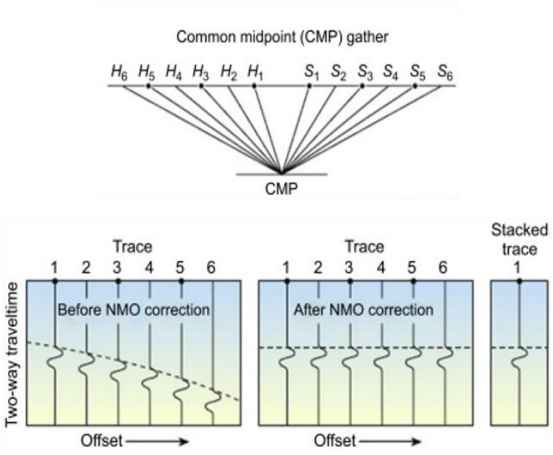

Figure 3.12 - Schematic images of CMP gather, before and after NMO correction, and stacked trace. (from https://www.sciencedirect.com/topics/engineering/imaging-depth).

Finally, a velocity model is used to migrate the stacked section. The post-stack seismic section is a normal incidence section. When the geology is extremely complex, the interfaces between the layers are slanted and irregular, and there are discontinuities, diffractions will appear in the seismic sections as hyperbolic events and the reflectors will not be in their correct positions. The migration process will move the dipping events into their supposedly true subsurface positions, will collapse the diffractions, will increase the spatial resolution and corrects amplitudes for geometric focusing effects and spatial smearing (Dobrin and Savit, 1988; Yilmaz, 2001a) making the seismic section more similar to actual geology. This process can be applied before the stack (pre-stack migration) or after this (post-stack migration). An extra step is necessary for the 3D processing, this step is the 3D Regularization and its purpose is to make uniform distribution of offsets by interpolating offset bin volumes, creating a seismic block itself.

3.4. New Ultra-High-Resolution 3D Marine Seismic System

Monrigal et al (2017) presented a new ultra-high-resolution 3D marine seismic system with sufficient resolution for the very detailed information required by geotechnical engineers for the design and positioning of the turbine foundations in offshore wind farms (Figure 3.13). This system uses frequency ranges up 2.5 kHz and 1-m bin size, and was designed taking into account all the elements needed to achieve imaging of the subsurface with vertical resolution of less than 50 cm, as follows:

- Short receiver spacing to match the source frequency and ensure adequate spatial sampling;
- High accuracy positioning in all three directions for both source and receivers;
- Adequate streamer length for velocity discrimination for the depth of imaging;
- A rapidly firing source and a stable, repeatable signature to ensure homogeneous data quality over the survey area;
- Shallow towing depth of the source to preserve the high frequency content;
- Sloping streamer to reduce the receiver ghost effect and ensure a full broadband spectrum.

This system is based on a multi-tip sparker source utilising negative discharge technology, guaranteeing a stable and highly repeatable impulsive source. It comprises two sources firing in flip-flop mode to optimise inline and crossline coverage. Its broad bandwidth (0.1–3.5 kHz) allows the imaging of the subsurface with metre-scale horizontal and decimetre vertical resolution, whilst offering good penetration in shallow marine sediments.

The streamers were specifically built with short, but variable, channel spacing (e.g. 8 channels at 1.0 m, 8 at 2.0 m, and 8 at 4.0 m). This configuration ensures adequate spatial sampling on the near traces whilst providing sufficient move-out on the far traces to derive velocity information for shallow depth imaging. A slanted streamer technology, which is a tilted streamer where the depth increases as offsets increases and without sag in the middle, was adopted to improve the resilience of the system to noise and ensures a broadband seismic response, allowing high-quality acquisition in conditions where conventional UHR surveying would have to be interrupted. Generally, the system uses four streamers which are towed with an inline separation of 4.0 m, resulting in a 14-m swath with a mid-point line separation of 2.0 m.

In order to determine source and receiver positions with high accuracy the system uses pairs of Differential GPS receivers located on both sources and on the buoys at the head/tail of each streamer. These modules are designed to operate in Precise Point Positioning (PPP) mode

when working in areas covered by a satellite-based augmentation system (SBAS), thus providing decimetre accuracy, allowing to compute de centre of the buoys and source, then the positions of each streamer, and hence for any receiver or channel.

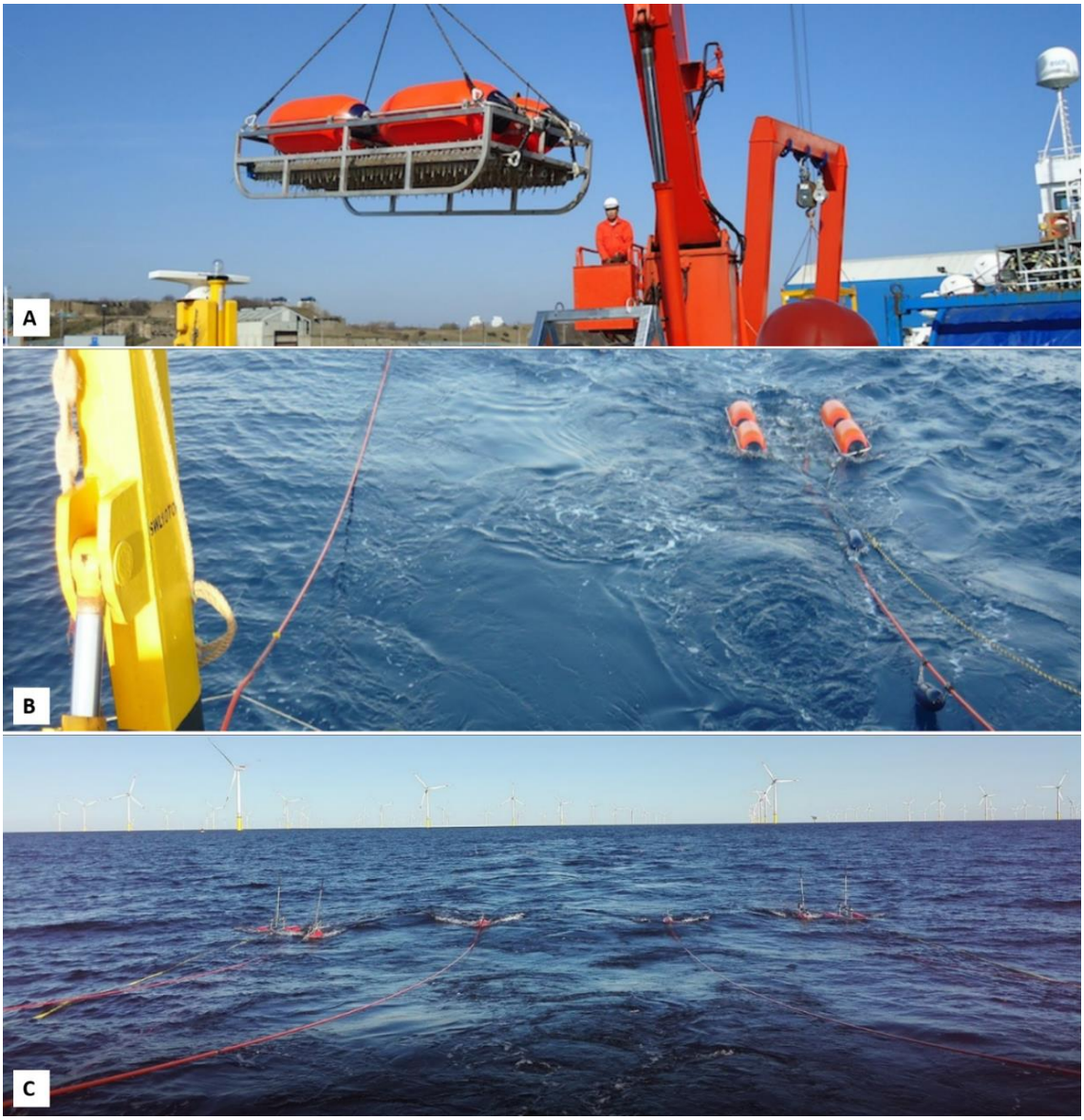

Figure 3.13 - Ultra High Resolution Seismic equipment by Geomarine Survey System. A) and B) Geo-Sparker source deployment. C) ultra-high-resolution 3D marine seismic system with 2 Geo-Sparker, 4 UHR streamer and DGPS antennas on the buoys. (Source https://www.geomarinesurveysystems.com).

A full processing sequence for this type of data was developed at Geosurveys, aiming at maintaining the broadband spectrum and retain or shorten the already very short (2–3 ms) seismic wavelet (Duarte, Wardell and Monrigal 2017). The main steps of this advanced processing for UHRS 3D shallow marine seismic surveys are: attenuating noise, extracting the source signature, determining the relative positions of the spread, geometry assignment, tide corrections, velocity analyses, stack, post-stack residual receiver deghosting, multiple suppression and migration.

3.5. Interpretation of 3D Seismic Data

The interpretation of a 3D seismic dataset is done visually and interactively, in powerful workstations, on vertical seismic sections, in inline and crossline directions, and in horizontal seismic sections, called horizontal time slices. The traditional seismic interpretation involves picking a reflection time surface associated with a layer boundary from a time migrated volume of data or a reflector from a depth migrated volume of data to determine the structure map for that layer boundary. Nowadays, the way seismic interpretation is done is a result of the power of 3D visualization of image volumes, velocity volumes, and attribute volumes, such as those associated with AVO analysis and acoustic impedance estimation. Now, this also involves manipulation of amplitudes contained in the data volumes to derive information about the depositional environment, depositional sequence boundaries, and the internal constitution of the sequence units themselves (Yilmaz, 2001a).

If that large amount of information is well correlated it can create a reliable geological model (Yilmaz, 2001a). The interpreter must combine the various components of the dataset (e.g. 3D seismic cube, 2D lines and well log data) in order to recognize seismic patterns that can give clues depositional environments and the structural geology of the area. If instead the seismic interpretation is not consistent, the seismic data itself is useless (Robinson et al., 1986).

UHRS, due its higher resolution, allows the interpretation of small objects such boulders, an important step to decrease the probability of failed foundation implementations for offshore geotechnical engineering. A careful interpretation of geological features in the seismic data is therefore the key for the success in high resolution seismic studies for foundations of offshore structures (Correia, 2017)

Chapter 4:

Problem Setup, Data and Methodology

4.1. Problem Setup

The main goal of this work was to develop methodologies to identify positioning errors and diagnose them onboard, in a short interval of time, in order to determine their categories and how they can affect the data. Besides this, it is intended to obtain enough information to decide which is the best rejection criteria to be applied when needed. For such purpose it is first necessary to establish a criterion to assess the quality of the data, in order to determine if it can be accepted or must be rejected.

Obtaining positioning data with high accuracy is extremely important for the kind of UHRS surveys that *Geosurveys* has been conducting. The study and geological characterization of near-surface sediment and others geological structures at shallow marine environment for geotechnical work, such as determining the positions of foundations for turbine implementations in Offshore Wind Farm, require very high seismic resolution. Horizontal seismic resolution can be strongly controlled by the quality of the positioning data because these values are used to calculate the positions of the seismic traces. Wrong positioning data will affect the offset calculation and the position of the reflection points causing an increase of difference between the seismic section and the actual geology. On the other hand, it makes it more difficult to accurately locate boulders and identify other risks or in-depth hazards, compromising the ability to obtain good information to optimize the installation of wind turbines, which in the end may result in increased operation costs.

There are many ways to assess the quality of the data provided by the positioning system used during data acquisition. Once the velocity of sound propagation in the water is determined (measured by a sound velocity profiling system), it is possible to convert the direct arrivals times into offsets and compare them with the offsets computed using the positioning data. The differences between these offsets can be used to evaluate the quality of the positioning data given by DGPS antennas.

There are different causes behind the navigation issues. The working mode of GPS antennas (standard or with differential corrections) in the seismic spread affects the accuracy of the positioning data provided by the system. Therefore, the most important problems which often

affect the data are caused by poor antennas performances, either when it stops working or stops providing coordinates. These problems can be easily detected in the NMEA files.

The working mode of the GPS antennas can be obtained by consulting the NMEA sentences, which include a field with this information. If one antenna stops working, the number of NMEA sentences will be smaller than the equivalent in other antennas. If the antenna is still working and in the meanwhile no coordinate information is being provided, the number of sentences for the different antennas in the seismic spread will be the same, but with null coordinates or other unrealistic values. Another important point is the number of satellites available which impact the accuracy of the coordinates provided. The problem becomes more critical and difficult to solve when the tail buoy antennas (DGPS antennas on the tail buoy of the streamer) do not provide any information, in contrast to what happens with source and lead buoys antennas (DGPS antennas on the front buoy streamer and source buoy) which is immediately evident with absurd offset values for channels closer to the seismic source. The acquisition system determines the channel positions from the defined geometry, and the streamer azimuth that is calculated from the coordinates provided by the lead and tail buoy antennas. Thus, when a tail buoy antenna stops working, a wrong azimuth is calculated and consequently the receiver positions will be wrong. In these cases, there is no control over the calculated azimuths, it is not easy to predict the system behaviour, and therefore the coordinates that the system assigns to the tail buoy antenna for azimuth calculation are wrong.

If it was possible to take control of azimuth calculation even when some tail buoy antenna does not provide any information, a good assessment criterion would be the comparison between streamers' azimuth when it is working properly and when a tail buoy antenna does not work. For example, if a streamer presents an azimuth value similar to the expected azimuth when tail buoy is not working, this part of the dataset could be rejected or corrected using unaffected streamer azimuth. Nevertheless, the best and easiest way that was found so far for this kind of analysis is the comparison between direct arrivals and offset computed by positioning data from GPS antenna of the acquisition system. This analysis cannot be done in real time, at present, because it includes direct arrivals picking for comparison. Therefore, the methodology presented here is to be performed offline.

Next, after a description of the dataset used for this work, we introduce the processing methodology of the original seismic data to obtain the Standard Stack, and then describe the analysis and evaluation of the quality of positioning data, identifying and diagnosing positioning errors and their categories. In the following chapter, the different types of errors are summarized and the implementation of criteria to reject data affected by this kind of problem is discussed.

Finally, an assessment after applying rejection criteria is done to verify the changes and its effects on the seismic volume in order to know how this problem affects de final stack section.

4.2. The Dataset: Seismic Acquisition Parameters and Processing Sequence

4.2.1. Data Acquisition

As mentioned before, the dataset used for this work consisted on a 3D seismic volume with 600 inlines and 3800 Crosslines with a CDP bin interval of 0.5 m, from a 3D UHRS data block named BLK2, that belongs to the NAPOLI 3D UHRS survey carried out in the Tyrrhenian Sea (Bay of Naples). These data were acquired and quality controlled by *Geomarine* and *Geosurveys* between 8th of October and 10th of October 2017. The multi-channel seismic spread consisted of:

(a) Two Geo-Source 400 tips FW sparkers towed at 40 cm deep firing at 800 Joules with 0.6 s of interval;

(b) Two Geo-Spark 2000XF power supplies;

(c) Four Geo-Sense Ultra High-Resolution 48 channels streamer towed in a slant with variable group interval: 1 m between channel 1 and 24 and 2 m between channels 25 and 48;

(d) Six multi-traces 48 channels systems, connected to the streamers (48 channels section) and to the reference hydrophones;

(e) Ten DGNSS antenna pairs for the positioning of front and tail buoys of the streamer and the source. The navigation and positioning were carried out with this arrangement to allow the positioning control of the entire seismic spread. Time trigger was supplied to the seismic spread using the Survey DGPS positioning system. This arrangement allows to control the positioning of the entire seismic spread.

The streamers were balanced for a slanted configuration with the head at 40 cm below sea surface and the tail at approximately 1 m. The Streamer's slant configuration allows wider signal frequency recovery and better ghost removal, as the deeper receivers with increasing offset will result in an incoherent stack of the receiver surface ghost. Tests were carried during the sea trials to assess the quality of the streamer balancing in order to get the desired streamer configuration (expected front and tail depth, without sag in the middle). The balancing was achieved using lead strips tapped along the streamer. Figure 4.1 shows the 3D acquisition geometry adopted for the NAPOLI 3D UHRS survey.

4.2.2. Acquisition Parameters

The streamers deployed in this survey have a total of 48 channels. The first 24 channels are spaced 1 m apart and the last 24 channels are spaced 2 m apart, making for a total streamer active length of 71 m. The shooting interval was performed in time – every 0.6s. Table 4.1 shows the general acquisition parameters.

Table 4.1 - Acquisition parameters of the 3D Napoli Survey

Sources	**2x Geo-Source 400 tips LW**
Sources Towing Depth	0.4 m
Shooting interval	0.6 s
Operating Power	800 J
Power Supply	2x Geo-Spark 2000FX
Multichannel Streamer	**4x Geo-Sense Ultra High-Resolution 48 channels**
Streamer Depth	0.4 - 1 m
Group Interval	Variable (ch1-ch24: 1m; ch25-ch48: 2m)
Group Active Length	71m
Recorder	**6XMultitrace48-Geomarine Survey systems**
Sample Interval	0.1 ms
Record Length	300 ms
Format	SEG-Y

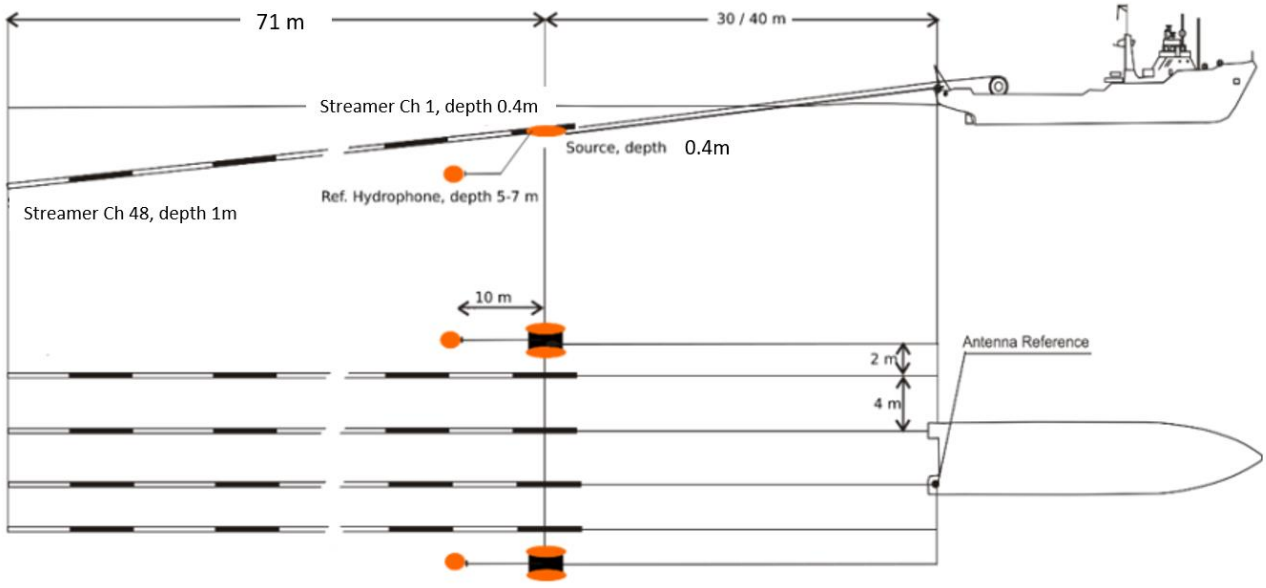

Figure 4.1 - Acquisition geometry scheme (adopted from Geosurveys reports).

4.2.3. Seismic Data Quality Control

The offshore QC was performed on this dataset to assess the data quality and seismic coverage, and guarantee the minimum data quality necessary to produce the final expected results. When the data did not match the agreed specifications, it was flagged and rejected. The QC was performed according to the workflow presented in figure 4.2 and the steps are described below

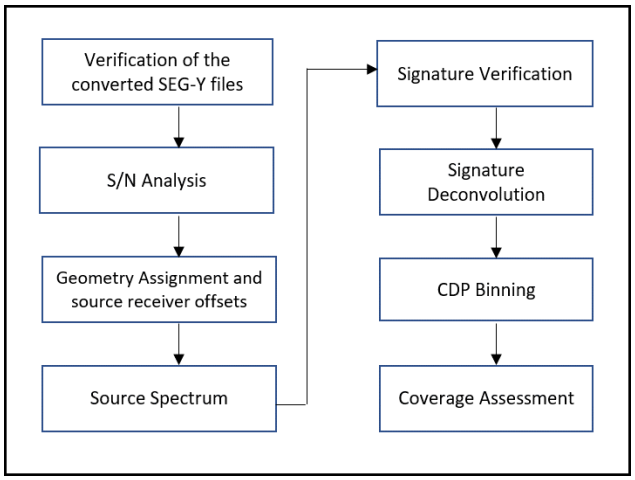

Figure 4.2 - Offshore seismic data quality control workflow (Geosurveys).

1. **<u>Verification of the converted SEGY files</u>**

After acquiring a seismic swath, the multi-trace files were converted into SEGY format. This quality control step consisted in verifying if:

1. The conversion was done properly, without corrupting the files;
2. The number of FFIDs was correct;
3. There were “bad shots”;
4. The data was considered good for processing, marginal or not good for processing.

All the data that was considered not good for processing was rejected, and then the rejected swaths were re-acquired.

2. **<u>Signal and noise analysis</u>**

The acquired seismic data was inspected in the shot and trace domains to assess noise types and then to do attenuation with adequate filters. The most significant types of noise recognized on the data were the following:

- Burst noise due to streamer surfacing, observed in the lines acquired in choppier seas, mainly in the near channels. Noise attenuation was done with adequate frequency bandpass filters;

- Directional noise – related with passing vessels. F-K filters were applied;
- Streamer tugging (front and tail tugging) – also removed, yielding better S/N ratio.

3. **Geometry assignment and source receiver offsets**

The *Geosuite Naviworks* software was used to determine the node positions for the seismic volume. The exact offsets from the antennas to the nearest nodes were measured offshore. *Naviworks* imports the multi-trace data logs and Wi-fi DGPS inputs from each source, and the streamers lead and tail buoy. This software calculates the position for all nodes in the system for every shot at the time of the triggering.

The seismic geometry headers were filled with the source and receiver positions from the *Naviworks* output files. The source and receiver positioning accuracy were checked by comparing the offsets calculated by the multi-trace using the source and receiver positions with direct arrival times. The offsets calculated from the DGPS derived source and receiver positions were converted to time using the measured sound velocity in the water (the sound velocity was measured by the mini sound velocity probe of the multibeam).

4. **Source spectra**

In order to assess the correct behaviour of the sources, a spectral display for all of the sources was carried out in all acquired lines.

5. **Signature verification and deconvolution**

The spectral response of the data was analysed using a reference wavelet derived from the direct arrival measured in the beginning of the survey, to assess the recorded signal stability.

6. **CDP Binning**

A CDP binning grid was created to assign In lines and Cross Lines values to the volume. A 2 m bin was used on the offshore QC processing to assess the coverage on the entire survey area, then. a 0.5 m bin was recalculated in the office.

7. **Coverage Assessment**

After seismic data quality control and analysis, geometry assignment (CDP binning of 2 m x 2 m) and bad shots removal, the seismic volume coverage was calculated, in order to verify if there were data gaps on the critical areas.

4.2.4. Seismic Data Processing

The 3D seismic processing workflow is basically divided into two stages, which are swath and volume processing. The main goals of the swath processing stage are to apply static

corrections and denoise; all the swaths then are merged at the end in order to create the seismic volume and to start the second stage.

This work presents only the volume processing stage since the swath processing was done previously. The seismic volume processed in this thesis is composed by 600 inlines and 3800 crosslines, the results of the processing steps showed in this thesis correspond to a small part of the dataset between In Lines 400 and 600, and Cross Lines 2000 and 2200 (100 m^2 area). However, some results of the processing and methodology developed are shown in chapter 5 for a larger area.

The main goal of the seismic volume processing was to create a migrated seismic section for further geological interpretation. The processing flow carried out consisted mainly on: 3D Regularization, Normal Moveout correction and CDP ensemble stacking using the velocity model obtained from velocity analysis, post-stack deconvolution in order to attenuate receiver ghost, interpolation, F-X-Y deconvolution, spatial filtering and migration. Figure 4.3 shows a summary of the main processing steps applied over the seismic volume used in this work.

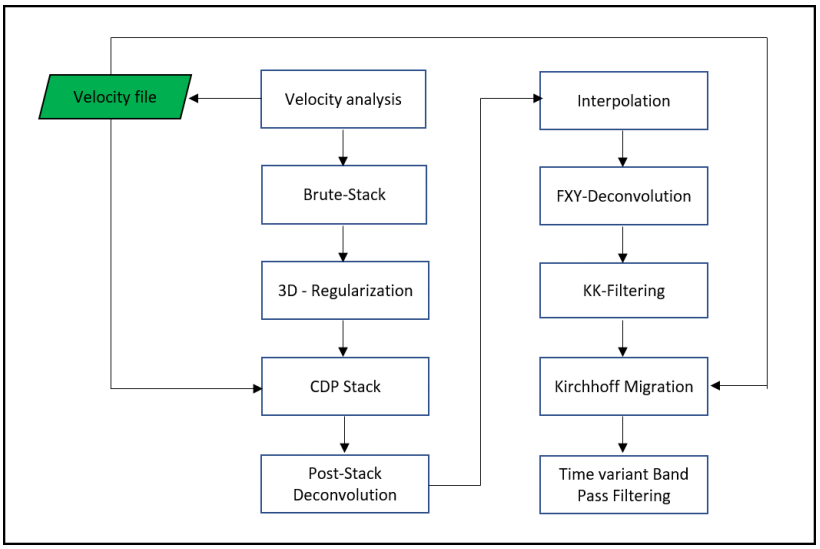

Figure 4.3 - Seismic data processing workflow. In green, velocity file from velocity analysis, in white boxes with blue borders, the processing steps.

1. Brute stack

In order to have an overview about the data to process, a brute stack was firstly obtained with a constant velocity (1.52 m/ms) (Figure 4.4). An area from the seismic volume was selected to perform the standard stack and other tests after applying the rejection criteria. In the brute stack section in figure 4.4, normal faults from the extensional basin mentioned in chapter 2 are observed. More detail of this extensional system is shown from figure 5.5 to figure 5.8.

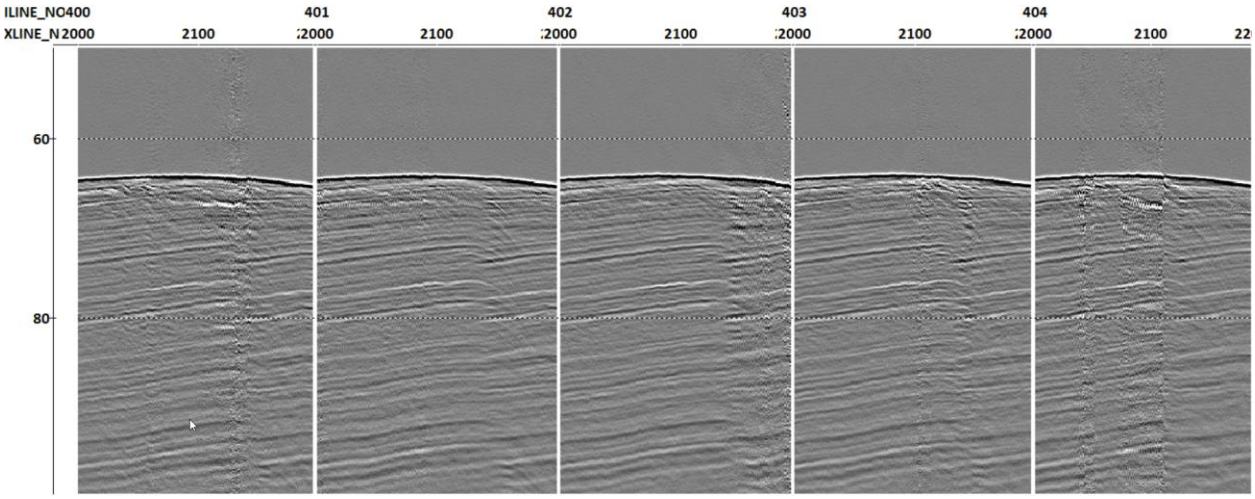

Figure 4.4 – Brute stack section with constant velocity (1.52m/ms) showing an overview of the seismic volume to be processed. Vertical scale in ms.

2. 3D Regularization

The goal of 3D regularization is to make a regular distribution of offsets by interpolation. Regularization fills the seismic volume gaps and is done using an F-Kx-Ky reconstruction that is accurate even for dipping seismic events.

The procedure works by spatial/temporal block overlaps. Then, for each block a Fourier coefficient is determined in a regular grid that will match the irregularly spaced input data by inverse Fourier transform. The coefficients are then transferred back to the X-Y-T domain through a direct Fourier Transform. In order to emphasize the benefits of this step, figures 4.5 and 4.6 show respectively the data before and after regularization.

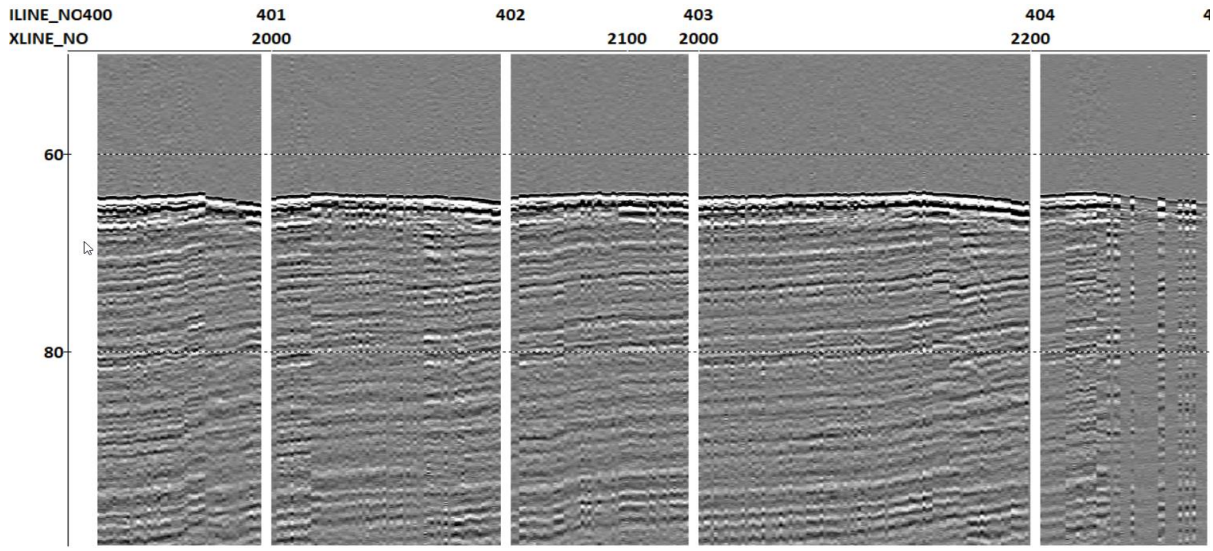

Figure 4.5 - Seismic volume showing 5 inline windows. Before 3D regularization. Vertical scale in ms.

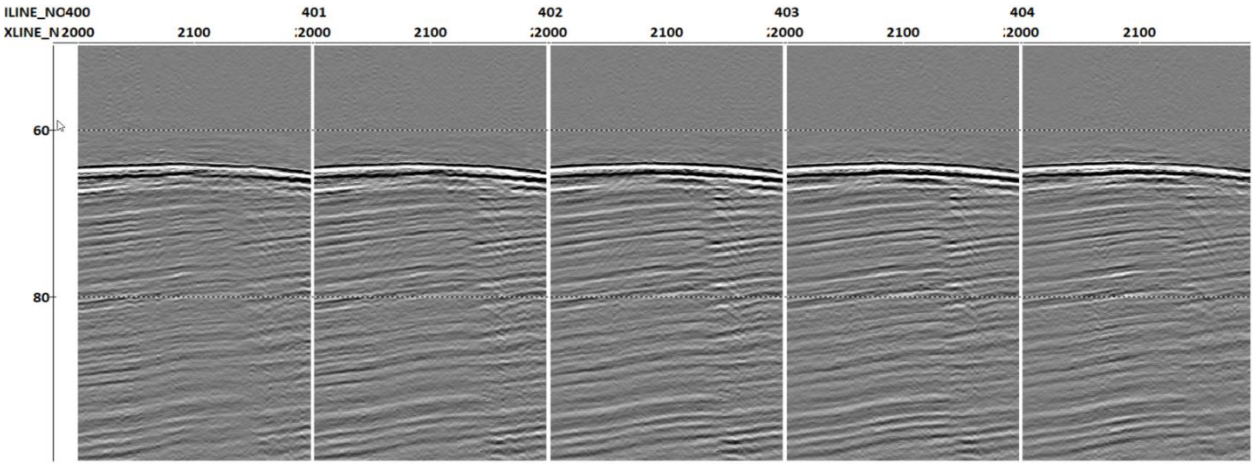

Figure 4.6 - Seismic volume after 3D regularization showing a uniform trace distribution. Vertical scale in ms.

Both figures 4.5 and 4.6 present the same interval of inlines and crosslines. It would be expected to have a total of 200 seismic trace for each inline window, this fact is not verified before 3D regularization in figure 4.5 which present only 317 seismic traces for the 5 windows. These few traces can be due to gaps in the coverage and some bad shots killed. After regularization, this problem was solved as it was seen in figure 4.6 which shows a regular trace density, with 1000 traces for the 5 windows.

3. CDP Stack

After regularization, a CDP stack was done to increase the signal to noise ratio and attenuate the receiver ghost (Figure 4.7), which is possible due to slant streamer acquisition geometry.

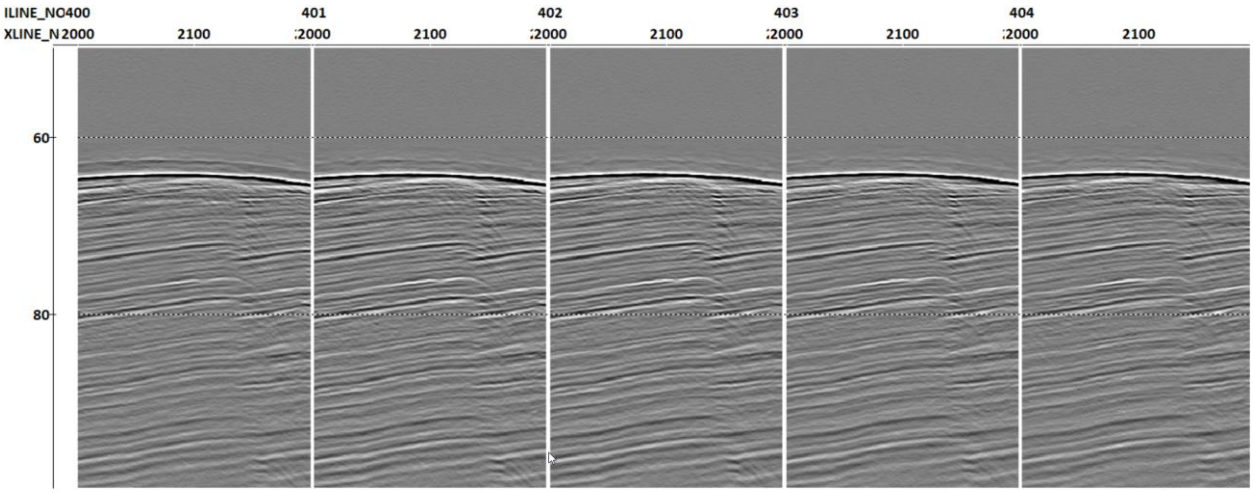

Figure 4.7 - CDP stack after regularization using velocity file from the velocity analysis. Vertical scale in ms.

To show the effect of 3D regularization, figure 4.8 allows checking if the improved result in figure 4.7, in comparison with brute stack section in figure 4.4, is mainly an effect of the regularization or of including the velocity file from the velocity analysis. The figure 4.8a shows a CDP stack after regularization using constant velocity (1.52 m/ms) and figure 4.8b shows CDP stack with the same velocity file as figure 4.7. Using this comparison, it becomes clear that the data quality achieved after the CDP stack is mainly a result of the regularization, since there was no significant difference between using a constant velocity or a velocity file. On the other hand, the stack sections without regularization, using a velocity file, are also very close to the brute stack because there is no very significant velocity variation in this area. The brute stack shown in figure 4.4 presents also some gaps in the coverage and bad shots; for these reasons, the trace density is not as regular as in the figure 4.6 showing only 970 seismic traces for the 5 inline windows and low data quality.

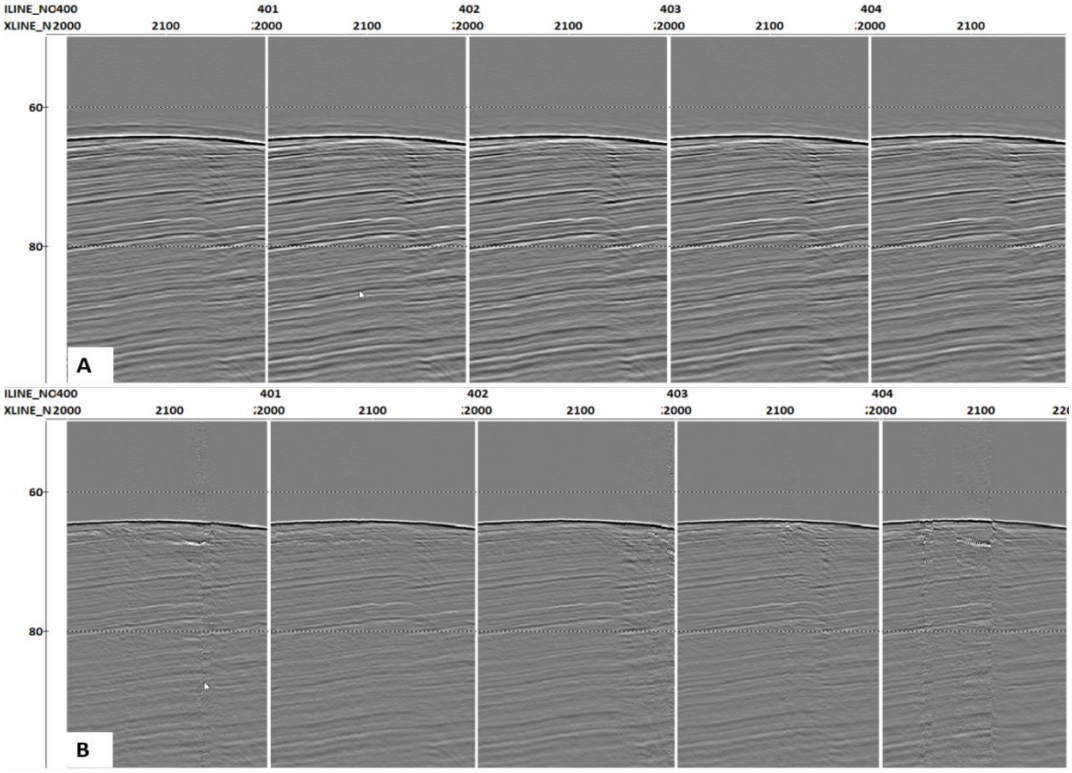

Figure 4.8 - A) CDP stack sections after 3D regularization with constant velocity. B) CDP stack using velocity file from velocity analysis, without 3D regularization. Vertical scale in ms.

4. Post Stack Deconvolution

Once the source signature was extracted, post-stack deconvolution was applied in order to remove the receiver ghost (Figure 4.9). This step aims also to compress the wavelet and increase the vertical seismic resolution, making it possible to distinguish different reflections which are very close in depth.

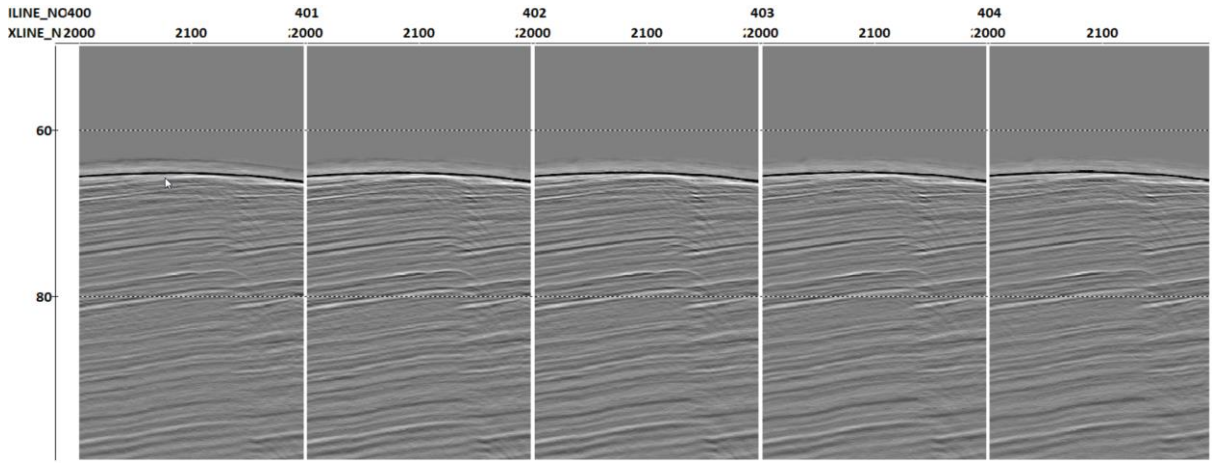

Figure 4.9 - Increasing of vertical seismic resolution after post-stack deconvolution. Vertical scale in ms.

5. Interpolation

This step was applied to infill residual data gaps. This is a pre-requirement for F-X-Y deconvolution and spatial filtering.

6. FXY Deconvolution

This processing step aims to eliminate noise in the three directions or domains of the seismic volume, time frequency, and spatial frequency at X and Y. This algorithm uses a predictive Wiener filter that is calculated for a spatial series obtained at each frequency through a Fourier transform. Each predictive filter is spatially applied considering a given grid. This F-X-Y domain predictive filter increases the coherence of the time domain events and eliminates the noise associated with these events that would be impossible to eliminate only by frequency domain filtering. The results of this processing step are showed in Figure 4.10.

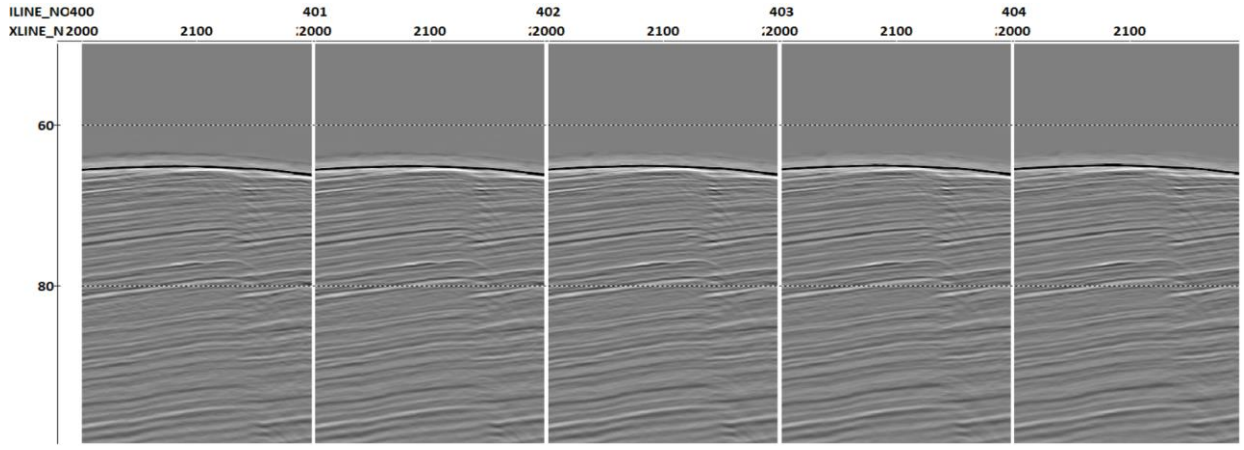

Figure 4.10 - Seismic volume after FXY deconvolution to eliminate noise in the three directions. Vertical scale in ms.

7. KK filtering

A filtering in K-K domain was applied over the time-slices to increase the seismic volume signal coherence (Figure 4.11). After this, noises in figure 4.11a with inline orientation were attenuated and the signal coherence improved (figure 4.11b).

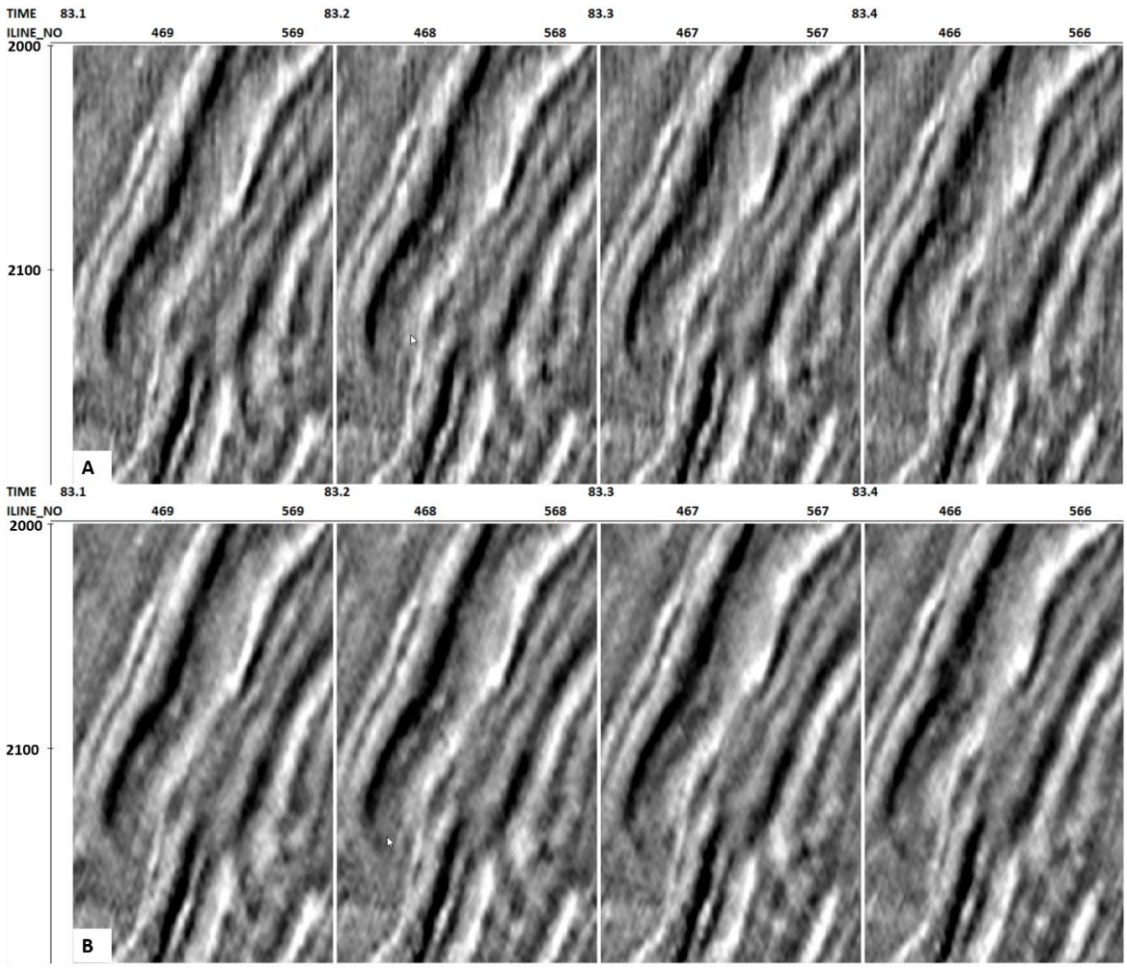

Figure 4.11 - Time slices. A) Before KK filtering, time slices showing some noise along inline direction. B) After KK filtering, the noises were attenuated resulting in improvement of the signal. Crossline number in vertical axis, inline number and time scale in horizontal axis.

8. 3D Kirchhoff Migration

Using the velocities from interactive velocity analysis, a 3D Kirchhoff Migration was performed in time (figure 4.12). The stack section is a normal incidence section (zero offset); as such, when the geology is very complex and when there are non-horizontal interfaces and discontinuities, diffractions will appear in the seismic sections as hyperbolae, masking the true geology, and the reflectors will not be in their true positions. Migration aims to collapse the energy of diffraction, eliminate hyperbolae, and place reflectors in their true positions, in order to

reconstruct the actual geology. As shown in figure 4.12, this step makes it much easier to identify the faults.

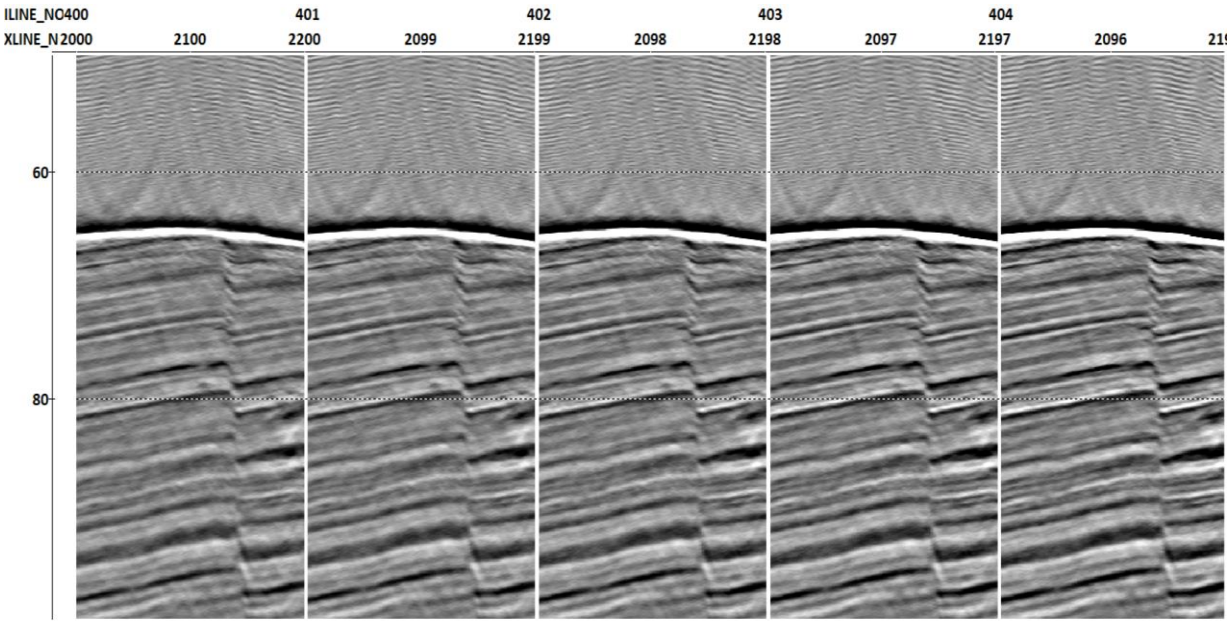

Figure 4.12 - Stack sections after 3D Kirchhoff Migration, showing a much clearer geology and much better fault imaging. Vertical scale in ms.

9. Time Variant Bandpass Filtering

After migration, a Time Variant Bandpass Filter (TVBPF) was applied to increase the signal to noise ratio. Figure 4.13 shows the result of the seismic volume processing after migration and TVBPF.

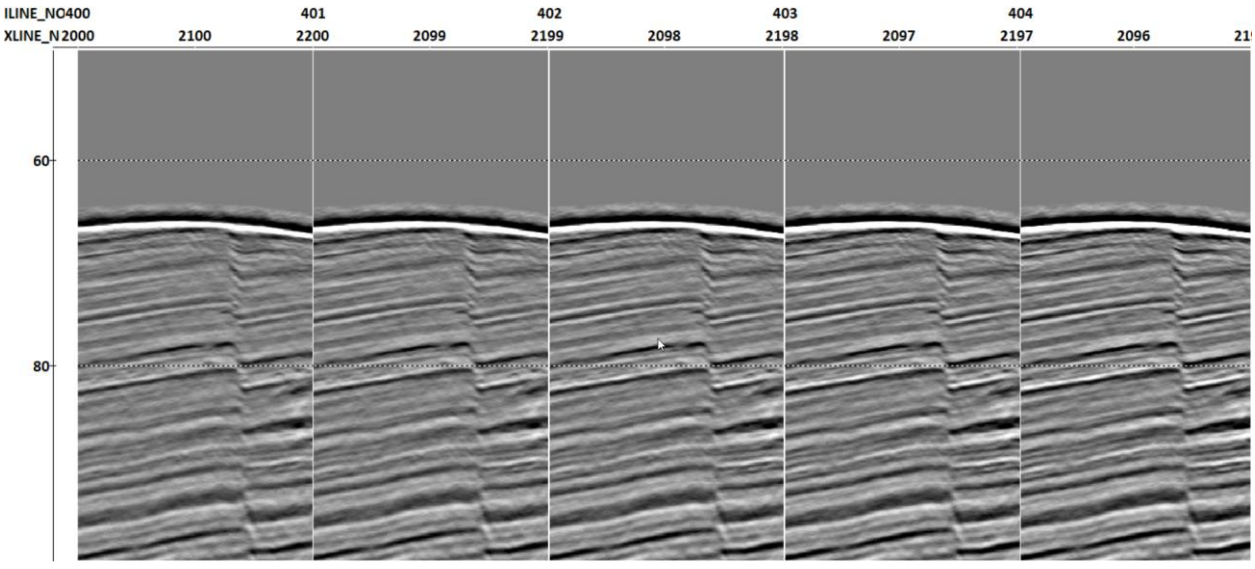

Figure 4.13 - Final result of the processing data after migration and time variant bandpass filter. Vertical scale in ms.

4.3. Navigation Quality Control

The actual offsets can be obtained from the direct arrival times. If the velocity of sound propagation in the water column is known (measured during the survey), it is possible to easily determine the offsets by the Equation 4.1, where $SVP_{shallow}$ (1530 m/s) is the sound velocity in shallow water measured by the mini sound velocity probe of the multibeam (the name assigned to this variable is a convention used by *Geosurveys*), and DA_{time} is the time of direct arrivals.

$$SVP_{Shallow}(m/s) = \frac{offset(m)}{DA_{time}(s)} \quad (4.1)$$

The offsets computed from the positioning data were then converted to time by dividing them by $SVP_{Shallow}$. These calculated times were compared with the direct arrival times, and significant differences in some areas of this seismic volume, which can be originated by positioning problems, were identified (Figure 4.14). After obtaining the actual offsets, the magnitude and polarity of positioning errors provided by the acquisition system can be determined by the difference with the actual offsets in distance or time. In this work, the errors were calculated in time using the Equation 4.2, where Error is the difference between actual offset and offset calculated with positioning data provided by DGPS antenna, which is the variable GPS_offset showed in the equation; the remaining variables were already defined in the previous equation (4.1).

$$Error = \frac{GPS\_Offset}{SVP\_Shallow} - DA_{time} \quad (4.2)$$

It is important to consider that from the previous equation several factors contribute to the error. As concerns the time of the direct arrivals, there are errors related to the picking and zero time. The offsets calculated with the positioning data have influence of the lead and tail buoy antenna, source antennas and geometry definition errors. Finally, there are errors in seismic wave propagation velocity measurement in the water column associated with the measuring device.

The roots of the positioning errors mentioned above compromise the positioning data provided by the acquisition system, leading to a decrease of the accuracy of seismic trace location. However, these factors create patterns that can be graphically detected allowing their control and reduction of the impacts on the acquired data.

The tail buoy antennas problem is a very common phenomenon and its detection is not so trivial. This has a big impact on the accuracy of the positions determined for all channels, especially the farthest, because it degrades the azimuth used to calculate the receiver positions along the streamers. The analysis of positioning problems in the last channels of each streamer gives clues about tail buoy antenna issues, since these will be the most affected channels.

Similarly, the first channel analysis provides information about lead buoy and source buoy antennas problems because this mainly affects near-offset calculations and this effect decreases as the distance increases.

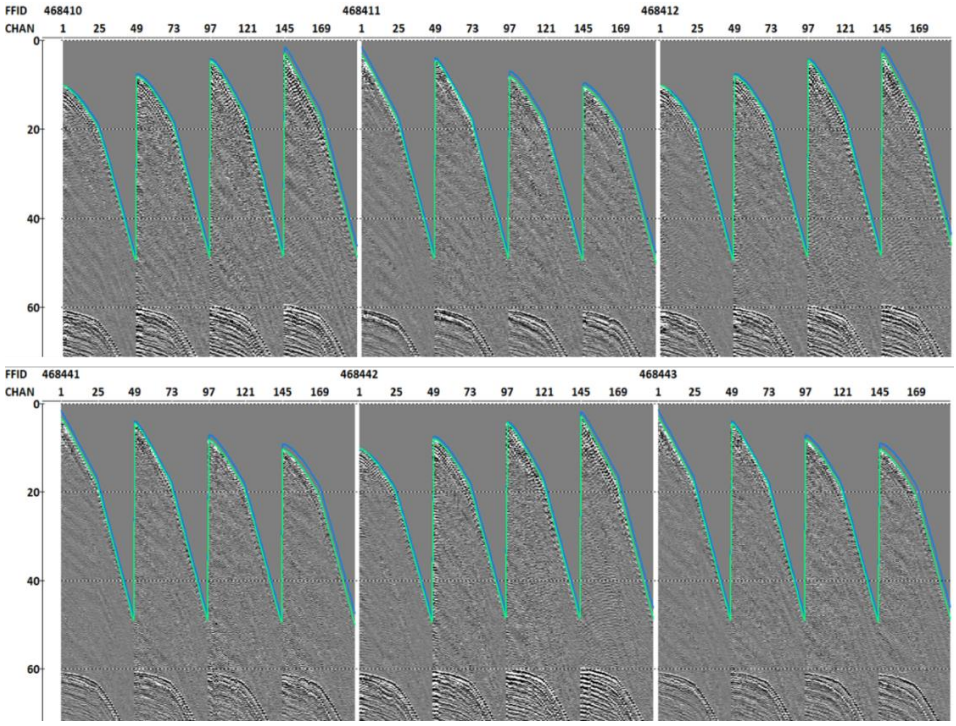

Figure 4.14 - Shot gather showing positioning problems detected due to the differences between direct arrival time (blue line) and estimated offset computed with GPS data and converted to time (green line). Vertical scale in ms.

In order to get an overview of the possible problems with streamer and source antennas, a univariate statistical analysis of the positioning error values of the first and last channels of each streamer for each source was performed (Table 4.2). The determined parameters allowed to detect anomalies in the distribution of the data, the polarity of the abnormal values and how often they appear in the data, and the variation interval of the most frequent values.

For all these cases, kurtosis reveals that it is a platykurtic curve (kurtosis <3), which means that there is a wide variation in the positioning error values, which is the expected behaviour for anomalous data. The data show a positive and negative asymmetric distribution indicating that the errors have different polarities for the different situations that will be analysed later. The magnitude of the error is indeed important for a quantitative analysis, but besides the absolute values of the errors, it is interesting to know the polarity because this can give clues to what is happening with the positioning data, making the diagnosis easier, which is the main objective of this work. Therefore, after a statistical analysis that confirms that these data are anomalous, it is then important to diagnose the errors to detect their causes and the most affected parts of the

data, in order to choose the most appropriate rejection criterion, if it is necessary to reject part of the data.

Table 4.2 - Basic univariate statistical analysis of the positioning error values of the first and last channel of each streamer and source.

Source 0								
Streamer	1		2		3		4	
Channel	1st	Last	1st	Last	1st	Last	1st	Last
Minimum	-1.6058	-1.4534	-1.4675	-2.2197	-1.8299	-1.7567	-1.6816	-2.7103
Maximum	0.4528	-0.2352	0.6252	-0.6407	0.6144	-0.5440	0.3244	-0.9622
Average	-0.7782	-0.8908	-0.5498	-1.5011	-0.7011	-1.0646	-0.7627	-1.7327
Median	-0.7877	-0.8994	-0.5333	-1.4965	-0.6342	-1.0662	-0.8186	-1.7082
Standard Deviation	0.3686	0.2862	0.3413	0.3197	0.4507	0.2366	0.3759	0.3553
Kurtosis	-0.0167	-0.7020	-0.2345	-0.1339	-0.3469	-0.1246	-0.3782	-0.6973
Asymetry	0.3563	0.2291	0.0665	-0.0336	-0.2060	-0.3329	0.3303	-0.2989
1st Quartile	-1.0251	-1.1384	-0.8070	-1.6812	-1.0270	-1.2162	-1.0174	-1.9949
3rd Quartile	-0.5587	-0.6992	-0.3085	-1.3202	-0.4007	-0.8844	-0.5010	-1.4261
Source 1								
Streamer	1		2		3		4	
Channel	1st	Last	1st	Last	1st	Last	1st	Last
Minimum	-1.0482	-1.6985	-1.3759	-2.4331	-1.7832	-1.7882	-2.1217	-2.7229
Maximum	0.8257	0.3164	0.7564	0.2455	0.9360	0.0399	0.4822	-0.2921
Average	-0.2551	-0.5969	-0.2628	-1.2353	-0.3293	-0.7953	-0.7134	-1.4441
Median	-0.2732	-0.5330	-0.2292	-1.2727	-0.3061	-0.7477	-0.6459	-1.2891
Standard Deviation	0.2884	0.3681	0.3567	0.5435	0.6065	0.4707	0.5706	0.6562
Kurtosis	-0.2571	0.0925	0.0373	0.2615	-0.7397	-0.8126	-1.0763	-1.3298
Asymetry	0.2255	-0.5102	-0.2678	0.3991	-0.0768	-0.3438	-0.1979	-0.3045
1st Quartile	-0.4652	-0.8475	-0.4869	-1.5124	-0.7547	-1.1682	-1.2067	-2.1240
3rd Quartile	-0.0422	-0.3462	-0.0195	-0.8909	0.1087	-0.3927	-0.2390	-0.8467

Diagnosis of the Positioning Errors

In order to make the diagnosis of positioning errors easy, two standard graphic types were adopted in this work (see figure 4.16 as example). The first one (Positioning Error: *FFID vs CHAN*) shows FFID and channel numbers in abscissa and ordinate axis respectively. The positioning error values calculated by equation 4.2, are overlaid on this chart with an appropriate colour scale to facilitate the identification of the affected parts of the seismic spread. The colour scale represents the positioning error values, so this allows to check easily the errors for the entire dataset. The second graphic is a histogram (figure 4.16) of the positioning error values and their frequencies on the dataset. This histogram allows to detect anomalous values to the expected GPS behaviour and gives clues about the polarities of the errors.

Problems related to the streamer

This section presents an example where the second streamer shows high values of positive polarity errors in the area marked in the red box for both sources (Figure 4.16). These values are higher for source 1 in both streamer sections. However, as this anomaly is not found in other cables, probably the main source of this anomalous pattern is the streamer itself. These anomalies are stronger on the first channels, indicating a lead buoy antenna problem. On the other hand, there was also an increase of about 2 meters in the offsets of the last channels of this streamer for this affected area compared to the rest where there is not such anomaly; this effect is marked in the seismic section shown in the figure 4.15 for channel 88.

In addition to the anomaly in question, the graphic *FFID vs CHAN* of the source 1 (figure 4.16 b) presents some weak vertical patterns of positioning errors with high negative polarity, indicating that there may be also a problem associated with this source. In general, this problem creates a positive or right asymmetry pattern with the average greater than the median, indicating that the larger values (right side) are anomalous to the normal behaviour of the data distribution curve. These types of errors can be easily detected, but it is important to consider that depending on the polarity of the error, the asymmetry of the distribution curve will be positive or negative.

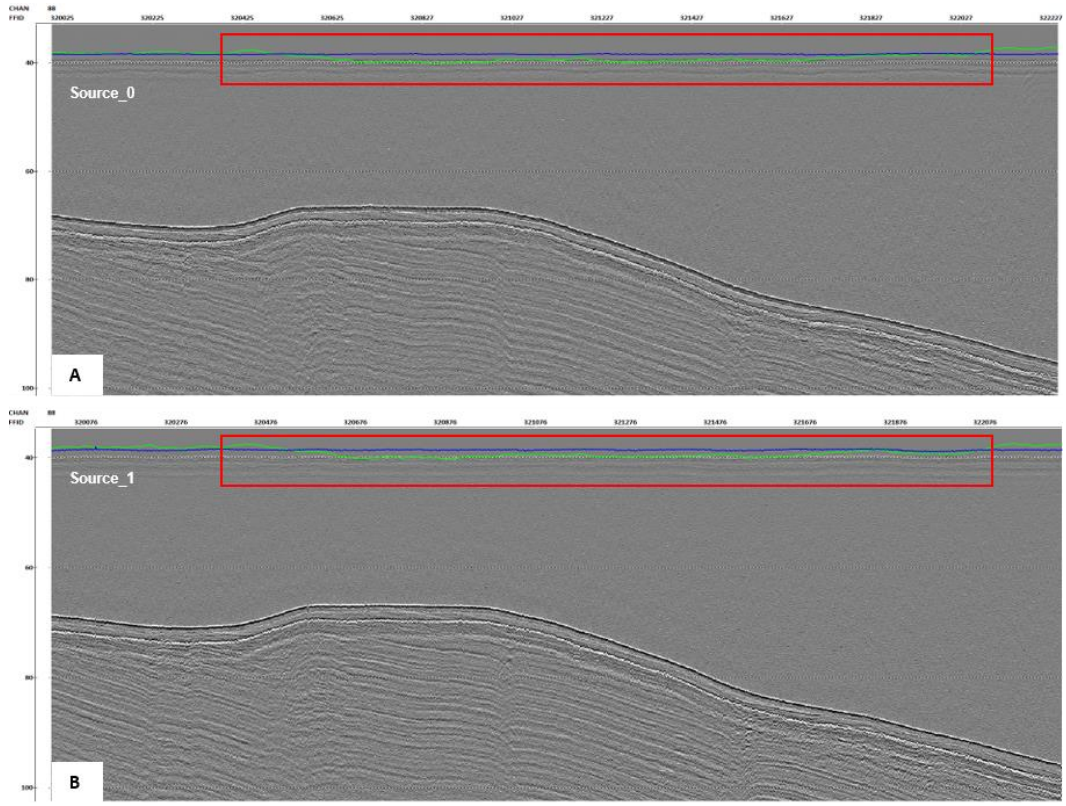

Figure 4.15 - Inversion of polarity in error values created by streamer buoys issues, a) source 0 and b) source 1. Direct arrivals time in blue line; offset computed with GPS data and converted to time in green line. Streamer 2, channel 88. Vertical scale in ms.

a)

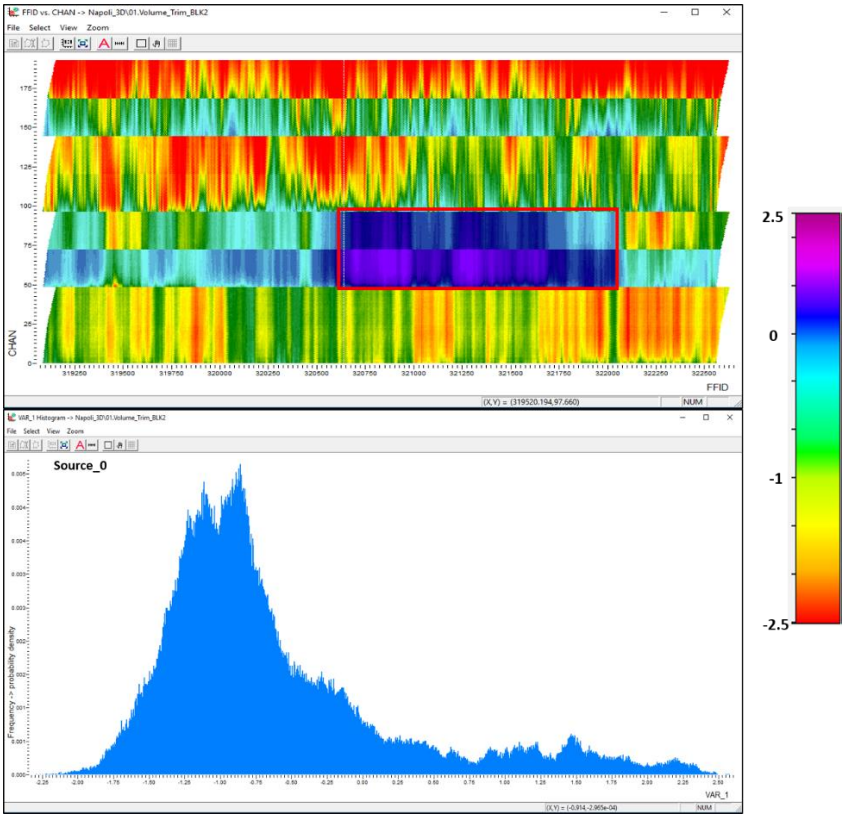

b)

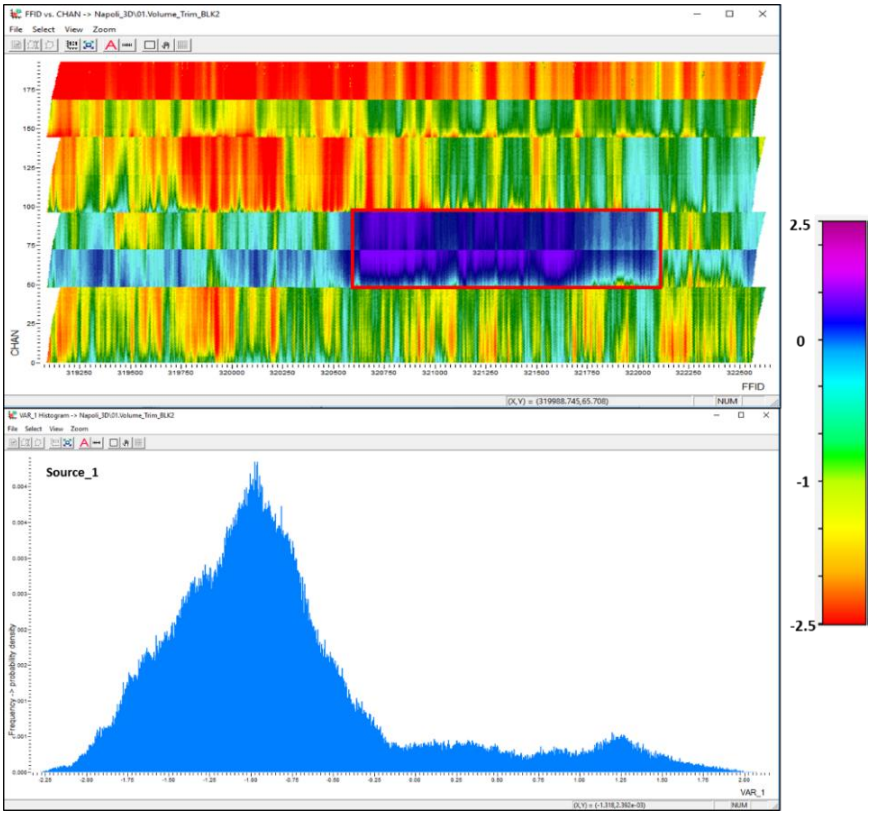

Figure 4.16 - FFID vs CHAN chart and Histogram showing anomalous values of the positioning errors identified in the second streamer due to an inversion of polarity of the error values, a) source 0; b) source 1. Source 0 closer to the first streamer. The colour scale represents the positioning error values calculated by equation 4.2.

Geometry assignment problem

This is one of the issues that most often affects the positioning of this dataset. The dataset used in this work shows evidence of errors in geometry definition, more precisely at the transition of the first group interval of channel to the second one. This problem affects the second section of streamers 2 and 4, resulting in unrealistic offsets for those channels. Thus at least ¼ of the dataset has wrong offsets because of this type of error.

Every streamer used to acquire this data has two active channel sections: the first section is composed by 24 channels, 1 m spaced, and the second section the same number of channels, 2 m spaced. A slight error in delimiting streamer sections can lead to errors such as increasing or decreasing the second section 1 m away from the actual positioning, resulting in unrealistic offsets for all channels in that section.

This error lead to a huge difference between the direct arrivals and offsets calculated with GPS data. This also results in a set of different values that normally appear separated from the rest in the histograms, creating a pattern similar to a bimodal distribution or even more than two modal values if there are other important causes of errors affecting the data (Figures 4.17 and 4.18).

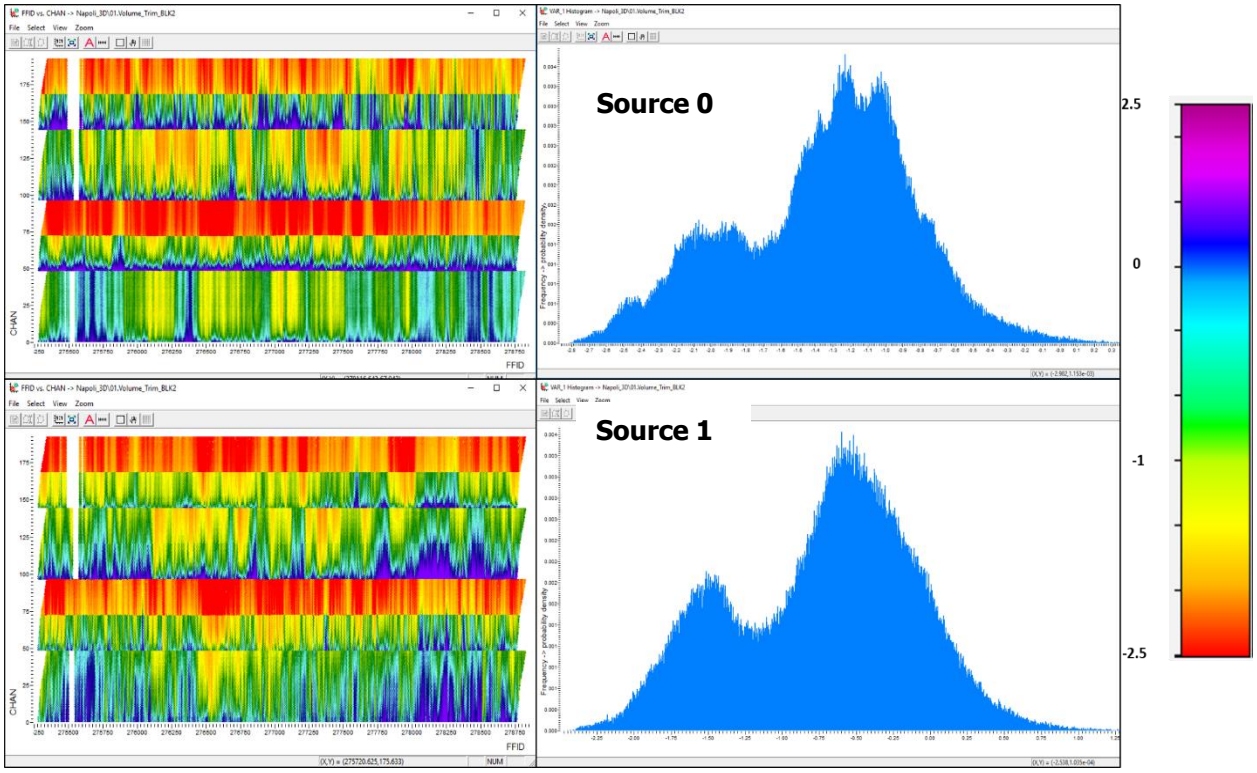

Figure 4.17 - FFID vs CHAN chart and Histogram showing pattern of the positioning problem leaded by geometry assignment issues. Source 0 closer to first streamer. The colour scale represents the positioning error values calculated by equation 4.2.

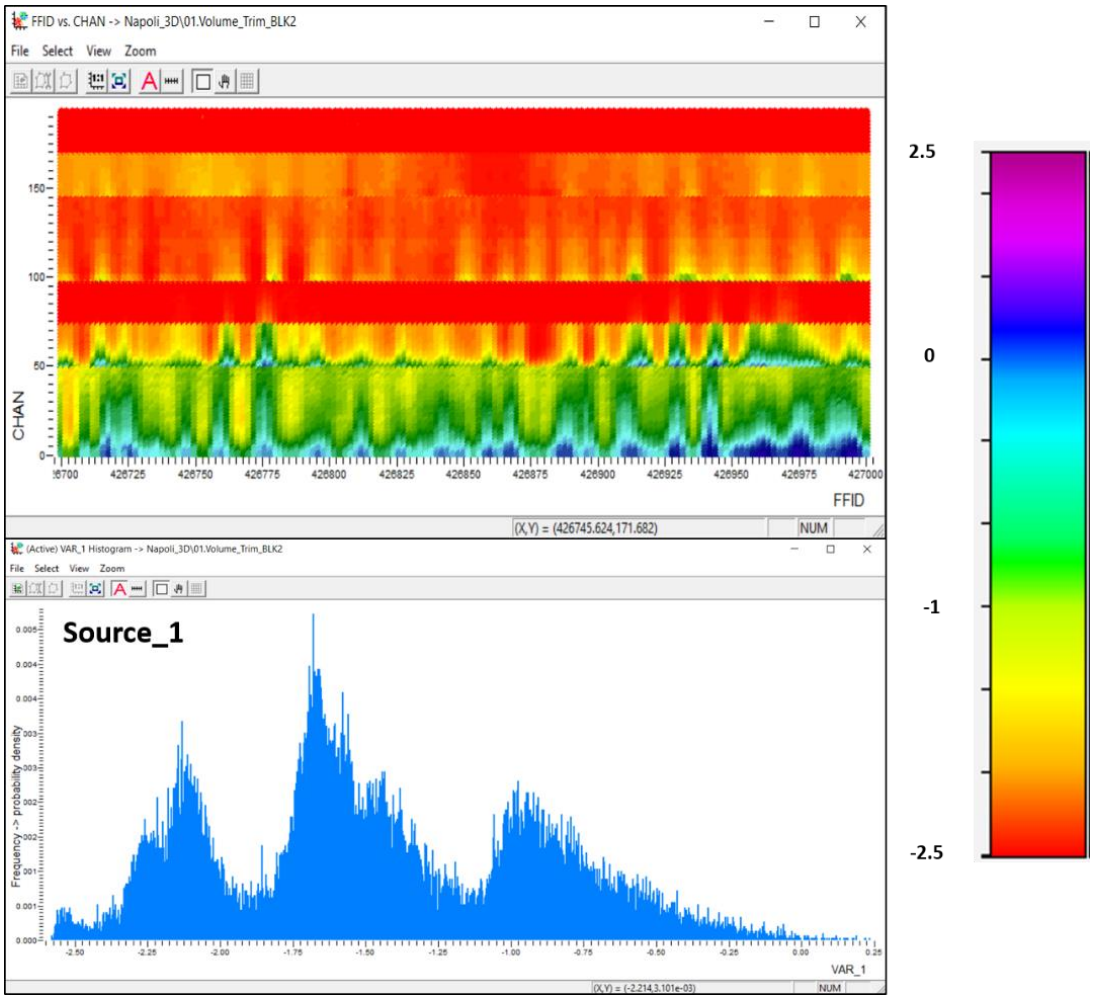

Figure 4.18 - Pattern with three modal values generated by geometry assignment issues. The colour scale represents the positioning error values calculated by equation 4.2.

Positioning errors related to source buoy antenna

Figure 4.19 presents a case where the errors have different polarity for different seismic sources. In the seismic section attached (Figures 4.19 and 4.20), the direct arrivals time is the blue line and the estimated times with the offsets obtained by the GPS data are represented by the green line.

For source 0, the estimated time is generally longer than the direct arrival time except at the last FFIDs, leading mainly to errors with positive polarity. Around the last FFIDs a visible pattern originated by the polarity inversion is formed for all streamers, and therefore it can be a problem related to that source. For source 1 it happens exactly the opposite, and for this reason the error has a negative polarity. As can be seen from the histograms, the data is once more strongly affected by the geometry definition problem which, mixed to the source problems, gave rise to patterns that indicate the existence of several error classes whose values are very frequent.

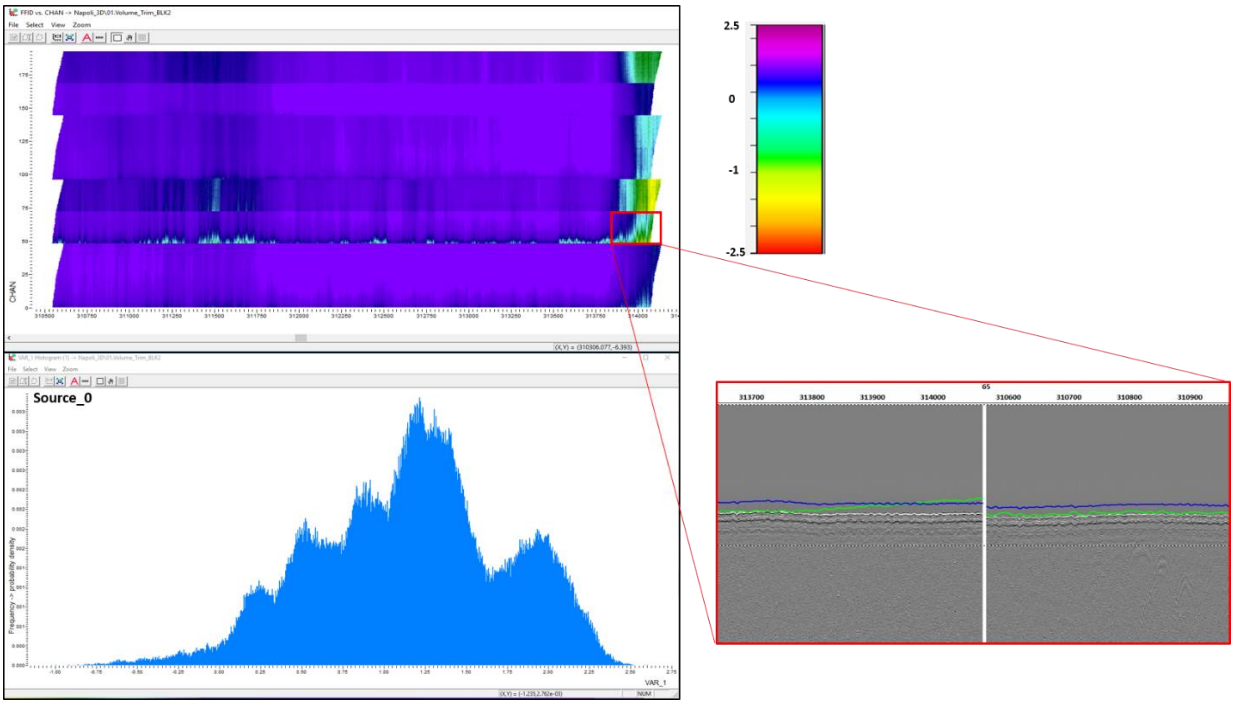

Figure 4.19 - FFID vs CHAN and Histograms for positioning error values showing anomalous vertical pattern, identified by the inversion of polarity of the error values. Direct arrivals time in blue line, offset computed with GPS data and converted to time in green lines. The colour scale represents the positioning error values calculated by equation 4.2.

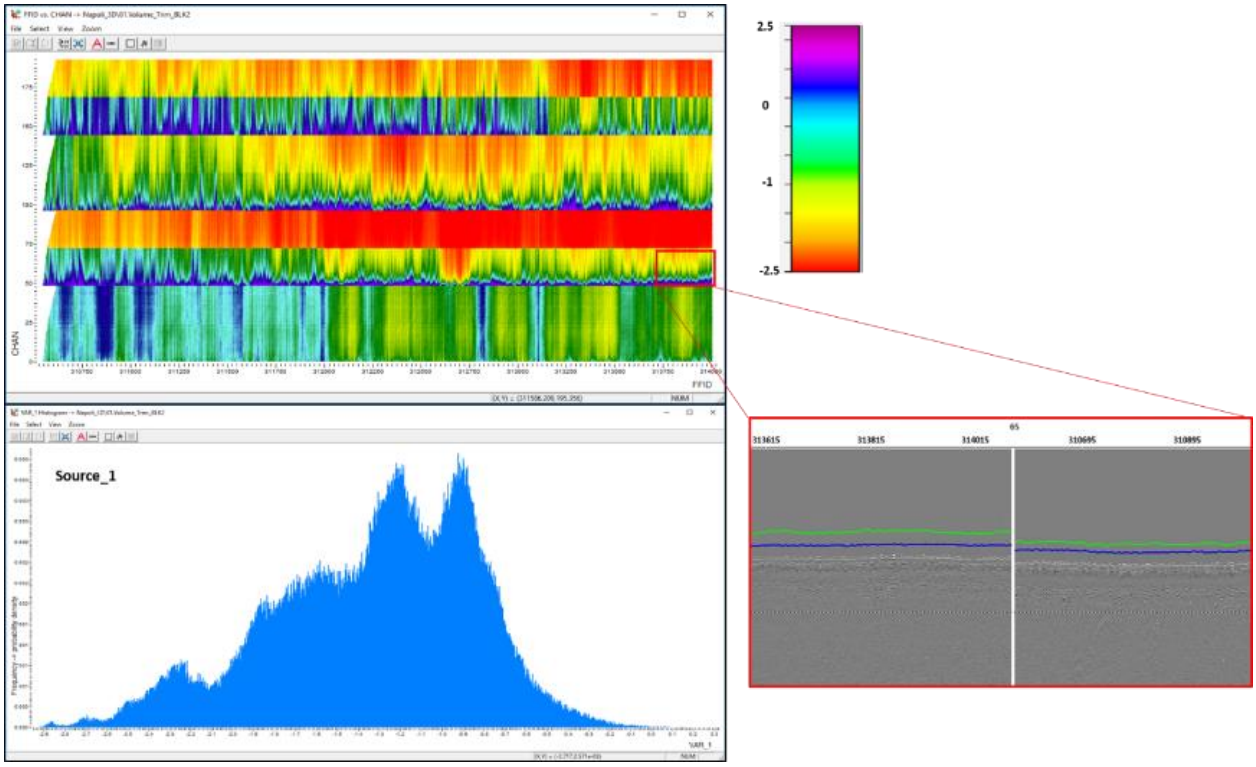

Figure 4.20 - Previous anomalous pattern in source 0 data not identified in source 1, indicating that the cause of this problem can be related to source 0. Direct arrivals time in blue line; offset computed with GPS data and converted to time in green line. Source 1 closer to first streamer. The colour scale represents the positioning error values calculated by equation 4.2.

Problems related to geometry assignment, source and lead buoy antennas

Figures 4.21 and 4.22 show different error patterns for each source. From the histograms it is possible to detect easily that this is an anomalous distribution. This fact is confirmed by the right asymmetry verified in the distribution of source 0, and the left asymmetry in the other source. The values show great variance and, therefore, geometry assignment errors with negative polarity do not form the bimodal pattern found in the previous cases. Despite this, it was possible to distinguish these values because they have a different pattern of distribution curve verified in the histograms, and these values are more noticeable for source 0.

The first section of streamer 2 presents a positive polarity error pattern that is well represented in source 1. This pattern is not too clear in the source 0 data where this appears with a strong alternation of the error values creating small vertical patterns. Seismic shows evidence of source instability due to large oscillations in offsets, especially for source 0. These oscillations are probably responsible by the alternating pattern between positive and negative values found in the first group of second streamer. This pattern may be due to a problem with lead buoy antenna of the second streamer, source 0 oscillations, and geometry assignment.

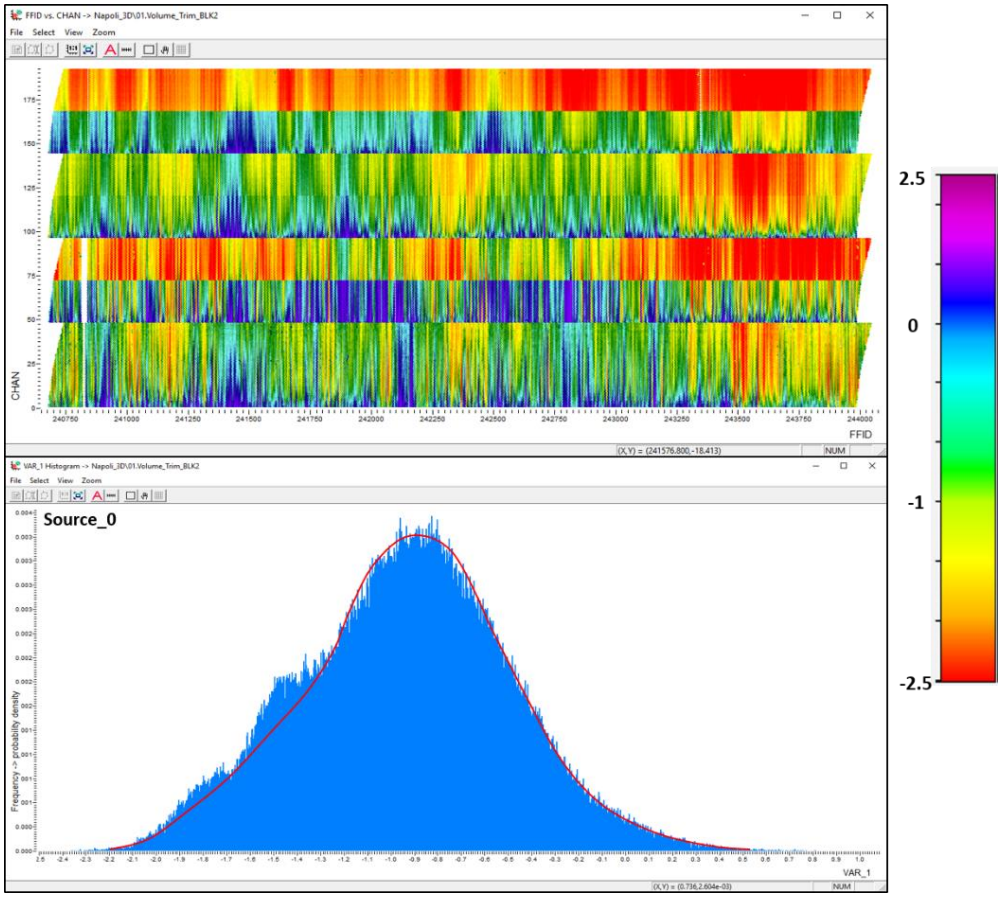

Figure 4.21 - Source 0, FFID vs CHAN chart and Histograms for positioning errors caused by different sources. The colour scale represents the positioning error values calculated by equation 4.2.

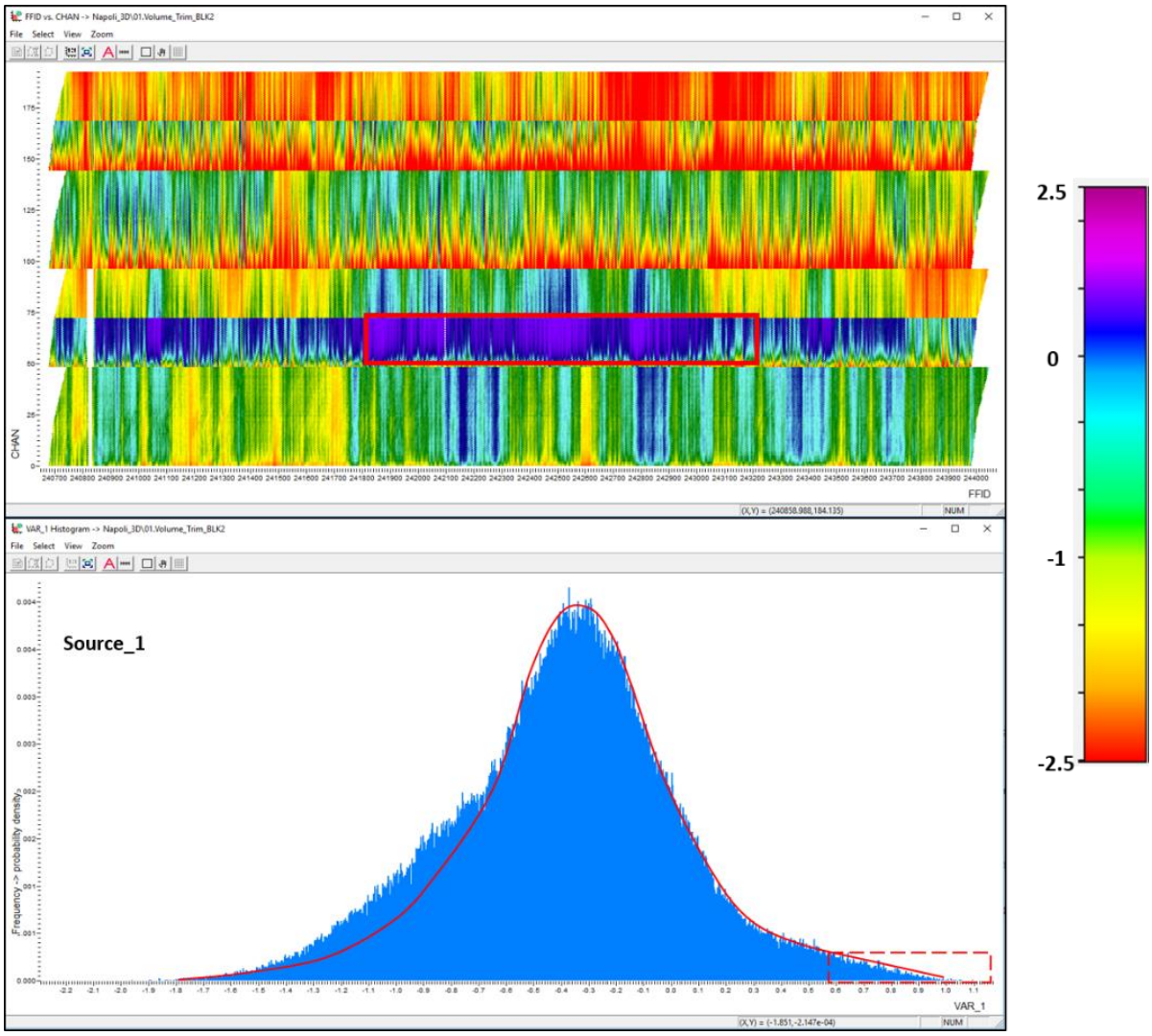

Figure 4.22 - Source 1, FFID vs CHAN chart and Histograms for positioning errors caused by different sources. This source is closer to first streamer. The colour scale represents the positioning error values calculated by equation 4.2.

Chapter 5:

Results and Discussion

5.1. Graphical Patterns and Categories of the Errors Detected

Usually, when GPS antennas are working, it is necessary time to reach the stability in the signal received as well as the coordinates provided. This time may depend on number of satellites available and the operating mode (Standard or Differential). Therefore, when the coordinates for a specific point are measured several times, different values around the true coordinates are found and the more measurements are done the closer these values will be to the correct values, until the stability is achieved, and the majority of measurements will be projected as close as possible to the correct values.

This normal GPS behaviour is similar to the normal gaussian distribution curve, and therefore any problem with the operation of GPS antennas will lead to an anomalous curve in relation to the normal Gaussian curve. This fact makes the detection of positioning problems easy, which is the main objective of this thesis.

Using *Histograms* and *FFID vs CHAN* charts for the values of the positioning errors previously calculated, it was possible to detect anomalies and diagnose the causes that lead to these errors which affect the dataset. This section presents the four main types of positioning errors detected, grouped by categories according to their causes.

5.1.1. Lead Buoy Antenna Issue

When a lead buoy antenna does not work properly within a certain interval of time, the positions of the channel in the concerned streamer will be affected. In these cases, the positioning errors will be more important in the first channels and decrease as offsets increase. This type of problem generates a pattern on the *FFID vs CHAN* chart that is different from the unaffected FFIDs and an asymmetric curve indicating the presence of abnormal values in the histograms (Figure 5.1).

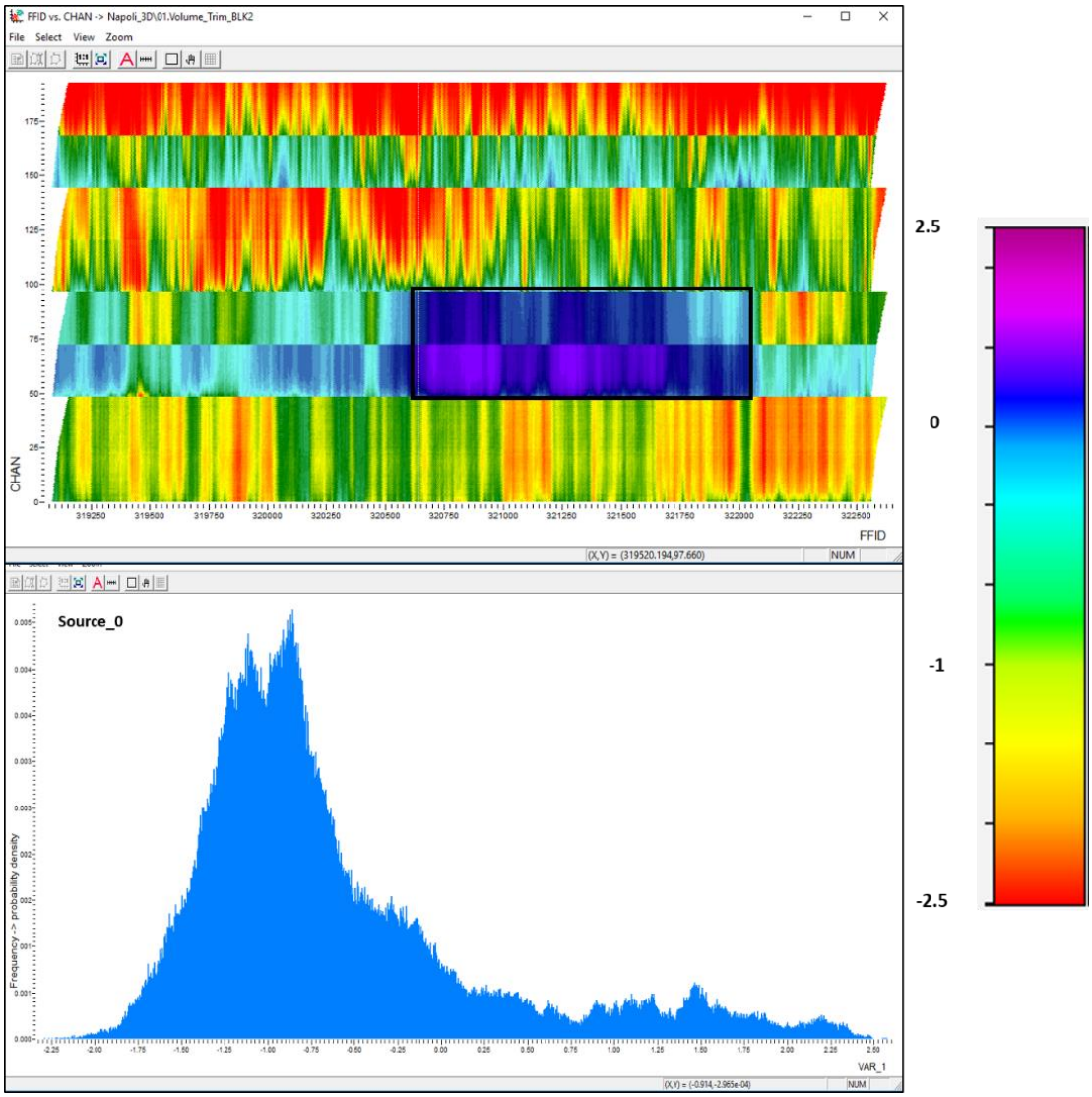

Figure 5.1 - Basic pattern of positioning error caused by lead buoy antenna problems. The colour scale represents the positioning error values calculated by equation 4.2.

5.1.2. Tail Buoy Antenna Issue

Similar to the case of the lead buoy, the tail buoy antenna problems mainly affect the last channels and generate a pattern where errors are higher in far-offsets (Figure 5.2). This problem needs more attention because the positions of all channels along the streamer are calculated considering the streamer azimuth that depends on the tail buoy position.

This problem is very common, and its detection is not so trivial because it does not always result in absurd offset values as it happens in the first channels when the lead buoy and source antennas are lost. Although errors are greater in far-offsets, the first channels are also affected, such that the computed CDP track can be too different from the real CDP track, and thus a pseudo off-track can be generated.

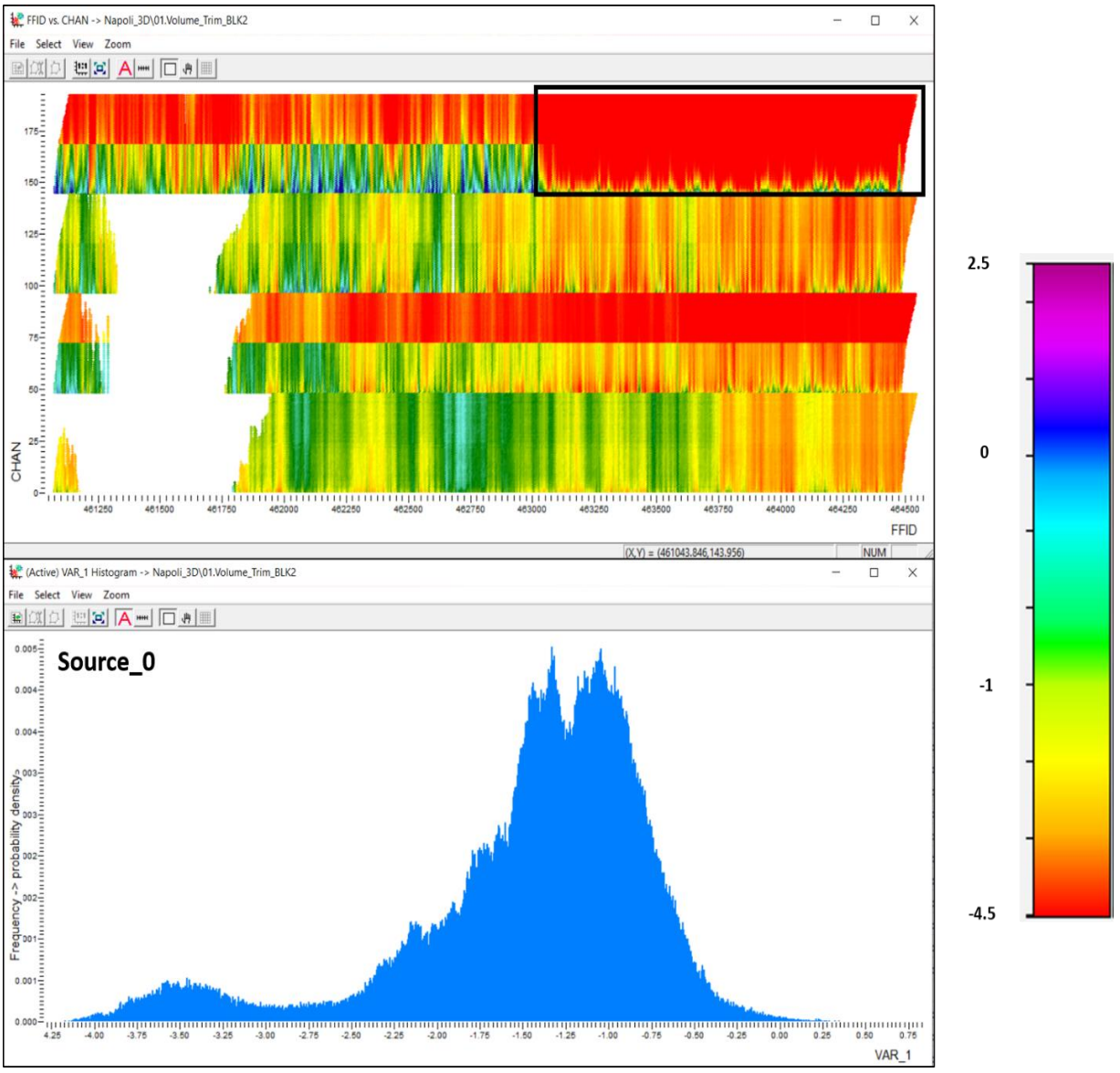

Figure 5.2 - Basic pattern of the positioning errors caused by tail buoy antenna problems. The colour scale represents the positioning error values calculated by equation 4.2

5.1.3. Source Buoy Antenna Issue

The positioning issues related to the source antennas were easily identified on the *FFID vs CHAN* charts. This leads to a different pattern from the rest of the data. This type of problem affects all channels in the four streamers, generating a vertical pattern where the positioning errors have different values (Figure 5.3). The channels closest to the source are the most affected when compared to the other channels. In the figure 5.3, the source with problem (source 0) is closer to the fourth streamer, and therefore the error identified by the vertical pattern decreases towards the first streamer.

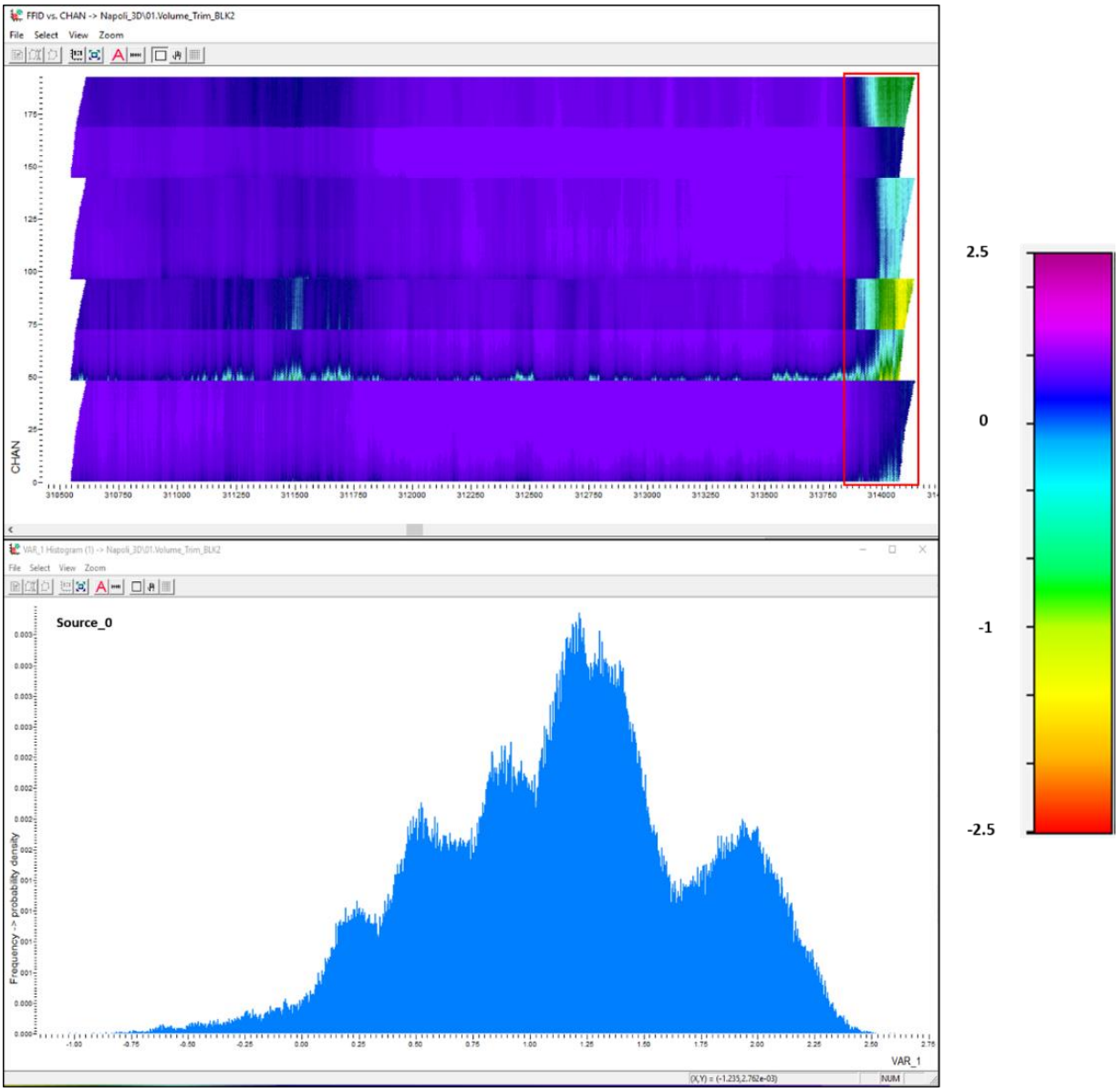

Figure 5.3 - Basic pattern of positioning error caused by source buoy antenna problems. The colour scale represents the positioning error values calculated by equation 4.2.

5.1.4. Geometry Assignment Issue

The problems related to the geometry assignment can be caused by errors in measurement of the distances between sources and receivers, lead buoy antenna and first channel, and distances between channels at transition from one streamer section to another. The last one is the most common positioning problem affecting the dataset analysed in this work.

This type of problem creates a pattern in the *FFID vs CHAN* graphics that splits the streamer sections abruptly (see black boxes in the upper image of figure 5.4). It becomes visible by a jump in the error value that is larger than the expected. As half of the streamer is affected, a

significant part of dataset is compromised and this leads to a second set of error values, resulting in a bimodal distribution (see histogram in Figure 5.4). This problem can be solved in the office by correcting the geometry and recalculating the channel positions using *Geosuite NaviWorks* software, but once this problem is detected during the acquisition, it should be corrected immediately, in order to decrease the time-consuming of post-processing/correction of the positioning data in the office.

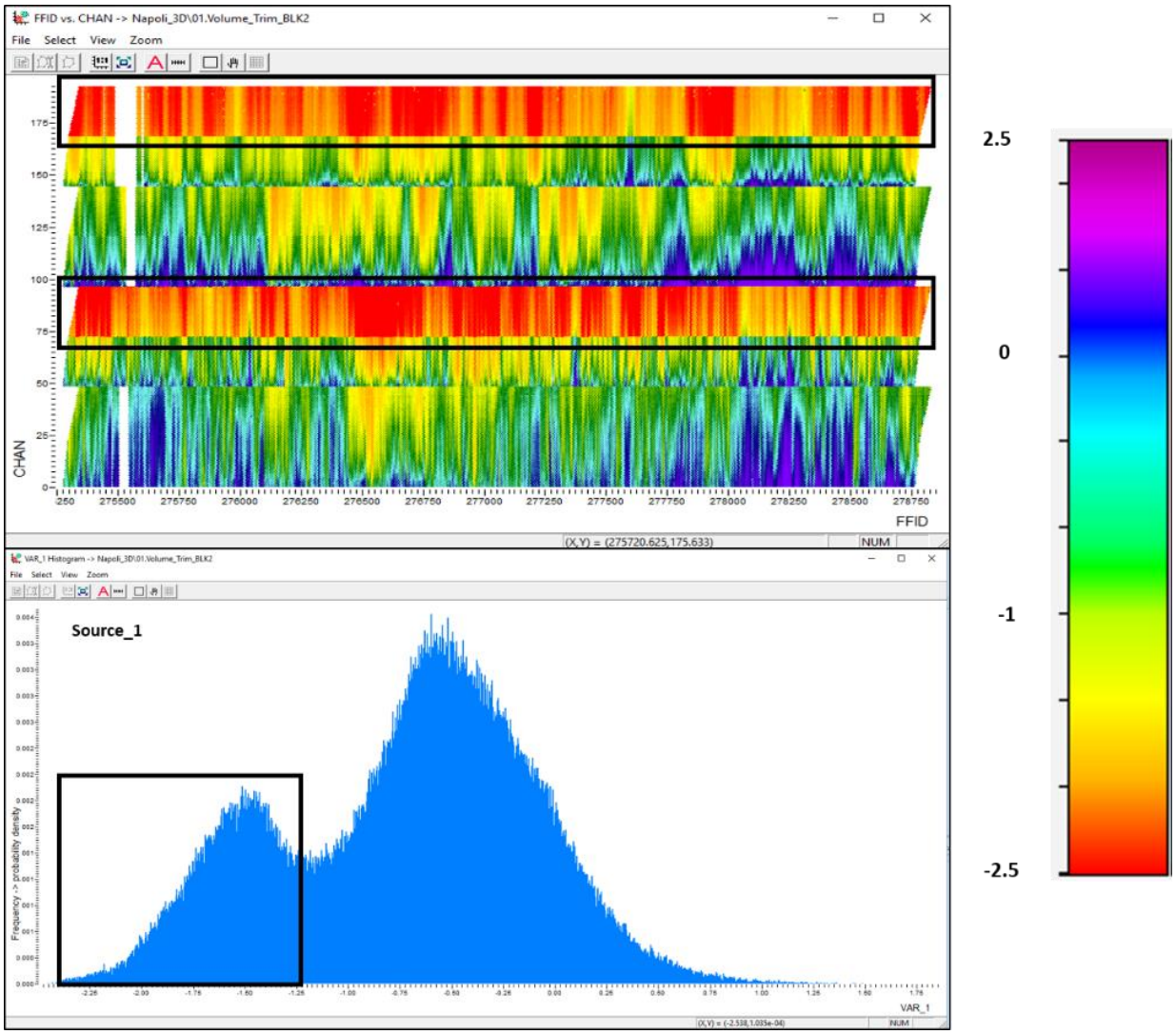

Figure 5.4 - Typical pattern of positioning error caused by geometry assignment problems. The colour scale represents the positioning error values calculated by equation 4.2.

5.2. Presentation and Evaluation of the Results on Time-Slices

After diagnosing the positioning errors and their causes, a rejection criterion was applied in order to assess the impact that these types of problems have on the data. Accordingly, a maximum limit for the acceptable range of error was chosen.

Many factors must be considered to determine the maximum acceptable limit of the error. In order to get easier the exact location of boulders and the identification of other in-depth hazards that threaten the optimization of the wind turbine installations, it is important to reduce as much as possible the difference between the actual geology and the seismic section obtained; this difference can be strongly affected by the positioning data.

The bin size was chosen as the main factor to determine the maximum acceptable error. Thus, the ideal criterion is to reject any difference between the offset calculated by the direct arrivals times and the offsets provided by the positioning data that is at least twice larger than the Bin size. The errors in the offsets are caused by the low accuracy in the positioning of the sources and receivers, and therefore the reflection midpoint calculated will have at least one uncertainty of half of the offset errors. If this uncertainty is larger than the bin size, there is a probability of adding seismic traces that belong to other Bin during the ensemble stack, changing the interpretation of the actual geology and leading to an increase of the discrepancy between the geology and the seismic section.

However, common sense and a weighting factor must exist if a huge part of the data presents this problem. In these cases, the maximum acceptable limit needs to be increased, in order to avoid gaps in the volume that can compromise the following processing steps (e.g. regularization).

In this work, two different rejection criteria were tested, the first will be farther called as Rejection A, and the second one as Rejection B. The characteristics of each criteria are described farther. For both cases, the maximum acceptable limits for the amplitude of the errors were higher than the Bin size (0.5 m), in order to avoid large gaps in the volume since this dataset is strongly affected by positioning errors. These two rejection criteria were applied on the original seismic volume, then two datasets with different trace density were generated and the same processing sequence were applied for each volume.

Since bad navigation is being rejected, the results are more evident on the time-slices towards the vessel navigation (inline). For this reason, this section presents the results obtained and its differences in the horizontal-slices in order to evaluate the quality of the rejection criteria tested.

Figure 5.5 shows two horizontal cuts in time (83 ms and 110 ms) in a seismic section, made for the three volumes generated, to evaluate the results obtained after applying the rejection criteria. The set of normal faults showed in figure 5.5 correspond to the NE–SW trending SE-dipping normal faults from the extensional system presented in figure 2.5, around Pozzuoli Bay. This can be also confirmed on the time-slices from figure 5.6 to figure 5.8.

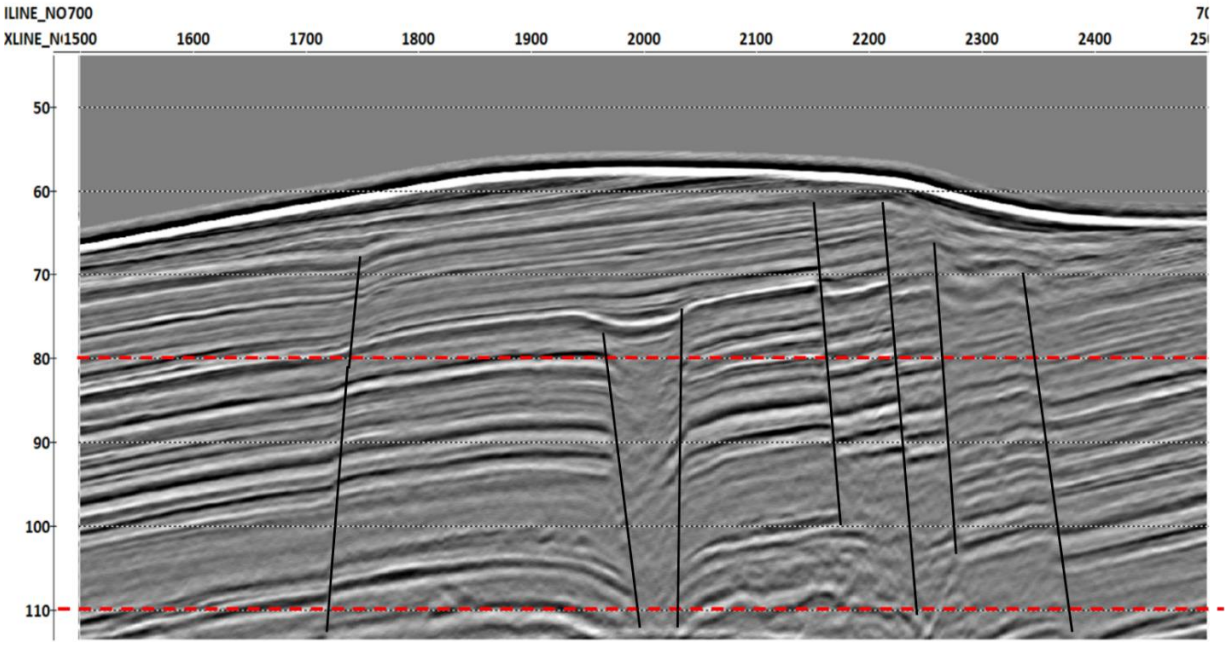

Figure 5.5 - Vertical seismic section from inline 700 and crossline between 1500-2500. Red lines showing the horizontal cuts in time (83 ms and 110 ms) used to evaluate the time-slices. Vertical scale in ms.

5.2.1. Time Slices Standard Stack

Figure 5.6 shows the horizontal sections of the original volume without rejection of the traces with bad positioning. These time-slices will be used as a standard for comparison with the volume where rejection criteria were applied.

5.2.2. Time Slices Rejection A

Figure 5.7 shows the horizontal sections at 83 ms and 110 ms. The rejection criterion applied (Rejection A) had a maximum error limit of 2 ms, which gives an uncertainty of 1.5 m in the position of the midpoint of reflection. The result of the processing of this dataset proved to be better than the standard stack in terms of continuity of reflectors and enhancement of faults.

5.2.3. Time Slices Rejection B

The final result of the seismic processing for the dataset on which the rejection criterion B was applied presented the worst result among the three datasets (see figure 5.8). For this criterion, a maximum limit of acceptable error equal to 1 ms (0.75 m of uncertainty in the positioning of the midpoint of reflection) was used and therefore many traces were rejected.

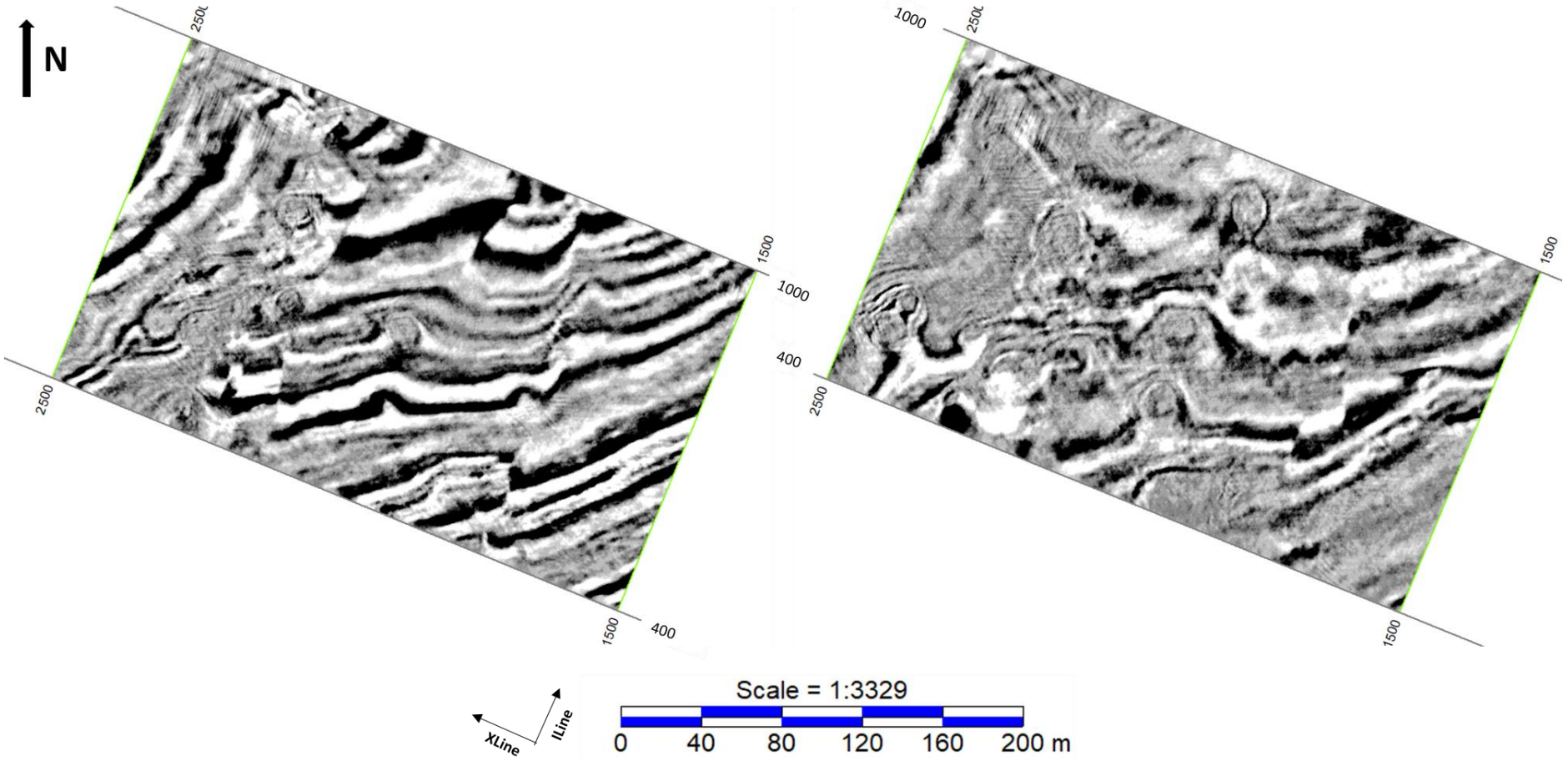

Figure 5.6 - Horizontal slices of the standard stack, without any rejection criterion. Left image at 83 ms and right image at 110 ms.

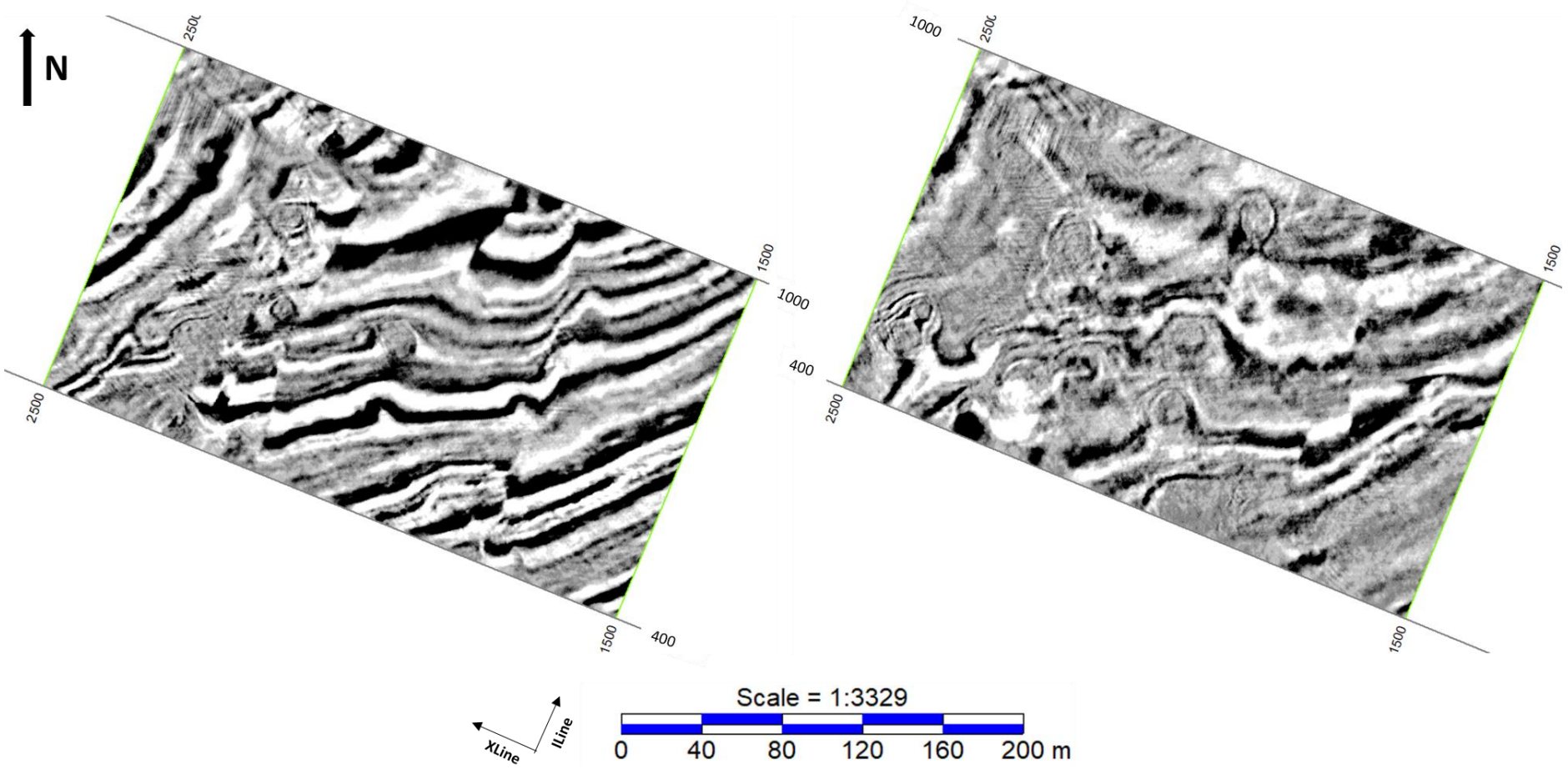

Figure 5.7 - Horizontal slices of the dataset on which rejection A was applied. Left image at 83 ms and right image at 110 ms.

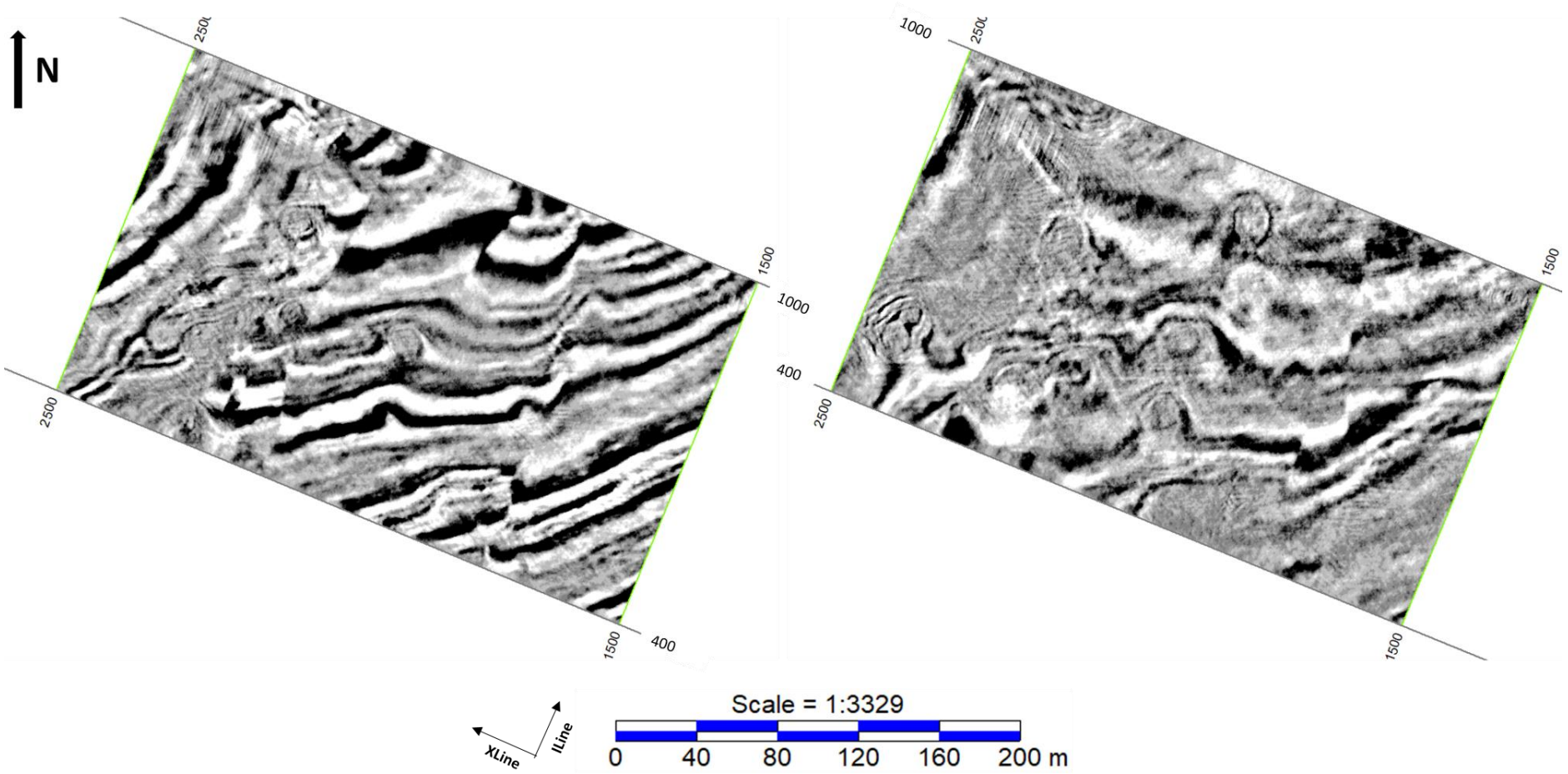

Figure 5.8 - Horizontal slices of the dataset on which rejection B was applied. Left image at 83 ms and right image at 110 ms.

5.3. Discussion

The *Histograms of positioning errors* showed anomalous distribution curves to the expected behaviour of working GPS antennas, revealing that there are problems in the positioning data provided. The graphical patterns created by these histograms along with the *FFID vs CHAN* charts for the positioning error values allowed to easily detect the main categories of errors that affect the data and its respective causes. Nevertheless, it is not always too easy to detect the source of problem trough these graphics because problems from different causes can occur at the same time disturbing the graphical patterns, making it more difficult to detect the causes of the positioning problems.

After detecting the positioning errors and applying rejection criteria A and B, the difference between the three processed datasets was noticeable. The quality control on the time-slices carried out in the *Kingdom Suite* software revealed that among the three datasets, that on which the rejection criterion A was applied presented the best results. With this criterion, the data showed more continuity in the reflectors, a better quality in terms of sharpness and the faults were better highlighted. The results obtained have great importance for a more detailed geological interpretation.

The dataset where the rejection criterion B (maximum positioning error limit of 1 ms) was applied, proved to be the poorest in terms of sharpness, continuity of reflectors and highlight of the faults. This result was expected because a large part of the data was affected by positioning errors greater than 1 ms, resulting in a decrease of the density of traces in the seismic volume, causing gaps in the coverage that the regularization cannot cover perfectly. Thus, the importance of weighing the acceptable limit values of errors in order to maintain a good trace density was confirmed. The time slices of the standard stack proved to be reasonable. However, it was not better than the result of rejection A (maximum positioning error limit of 2 ms) when comparing aspects such as the continuity of reflectors and definition of important geological structures for geological interpretation.

The differences between the three datasets are most evident in the near surface parts (close to the seabed). As depth increases, it becomes more difficult to find significant differences between the Standard Stack and Rejection A. However, it was possible to notice a slight difference in the highlight of the faults, which was more noticeable in the time-slices of the dataset on which the rejection criterion A was applied.

Chapter 6:

Conclusions

6.1. Concluding Remarks

In general, the objectives set for this work were fully achieved. Now, a new effective, efficient, and easy to apply method can be used during offline QC to control the quality of the positioning data provided by the GPS antennas. This method allows a better quality control of that, which besides feathering, is the biggest criterion for navigation rejection. This will also allow to build a seismic section closer to actual geology with the midpoints of reflections in their true positions, making possible the exact identification of the location of boulders and other structures or in-depth hazards that can compromise the installation of wind turbines.

With the Navigation QC procedure developed in this work it is now possible, not only to identify the presence of the positioning errors, but also to diagnose the causes that lead to these problems, allowing a response in the field in a short interval of time. Thus, the regular occurrence of these errors and subsequent time-consuming post-processing of positioning data in the office and associated increase of the costs will be avoided.

The positioning error was defined as the difference between the expected offset, calculated from the direct arrival times, and the offset calculated from the positioning data provided by the GPS antennas, used in the seismic spread to determine the position of each receiver, or their equivalent time. The solutions found were tested in the *RadExPro* software and two graphical patterns were adopted for the visualization and diagnosis of the most common positioning errors. These are the "*FFID vs CHAN"* charts for the positioning error values determined by equation 2, with a colour scale that makes the location of the seismic spread area affected and the causes of the problems easy, and the "*Histograms*" that present the error values, allowing the detection of abnormal behaviours to the normal operating mode of the GPS antennas and create patterns that also give clues as what is happening with positioning data, making the diagnoses easier.

In addition to diagnosing errors, a method to reject the affected data was also discussed. The proposed rejection criterion was based on the bin size in order to avoid adding seismic traces that actually belong to a certain bin but which have moved to adjacent bins due to positioning problems. The rejection method applied proved to be effective because it has the ability to reject only the affected channels and not the entire shot; this fact makes it possible to find a balance

between rejecting badly positioned traces and maintaining the regularity of the Bin grid or the trace density in order to avoid large gaps in the seismic volume and compromise processing steps such as regularization and interpolation. The results presented in previous chapter indicate that there should be a weighting factor, and that a maximum error limit slightly higher than the bin size must be accepted when a large part of the data is affected; this principle will also help to avoid gaps in coverage.

6.2. Suggestions for Future Work

Geosurveys is a company that is strongly investing in data quality control, carrying out its tasks effectively and in a short period of time, in order to reduce the costs associated with the time consumed in these operations. It has therefore invested in the development of methodologies and tools for real-time quality control. The quality control of the positioning data developed in the scope of this thesis is essentially based on the difference between offsets obtained from the direct arrivals time and the offsets calculated with the data provided by the GPS antennas, which is intended to be evaluated. Thus, this method is limited to the direct arrivals time picking, which is not performed in real time at present; for this reason, it was developed only for offline QC.

In order to improve the method developed in this work and make it applicable for real time QC, the following points describe the suggestions for future work to be developed and improved within the scope of *Geosurveys* research and development works:

- *Real time Direct arrivals picking*. Development of an effective method for real time direct arrivals picking during acquisition. This implementation will allow the quality control of the positioning data in real time using the offset differences method developed in this work and reduce the time associated with this operation as well as the costs.

- *Improving the rejection criteria*: The rejection criteria and their application are two points that can also be improved in order to optimize the solution presented here. The suggestion for this case is to develop rejection criteria based on the main sources of positioning errors presented in section 5.1, since the dataset is affected in different ways depending on the cause of errors. The rejection criteria to be developed should reject only the most affected channels and examples are given below:

    1. For the errors caused by lead buoy antennas, only the first channels of affected streamer should be rejected;

2. When source antennas are causing the errors, just the first channels which present absurd offset values should be rejected;
3. Tail buoy errors should essentially imply rejection of the last channels. Depending on the magnitude of the error, some channels in the first section of the streamer may be affected as well and therefore also rejected;
4. Traces with positioning errors due to geometry assignment must not be rejected, just correcting the geometry and recalculate the positions of the receivers.

- *Correct positioning problems caused by bad functioning of the tail buoy antennas*. It is first necessary discover the behaviour of the acquisition system when tail buoys antennas stop working. The positions of all receivers in the streamer are calculated along an azimuth between the lead and the tail buoy. When a tail buoy antenna stops working properly, the acquisition system assigns random coordinates, resulting in an incorrect azimuth and respectively the positions of the channels. Taking control of the behaviour of the acquisition system when this phenomenon occurs will allow to recalculate the wrong azimuth assigned by the system and correct or recalculate the true positions using the expected azimuth or the average of the azimuths of the other unaffected streamers.

References

Acocella, V. (2010). Evaluating fracture patterns within a resurgent caldera: Campi Flegrei, Italy. *Bulletin of Volcanology 72, 623-638*.

Acocella, V., Funiciello, R., Marotta, E., Orsi, G., & de Vita, S. (2004). The role of extensional structures on experimental calderas and resurgence. *Journal of Volcanology and Geothermal Research 129, 199-217.*

Aiello, G., Angelino, A., D'Argenio, B., Marsella, E., Pesoli, N., Ruggieri, S., & and Siniscalchi, A. (2005). Buried volcanic structures in the Gulf of Naples (Southern Tyrrhenian Sea, Italy) resulting from high resolution magnetic survey and seismic profiling. *Annals of geophysics, vol. 48, n 6*.

Aiello, G., Budillon, F., Conforti, B., D'Argenio, B., Ferraro, L., Marsella, E., . . . Tonielli, R. (2011). Geological Survey of the Naples Bay (CARG Project).

Aiello, G., Budillon, V., Cristofalo, G., D'Argenio, B., De Alteriis, G., De Lauro, M., & Toniell‌i, R. (2001). Marine geology and morphobathymetry in the Gulf of Naples (South-Eastern Tyrrhenian sea, Italy). in F. M. Faranda, G. Letterio, & G. Spezie, *(Eds). Mediterranean ecosystems: Structures and processes* (pp. 1-8). *Milan: Springer Science & Business Media.*

Aiello, G., Marsella, E., & Di Fiore, V. (2012). New seismo-stratigraphic and marine magnetic data of the Gulf of Pozzuoli (Naples Bay, Tyrrhenian Sea, Italy): inferences for the tectonic and magmatic events of the Phlegrean Fields volcanic complex (Campania). *Springer*.

Alfaro, J. C., Corcoran, C., Davies, K., Pineda, F. G., Hampson, G., Hill, D., . . . Kragh, E. (2007). Reducing Exploration Risk. Oilfield Review. *Spring, 26 – 43.*

Amore, O. F., Bonardi, G., Ciampo, G., De Capoa, P., Perrone, V., & Sgrosso, I. (1988).). Relazioni tra "Flysch Interni" e domini appenninici: reinterpretazione delle formazioni di Pollica, S. Mauro e Albidona e il problema dell'evoluzione inframiocenica delle zone esterne Appenniniche. *Memorie della Società Geologica Italiana 41, 285–297.*

Arnò, V., Principe, C., Rosi, M., Santacroce, R., & Sheridan, M. F. (1987). Eruptive history. Somma Vesuvius. Quaderni de "La Ricerca Scientifica, Progetto Finalizzato". *Geodinamica 114 (8): 53–103*.

Ashcroft, W. (2011). A Petroleum Geologist's Guide to Seismic Reflection. *Wiley-Blackwell*.

Aucelli, P. P., Cinque, A., Mattei, G., & Pappone, G. (2017). Late Holocene landscape evolution of the Gulf of Naples (Italy) inferred from geoarchaeological data. *Journal of Maps, 13:2, 300-310*.

Barberi, F., Cassano, E., La Torre, P., & Sbrana, A. (1991). Structural evolution of CampiFlegrei Caldera in light of volcanological and geophysical data. *Journal of Volcanology and Geothermal Research 48 (1–2), 33–49.*

Bonardi, G., D'Argenio, B., & Perrone, V. (1988). Geological map of Southern Apennines. *Memorie - Società Geologica Italiana, 41*.

Bone, M. R., Giles, B. F., Tegland, E. R. (1976). 3-D high resolution data collection, processing and display. *Houston, Texas, 46th annual SEG meeting.*

Brown, A. R. (2011). Interpretation of three-dimensional seismic data. *AAPG Memoir 42 and SEG Investigations in Geophysics No. 9.*

Bruno, P. P., Rapolla, A., & Di Fiore, V. (2003). Structural setting of the Gulf of Naples (Italy) seismic reflection data: Implications for Campanian volcanism. *Tectonophysics, 372(3), 193–213*.

Budillon, F., Conforti, A., Tonielli, R., D'Argenio, B., & Marsella, E. (2011). Morfobatimetria del Golfo di Pozzuoli. In L. Lirer (*Eds). I Campi Flegrei, storia di un campo vulcanico. Quaderni dell'Accademia Pontaniana, Napoli, pp. 105–120.*

Buia, M., Hill, D., Houbiers, M., Laura, S., Menlikli, C., Moldoveanu, N., & Snyder, E. (2008). Shooting Seismic in Circles. *Oilfield Review, Autumn, 18 – 31*.

Cinque, A., Aucelli, P. P., Brancaccio, L., Mele, R., Milia, A., Robustelli, G., & …Sgambati, D. (1997). Volcanism, tectonics and recent geomorphological change in the Bay of Napoli. . *4th Int. Conf. on Geomorph. - Italy 1997, Guide for the excursion, suppl III, t. 2, 123–141.*

Correia, F. (2017). Quality Control of Ultra High Resolution Seismic data acquisition in Real-Time. *Master thesis, University of Aveiro*.

De Natale, G., Troise, C., Pingue, F., Mastrolorenzo, G., Pappalardo, L., Battaglia, M., & Boschi, E. (2006). The Campi Flegrei Caldera: unrest mechanisms and hazards. In G. De Natale, C. Kilburn, & C. Troise, *(Eds). Mechanisms of Activity and Unrest at Large Calderas. Geological Society, London, Special Publications, 269, pp. 25–45.*

De Pippo, T., Di Cara, A., Guida, M., Pescatore, T. S., & Renda, P. (1984). Contributi allo studio del Golfo di Pozzuoli: lineamenti di geomorfologia. . *Memorie della Società Geologica Italiana 27, 151–159.*

De Vivo, B., Rolandi, G., Gans, P. B., Calvert, A., Bohrson, W. A., Spera, F. J., & Belkin, H. E. (2001). New constraints on the pyroclastic eruptive history of the Campanian volcanic Plain (Italy). *Mineralogy and Petrology, 73(1–3), 47–65*.

Deino, A. L., Orsi, G., de Vita, S., & Piochi, M. (2004). The age of Neapolitan Yellow Tuff caldera forming eruption (Campi Flegrei caldera, Italy) assessed by $_{40}$Ar/$_{39}$Ar dating method. *Journal of Volcanology and Geothermal Research, 133, 157–170*.

Della Vedova, B., Marson, I., Panza, G. F., & Suhadolc, P. (1991). Upper mantle properties of the Tuscan-Tyrrhenian area: A framework for its recent tectonic evolution. *Tectonophysics,195,311 – 318*.

Della Vedova, B., Pellis, G., Foucher, J. P., & Rehault, J. P. (1984). Geothermal structure of the Tyrrhenian Sea. *Mar. Geol.,55, 271 – 289*.

Dello Iacono, D., Zollo, A., Vassallo, M., Vanorio, T., & Judenherc, S. (2009). Seismic images and rock properties of the very shallow structure of Campi Flegrei caldera (southern Italy). *Bulletin of Volcanology 71, 275–284*.

Di Girolamo, P., Ghiara, M. R., Lirer, L., Munno, R., Rolandi, G., & Stanzione, D. (1984). Vulcanologia e petrologia dei Campi Flegrei. *Bollettino della Società Geologica Italiana 103, 349–413*.

Di Vito, M. A., Isaia, R., Orsi, G., Southon, J., De Vita, S., D'Antonio, M., & . . . Piochi, M. (1999). Volcanism and deformation in the past 12 ka at the Campi Flegrei caldera (Italy). *Journal of Volcanology and Geothermal Research 91, 221–246*.

Dobrin, M., & Savit, C. (1988). Introduction to Geophysical Prospecting. . *McGraw-Hill, 4th Edition 867*.

Duarte, H., Wardell, N., & Monrigal, O. (2017). Advanced processing for UHR 3D shallow marine seismic surveys. *European Association of Geoscientists & Engineers, Near Surface Geophysics, 2017, 15, 347-358*.

Dvorak, J., & Berrino, G. (1991). Recent ground movement and seismic activity in Campi Flegrei, southern Italy: episodic growth of a resurgent dome. . *Journal of Geophysical Research 96, 2309–2323*.

Dvorak, J., & Mastrolorenzo, G. (1991). The mechanisms of recent vertical crustal movements in CampiFlegrei caldera, southern Italy. *Special Paper—Geological Society of America 263, 1–54*.

Faccenna, C., Mattei, M., Funiciello, R., & Jolivet, L. (1997). Styles of back-arc extension in the central Mediterranean. *Terra Nova, 9, 126 – 130*.

Fedele, L., Morra, V., Perrotta, A., Scarpati, C., Putignano, M. L., Orrù, P., & Conforti, A. (2015). Note illustrative della Carta Geologica d'Italia alla scala 1:50.000, foglio 465 Isola di Procida . *ISPRA*.

Fevola, F., Fusi, N., & Mirabile, L. (1993). Rilievi di sismica monocale ad alta risoluzione: aspetti dell'avoluzione geomorfologica del Golfo di Napoli. *Annali dell Istituto Universitario Navale, Napoli 60, 61–71*.

Finetti, I. R. et al. (2001). Crustal section based on CROP seismic data across the North Tyrrheniannorthern Apennines-Adriatic Sea. *Tectonophysics,*.

Florio, G., Fedi, M., Cella, F., & Rapolla, A. (1999). The Campanian Plain and Phlegrean Fields: structural setting from potential field data. *Journal of Volcanology and Geothermal Research 91, 361–379*.

Fusi, N., Mirabile, L., Camerlenghi, A., & Ranieri, G. (1991). Marine geophysical survey of the Gulf of Naples (Italy): relationships between submarine volcanic activity and sedimentation. *Mem. Soc. Geol. It., 47, 95-114*.

Gvirtzman, Z., & Nur, A. (2001). Residual topography, lithospheric structure and sunken slabs in the central Mediterranean. *Earth Planet. Sci. Lett.,187,117 – 130*.

Hatton, L., Worthington, M. H., & Makin, J. (1986). Seismic Data Processing - Theory and Practice. *177*.

Heigl, W. M., Radtke, R. P., Stokes, R. H., & Glowka, D. A. (2013). A low-frequency downhole sparker for borehole seismic applications. *CSEG Recorder*.

Iannace, A., Merola, D., Perrone, V., Amato, A., Cinque, A., Santacroce, R., & D'Argenio, B. (2015). Note Illustrative della Carta Geologica d'Italia alla scala 1:50.000 fogli 466–485 Sorrento-Termini.

Insinga, D., Di Meglio, A., Molisso, F., & Sacchi, M. (2002). Stratigrafia e caratteristiche fisiche dei depositi olocenici del porto di Miseno, Golfo di Pozzuoli (Tirreno centroorientale). *Il Quaternario 15, 9–19*.

Judenherc, S., & Zollo, A. (2004). The Bay of Naples (Southern Italy): constraints on the volcanic structures inferred from a dense seismic survey. *Journal of Geophysical Research 109, B10312*.

Kastens, K. A., & Mascle, J. (1988). ODP leg 107 in the Tyrrhenian Sea: Insights into passive margin and back-arc basin evolution. *Geol. Soc. Am. Bull.,100, 1140 –1156*.

Kearey, P., & Brooks, M. (1991). An Introduction to Geophysical Exploration. *Blackwell Science*.

Kearey, P., Brooks, M., & Hill, I. (2002). An Introduction to Geophysical Exploration. *Blackwell Science 3rd Edition*.

Latmiral, G., Segre, A., Bernabini, M., & Mirabile, L. (1971). Prospezioni sismiche per riflessione nei Golfi di Napoli e Pozzuoli ed alcuni risultati geologici. *Boll.Soc. Geol. Ital., 90, 163-172*.

Lavecchia, G. (1988). The Tyrrhenian-Apennines system: Structural setting and seismotectogenesis. *Tectonophysics,147, 263 – 296*.

Lirer, L., Luongo, G., & Scandone, R. (1987). On the volcanological evolution of Campi Flegrei. *EOS, Transactions of the American Geophysical Union 68, 226–234*.

Malinverno, A., & Ryan, W. B. (1986). Extension on the Tyrrhenian Sea and shortening in the Apennines as result of arc migration driven by sinking of the lithosphere. *Tectonics,5, 227 – 245*.

McQuillin, R., & Ardus, D. A. (1977). Exploration of the Geology of Shelf Seas. *Graham & Trotman, 234*.

McQuillin, R., Bacon, M., & Barclay, W. (1984). An Introduction to Seismic Interpretation. *Graham & Trotman*.

Milia, A. (1996). Evoluzione tettono-stratigrafica di un bacino peri-tirrenico: il Golfo di Napoli. *Ph.D. Thesis, (Università degli Studi di Napoli «Federico II»)*.

Milia, A. (2010). The stratigraphic signature of volcanism off Campi Flegrei (Bay of Naples, Italy). *Geological Society of America Special Papers, 464, 155–170*.

Milia, A., & Giordano, F. (2002). Holocene stratigraphy and depositional architecture of eastern Pozzuoli Bay (eastern Tyrrhenian Sea margin, Italy): the influence of tectonics and wave-induced currents. *Geo-Marine Letters 22 (1), 42–50*.

Milia, A., & Torrente, M. M. (1999). Tectonics and stratigraphic architecture of a peri-Tyrrhenian half-graben (Gulf of Naples, Italy). *Tectonophysics, 315(1), 301–318*.

Milia, A., & Torrente, M. M. (2000). Fold uplift and syn-kinematic stratal architectures in a region of active transtensional tectonics and volcanism, Easter Tyrrhenian Sea. *Geological Society of America Bulletin 112, 1531–1542*.

Milia, A., & Torrente, M. M. (2003). Late-Quaternary volcanism and transtensional tectonics in the Gulf of Naples, Campanian continental margin, Italy. *Mineralogy and Petrology, 79, 49–65*.

Milia, A., & Torrente, M. M. (2007). The influence of paleogeographic setting and crustal subsidence on the architecture of ignimbrites in the Gulf of Naples (Italy). *Earth and Planetary Science Letters, 263(3), 192–206*.

Milia, A., Mirabile, L., Torrente, M. M., & and Dvorak, J. J. (1998). Volcanism offshore of vesuvius volcano in Naples Bay. *Springer-Verlag*.

Milia, A., Mirabile, L., Torrente, M. M., & Dvorak, J. J. (1998). Volcanism offshore of vesuvius volcano in Naples Bay. *Springer-Verlag*.

Monrigal, O., De Jong, I., & Duarte, H. (2017). An ultra-high-resolution 3D marine seismic system for detailed site investigation. *European Association of Geoscientists & Engineers, Near Surface Geophysics, 2017, 15, 335-345*.

Orsi, G., De Vita, S., & Di Vito, M. (1996). The restless, resurgent Campi Flegrei nested caldera (Italy): constraints on its evolution and configuration. *Journal of Volcanology and Geothermal Research 74, 179–214*.

Orsi, G., De Vita, S., Di Vito, M., & Isaia, R. (2002). a restless, resurgent structure in a densely populated area, in The Cultural Response to the Volcanic Landscape. *edited by Balmuth, M., (Archeol. Inst. of America, Boston, CA)*.

Pappalardo, L., Civetta, L., D'Antonio, M., Deino, A. L., Di Vito, M. A., Orsi, G., . . . Piochi, M. (1999). Chemical and Sr-isotopical evolution of the Phlegraean magmatic system before the Campanian Ignimbrite (37 ka) and the Neapolitan Yellow Tuff (12 ka) eruptions. *Journal of Volcanology and Geothermal Research 91, 141–166*.

Passaro, S., Barra, M., Saggiomo, R., Di Giacomo, S., Leotta, A., Uhlen, H., & Mazzola, S. (2012). Multi-resolution morpho-bathymetric survey results at the Pozzuoli-Bay underwater archaeological site (Naples, Italy). *Journal of Archaeological Science 40,1268–1278*.

Passaro, S., Tamburrino, S., Vallefuoco, M., Gherardi, S., Sacchi, M., & Ventura, G. (2016). High-resolution morpho-bathymetry of the Gulf of Naples, Eastern Tyrrhenian Sea. *Journal of Maps, 12(sup1), 203–210*.

Patacca, E., Sartori, R., & Scandone, P. (1990). Tyrrhenian basin and Apenninic arcs: Kinematic relations since Late Tortonian times. *Mem. Sci.Geol. It.,45, 425 – 451*.

Patacca, E., Sartori, R., & Scandone, P. (1993). Tyrrhenian basin and Apennines. Kinematic evolution and related dynamic constraints. in E. Boschi, E. Mantovani, & A. Morelli, *Recent Evolution and Seismicity of the Mediterranean Region. NATO ASI Ser., Ser. C, vol. 402, Kluwer Acad., Norwell, Mass., pp.161 – 171.*

Pereira, C. M. (2017). Challenges in Flex Binning Ultra High Resolution Seismic Reflection Data. *Master thesis, University of Aveiro.*

Pereira, L. A. (2009). Seismic Attributes in Hydrocarbon Reservoirs Characterization*. Master thesis, University of Aveiro.*

Pescatore, T., Diplomatico, G., Senatore, M., Tramutoli, M., & Mirabile, L. (1984). Contributi allo studio del Golfo di Pozzuoli: aspetti stratigrafici e strutturali. *Memorie della Società Geologica Italiana 27, 133–149*.

Ribeiro, T. (2011). Multichannel Seismic Investigation of the Gran Burato area, off W Galicia. *Master thesis, University of Aveiro*.

Robinson, E. A., Durrani, T. S., & Peardon, L. (1986). Geophysical Signal Processing. *Prentice – Hall, 1 – 25*.

Rolandi, G., Bellucci, F., Heizler, M. T., Belkin, H. E., & De Vivo, B. (2003). Tectonic controls on the genesis of ignimbrites from the Campanian Volcanic Zone, southern Italy. *Mineral and Petrology 79, 3–31*.

Rollet, N., Déverche`re, J., Beslier, M.-O., Guennoc, P., Réhault, J.-P., Sosson, M., & Truffert, C. (2002). Back arc extension, tectonic inheritance, and volcanism in the Ligurian Sea, western Mediterranean. *Tectonics,21(3), 1015*.

Rosenbaum, G., & Lister, G. S. (2004). Neogene and quartenary rollback evolution of the tyrrhenian sea, the Apennines, and the Sicilian Maghrebides. *TECTONICS, VOL. 23, TC1013*.

Rosenbaum, G., Lister, G. S., & Duboz, C. (2002a). Reconstruction of the tectonic evolution of the western Mediterranean since the Oligocene. *Journal of the Virtual Explorer,8, 107 – 130*.

Rosi, M., & Sbrana, A. (1987). Phlegraean Fields. *Quad. Ric. Sci., 114 (9), pp. 175*.

Rosi, M., Principe, C., & Vecci, R. (1993). The 1631 Vesuvius eruption. A reconstruction based on historical and stratigraphic data. *Journal of Volcanology and Geothermal Research 58:151–182*.

Sacchi, M. A. (2009). Risultati preliminari della campagna oceanografica CAFE_07 - Leg 3 nei Golfi di Napoli e Pozzuoli, Mar Tirreno Orientale. *Quaderni di Geofisica 64, 3–26*.

Sacchi, M., Pepe, F., Corradino, M., Insinga, D. D., Molisso, F., & Lubrito, C. (2014). The Neapolitan Yellow Tuff caldera offshore the Campi Flegrei: stratal architecture and kinematic reconstruction during the last 15 kyr. *Marine Geology 354,15-33*.

Santacroce, R. (1987). Somma-Vesuvius. *Quad. Ric. Sci., 114 (8), pp. 251*.

Santacroce, R., & Sbrana, A. (2003). Carta Geologica del Vesuvio - Scala 1.15.000, Progetto CARG, Carta Geologica d'Italia. *S.EL.CA., Firenze*.

Santacroce, R., Cioni, R., Marianelli, P., Sbrana, A., Sulpizio, R., Zanchetta, G., & Joron, J. L. (2008). Age and whole rock–glass compositions of proximal pyroclastics from the major explosive eruptions of Somma-Vesuvius: A review as a tool for distal tephrostratigraphy. *Journal of Volcanology and Geothermal Research, 177(1), 1–18*.

Scandone, R., Bellucci, F., Lirer, L., & Rolandi, G. (1991). The structure of the Campanian Plain and the activity of Neapolitan Volcanoes (Italy). *Journal of Volcanology and Geothermal Research 48, 1–31*.

Scarpati, C., Perrotta, A., Lepore, S., & Calvert, A. (2013). Eruptive history of Neapolitan volcanoes: constraints from 40Ar-39Ar dating. *Geological Magazine 150, 412–425*.

Sheriff, R. E. (1996). Understanding the Fresnel Zone.Geophysical Corner.

Sheriff, R. E., & Geldart, L. P. (1995). Exploration Seismology. *Cambridge University Press, Cambridge*.

Sheriff, R. E., & Matisoff, B. S. (1991). Encyclopedic Dictionary of Applied Geophysics. *Geophysical References Series*.

Simkin, T., & Siebert, L. (1994). Volcanoes of the world. *Geosciences Press, Tucson, Arizona, pp 1–349*.

Speranza, F., Villa, I. M., Sagnoti, L., Florindo, F., Cosentino, D., Cipollari, P., & Mattei, M. (2002). Age of the Corsica-Sardinia rotation and Liguro-Procençal Basin spreading: New paleomagnetic and Ar/Ar evidence. *Tectonophysics,347, 231 – 251*.

Telford, W. M., Geldart, L. P., & Sheriff, R. E. (1990). Applied Geophysicis. . *Cambridge University Press, 2nd Edition*.

Vezzoli, L. (1988). Island of Ischia. *Quad. Ric. Sci., 114 (10), pp. 133*.

Volkhard, S. A. (2017). Geophysical Site Investigation for Offshore Wind Farm Development. *Technical report, Fraunhofer*.

Wohletz, K., Orsi, G., & De Vita, S. (1995). Eruptive mechanism of the Neapolitan Yellow Tuff interpreted from stratigraphic, chemical and granulometric data. *Journal of Volcanology and Geothermal Research 67, 263–290*.

Yilmaz, O. (2001a). Seismic Data Analysis: Processing, Inversion, and Interpretation of Seismic Data, Vol.1.

Yilmaz, O. (2001b). Seismic Data Analysis: Processing, Inversion, and Interpretation of Seismic Data, Vol. 2.

Internet References

https://www.cgg.com/en

https://www.geomarinesurveysystems.com/products

https://www.sciencedirect.com/topics/engineering/imaging-depth

http://www.shippingherald.com

https://www.worldatlas.com/aatlas/infopage/tyrrheniansea.html

https://www.wordatlas.com/gulfnaples.html